The Dissertation Committee for Jacinto Lopez-Toledo
certifies that this is the approved version of the following dissertation:

Heat and Mass Transfer Characteristics of a Wiped Film Evaporator

Committee:

A. Frank Seibert, Supervisor

Gary T. Rochelle, Supervisor

James R. Fair

Roger T. Bonnecaze

Benny D. Freeman

Richard L. Corsi

Heat and Mass Transfer Characteristics of a Wiped Film Evaporator

by

Jacinto Lopez-Toledo, B. S., M. S.

DISSERTATION

Presented to the Faculty of the Graduate School of

The University of Texas at Austin

in Partial Fulfillment

of the Requirements

for the Degree of

DOCTOR OF PHILOSOPHY

THE UNIVERSITY OF TEXAS AT AUSTIN

August 2006

Heat and Mass Transfer Characteristics of a Wiped Film Evaporator

Publication No. _____

Jacinto Lopez-Toledo, Ph.D.
The University of Texas at Austin, 2006

Supervisors: A. Frank Seibert
Gary T. Rochelle

A new mechanistic model to analyze simultaneous heat and mass transfer in vertical wiped film evaporators (WFE) is proposed. The well-studied falling film evaporator (FFE) is taken as the base case for the wiped film evaporator. A heat transfer enhancement factor, β_h, is defined as the ratio of the heat transfer coefficient for a wiped film evaporator, h_p^{WFE}, to the heat transfer coefficient of a falling film evaporator, h_p^{FFE}: $\beta_h = \dfrac{h_p^{WFE}}{h_p^{FFE}}$. Assuming heat and mass transfer analogy, the mass transfer coefficient for the wiped film evaporator (k_L^{WFE}) can be predicted using the heat transfer enhancement factor multiplied by the mass transfer coefficient for the falling film evaporator: $k_L^{WFE} = \beta_h \times k_L^{FFE}$. Four different combinations for the calculation of β_h are considered: two models for h_p^{WFE} and two models for h_p^{FFE}.

The model was tested initially using the water-sucrose experimental data from Frank and Lutcha [25]. Further validation of the model was done

with collected experimental data in this study, using three chemical systems covering a wide range of physical properties: water-sucrose, water-glycerol, and water-ethylene glycol. Different operating conditions like rotational speed and feed rate, as well as initial concentration were also run. The proposed model predicts the exiting concentration of water with good accuracy when a good prediction of the physical properties exist.

The mechanistic model takes into account several characteristics of the WFE: length, diameter, number of blades, and rotational speed. Some features of a WFE are not considered directly by the proposed model, such as the blade geometry, blade spacing, and blade clearance. These characteristics are often included in the correlation for the prediction of the heat transfer coefficient (h_p^{WFE}), and are therefore indirectly considered by the model.

An Excel computer program (WFE-SRP) incorporates the mechanistic model. WFE-SRP is able to use the DIPPR equations [22] or group contribution methods (GCM) to predict physical properties. New components can be added to the computer program, as long as the DIPPR equations or functional groups are available in the included methods.

WFE-SRP can also perform an isothermal flash calculation. When some conditions are met (i.e., small temperature profile in the WFE), a flash calculation can represent a WFE, predicting the exiting composition, flowrates, and heat duty. When a temperature profile exists in the WFE, an isothermal flash does not work.

Table of Contents

List of Tables

List of Figures

Nomenclature

Roman Letters

a_{ij}	Constant in Equation 5.16
A	Heat Transfer Area [m^2]
C_p	Heat Capacity [J/kg-K]
D	Diameter [m]
D_L	Liquid Diffusion Coefficient [m^2/s]
g	Gravity Constant [m^2/s]
h	Heat Transfer Coefficient [W/m^2K]
h_o	Heat Transfer Coefficient for Hot Fluid [W/m^2K]
h_p	Heat Transfer Coefficient for the Process Side [W/m^2K]
K	Equilibrium Constant [$-$]
k_L^{FFE}	Mass Transfer Coefficient for FFE [m/s]
k_L^{WFE}	Mass Transfer Coefficient for WFE [m/s]
k_{wall}	Wall Thermal Resistance [W/m-K]
L	Length [m]
N	Rotational Speed [s^{-1}]
N_b	Number of Blades [$-$]
N_L	Mass Transfer Rate for Liquid Phase [kg/s]
Nu	Nusselt number [$-$]

P	Total Pressure [Pa]
P^s	Vapor Pressure [Pa]
Pr	Prandtl Number [−]
q	UNIQUAC Surface Area Parameter [−]
Q	Total Transferred Heat [W]
r	UNIQUAC Volume Parameter [−]
Re_f	Film Reynolds Number [−]
Re_N	Rotational Reynolds Number [−]
Sc_L	Schmit Number [−]
T_p	Hot Fluid Temperature [°C]
T_v	Evaporation Temperature [°C]
U_{ov}	Overall Heat Transfer Coefficient [W/m^{2}K]
w_h	Hot Oil Flow Rate [kg/s]
wt	Weight fraction [−]
x	Liquid Mole Fraction [−]
x_F	Feed Mole Fraction [−]
x^*	Liquid Equilibrium Mole Fraction [−]
y	Vapor Mole Fraction [−]
Z	Dimensionless Length in Equation 3.3[−]

Greek Letters and Symbols

β	Enhancement Factor [−]

β_h	Heat Transfer Enhancement Factor [−]
δ	Film Thickness [m]
δ_L	Characteristic Length in Falling Film [m]
δ_{wall}	Wall Thickness [m]
Δ	Increment [−]
λ	Thermal Conductivity [W/m-K]
λ_w	Heat of Vaporization of Water [J/kg]
ϕ	UNIQUAC Volume Fraction [−]
μ	Viscosity [Pa · s]
ρ	Density [kg/m^3]
σ	Surface Tension [N/m]

Superscripts

FFE	Falling Film Evaporator
WFE	Wiped Film Evaporator

Subscripts

L	Liquid
V	Vapor

Abbreviations and Acronyms

BR-AK	Bott and Romero-Ahmed and Kaparthi
BR-N	Bott and Romero-Numrich
BR-AK	Bott and Sheikh-Ahmed and Kaparthi
BR-N	Bott and Sheikh-Numrich
FFE	Falling Film Evaporator
FFEn	Falling Film Evaporation
FFEs	Falling Film Evaporators
HTC	Heat Transfer Coefficient
GCM	Group Contribution Methods
SRP	Separations Research Program
WFE	Wiped Film Evaporator
WFEn	Wiped Film Evaporation
WFEs	Wiped Film Evaporators
WFE-SRP	Wiped Film Evaporator - Separations Research Program

Chapter 1

Introduction

1.1 Evaporation

Evaporation is an operation used to remove a liquid from a solution, suspension, or emulsion by boiling off a portion of the liquid. It is thus a thermal separation, or thermal concentration, process. We define the evaporation process as one that starts with a liquid product and ends up with a more concentrated, but still liquid and still pumpable concentrate as the main product from the process. There are actually a few instances where the evaporated, volatile component is the main product.

Standiford [90] defines the unit operation of evaporation as the removal of volatile solvent from a solution or a relatively dilute slurry by vaporizing the solvent. In nearly all industrial applications the solvent is water, and in most cases the nonvolatile residue is the valuable constituent. Evaporation differs from distillation in that when the volatile stream consists of more than one component no attempt is made to separate these components. Although the product of an evaporator system may be a solid, the heat required for vaporization of the solvent must be transferred to a solution or a slurry of the solid in its saturated solution in order that the device be classified as

an evaporator rather than a dryer. It is not unusual for an evaporator to be used to produce a solid as its only product. For instance, table salt is produced by feeding a saturated brine to an evaporator, precipitating the salt as water is removed. A side stream of salt crystals in brine is withdrawn to a filter or centrifuge where the salt is recovered in essentially dry form; the filtrate is returned to the evaporator as a supplementary feed. Thus the heat required for evaporation of the water is transferred to a slurry in the evaporator even though the only material leaving the system is a solid, except for the evaporated water; usually a small bleed of brine is necessary to purge from the system the impurities entering with the feed brine.

An evaporator consists of a heat exchenger or heated bath, valves, manifolds, controls, pumps, and condenser [28]. The most common designs are jacketed tanks, tubular heat exchangers, plate-and-frame heat exchangers, and wiped film evaporators.

Evaporators are used in a wide variety of applications such as [90]:

1. Reducing the volume to economize on packaging, shipping, and storage costs, *for instance of salt, sugar, caustic soda, orange juice, and milk*
2. Obtaining a product in its most useful form, *for instance salt from brine or sugar from cane juice*
3. Eliminating minor impurities, *for instance, from salt, sugar*
4. Removing major contaminants from a product, *for instance diaphragm cell caustic soda solutions contain more salt than caustic when produced*

but practically all the salt can be precipitated by concentrating to a 50% NaOH solution

5. Concentrating a process stream for recovery of resources, *for instance pulp mill spent cooking liquor, if concentrated sufficiently in an evaporator, can be burned in a boiler to produce steam, yielding also an ash that can be used to reconstitute fresh cooking liquor*
6. Concentrating wastes for easier disposal, such as *nuclear reactor wastes, dyestuff plant effluents, and cooling tower blowdown streams*
7. Transforming a waste into a valuable product, such as *spent distillery slop after alcohol recovery, which can be concentrated to produce an animal feed*
8. Recovering distilled water from impure streams such as *sea water and brackish waters.*

In most cases it is essential that the product is subjected to minimal thermal degradation during the evaporation process, requiring that temperature and time exposure must be minimized. This and other requirements brought on by the physical characteristics of the processed product have resulted in the development of a large range of different evaporator types. Additional demands for energy efficiency and minimized environmental impact have driven development toward very innovative plant configurations and equipment design [72].

1.1.1 Function of an Evaporator

The main function of an evaporator is to concentrate a solution or to recover a solvent. Minton [63] mentions that the evaporator design consists of three principal elements: **heat transfer, vapor-liquid separation,** and **efficient utilization of energy**. For evaporators to be efficient, the equipment selected and used must be able to accomplish several things [63]:

1. **Transfer large amounts of heat to the solution with a minimum amount of metallic surface area.** This requirement, more than all other factors, determines the type, size, and cost of the evaporator system.

2. **Achieve the specified separation of liquid and vapor and do it with the simplest devices available.** Separation may be important for several reasons: value of the product otherwise lost; pollution; fouling and corrosion of the equipment downstream with which the vapor is contacted.

3. **Make efficient use of the available energy.** This may take several forms. Evaporator performance often is rated on the basis of steam economy, pounds of solvent evaporated per pound of steam used. Heat is required to raise the feed temperature from its initial value to that of the boiling liquid, to provide the energy required to separate liquid solvent from the feed, and to vaporize the solvent. The greatest increase in energy economy is achieved by re-using the vaporized solvent as a

heating medium. Energy efficiency may be increased by exchanging heat between the entering feed and the leaving residue or condensate. When this method is used, each evaporator is known as an effect.

4. **Meet the conditions imposed by the liquid being evaporated or by the solution being concentrated.** Factors that must be considered include product quality, salting and scaling, corrosion, foaming, product degradation, holdup, and the need for special types of construction.

Steam-heated evaporators are the most widely used in industry. The three principal requirements of these evaporators are [90]:

- Transfer to the liquid of large amounts of heat needed to vaporize the solvent.
- Efficient separation of the evolved vapor from the residual liquid.
- Accomplishing these aims with the least expenditure of energy justifiable by the capital cost involved.

1.2 Criteria for the Selection of the Evaporator

During the design of evaporation plants, numerous and sometimes contradictory requirements have to be considered. They determine which type of construction and arrangement is chosen as well as the resulting process and economic data. The most important requirements are [72]:

- Capacity and operational data, including *quantities, concentrations, temperatures, annual operating hours, change of product and controls automation.*
- Product characteristics, including *heat sensitivity, viscosity and flow properties, foaming tendency, fouling and precipitation and boiling behavior.*
- Required operating media, such as *steam, cooling water, electric power, cleaning agents and spare parts.*
- Capital and operating costs.
- Standards and conditions for manufacture, delivery, acceptance.
- Choice of materials of construction and surface finishes.
- Site conditions, such as *available space, climate (for outdoor sites), connections for energy and product, service platforms.*
- Legal regulations covering safety, accident prevention, sound emissions, environmental requirements, and others.

1.3 Types of Evaporator

Standiford [90] presents a classification of evaporators based on the heating medium (steam) used to transfer heat. He classifies the steam-heated evaporators as **natural circulation, forced circulation**, and **film-type.**

The simplest evaporator is the batch evaporator [28], shown in Figure 1.1. It has a jacketed vessel heated with steam or hot fluid. The product

is metered into a tank to a specified level through a feed nozzle. Heat is applied and the batch is allowed to heat to its boiling point. Vapors are removed until the desired concentration of the product is reached and the heat is then removed. This evaporator is not well-suited for temperature-sensitive materials because the residence time is usually long and the static head of the liquid increases the boiling point of the product at the bottom of the tank.

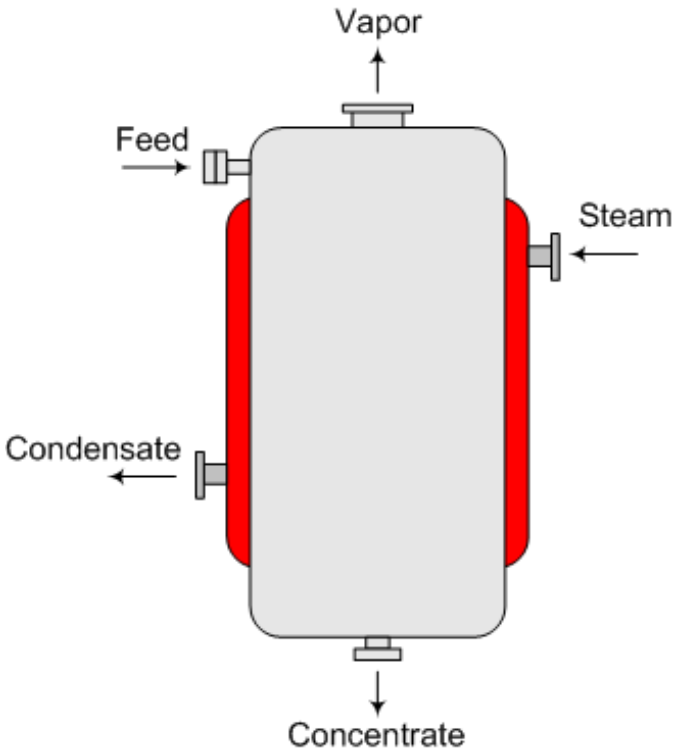

Figure 1.1: Batch evaporator

1.3.1 Natural Circulation Evaporators

These evaporators were the first developed commercially and still represent probably the largest number of units in operation [90]. Glover [28] mentions that they are normally used for simple applications where the product is clean and temperature-stable, whereas forced-circulation evaporators are used for viscous, salting and scale-forming products. The most common natural-circulation evaporators are horizontal tube, short vertical tube, and long vertical tube.

1.3.1.1 Horizontal Tube Evaporator

This is the oldest type of chemical evaporator [28], shown in Figure 1.2. It is the only evaporator where the heating medium is inside the tubes. Its principal advantage lies in the relatively small headroom required.

1.3.1.2 Short-Tube Vertical Evaporator

This is also called a calandria vertical evaporator. It is still in widespread commercial use [28]. Its principal use at present is in the evaporation of cane-sugar juice [86]. Circulation past the heating surface is induced by boiling in the tubes, which are usually 50.8 to 76.2 mm in diameter by 1.2 to 1.8 m long. The body is a vertical cylinder, usually of cast iron, and the tubes are expanded into horizontal tube sheets that span the body diameter. The circulation rate through the tubes is many times the feed rate, so there must be a return passage from above the top tube sheet to below the bottom tube sheet.

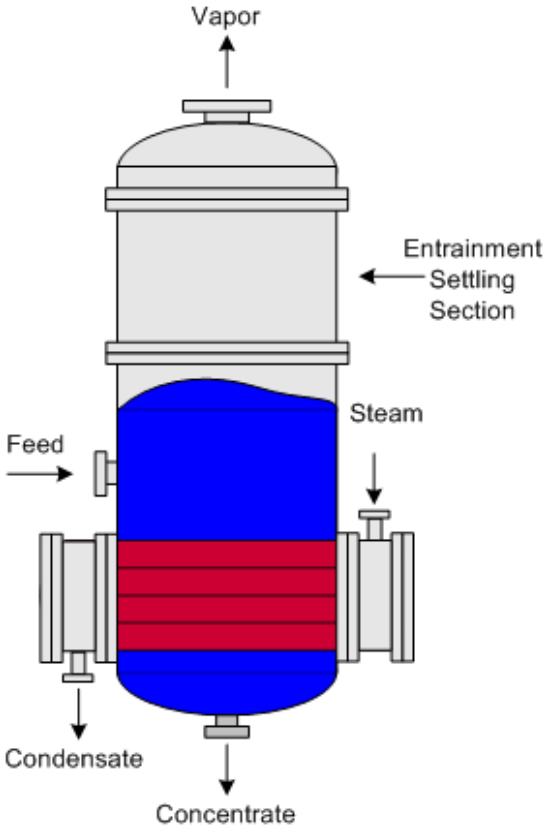

Figure 1.2: In a horizontal tube evaporator, the heating medium flows inside the tubes [28].

Most commonly used is a central well or downtake as shown in Figure 1.3.

Advantages of the short-tube vertical evaporator include [28]:

- low head-space required
- suitable for liquids that have moderate tendency to scale
- fairly high heat-transfer coefficients can be obtained with thin (up to 5-10 cP) liquids

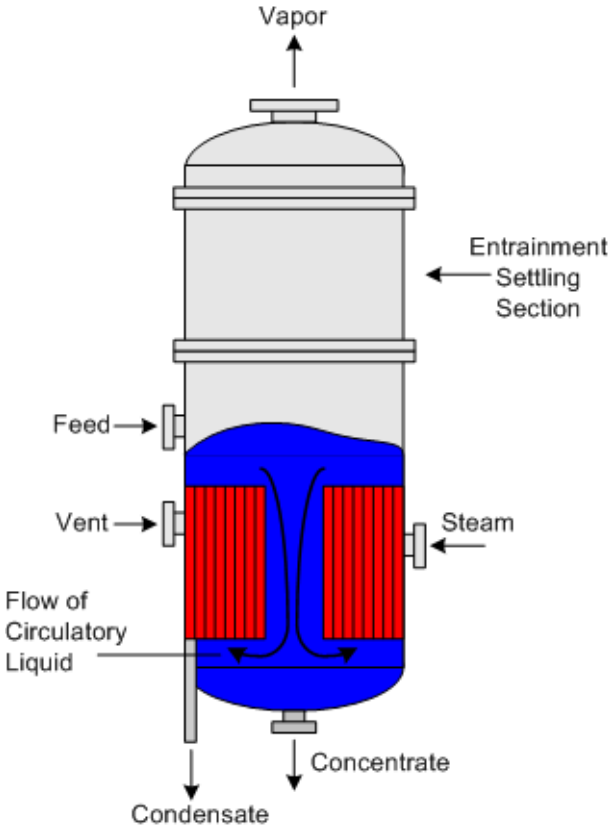

Figure 1.3: In a short-tube vertical evaporator, the process liquid is inside the tubes and the heating medium outside the tubes [28].

- relatively inexpensive to manufacture

1.3.1.3 Long-Tube Vertical Evaporator

This is also known as a rising-film evaporator, shown in Figure 1.4. It is one of the most widely used tubular evaporators [28]. A shell-and-tube heat exchanger mounted to a vapor-liquid separator, it requires little floor space, but high head room.

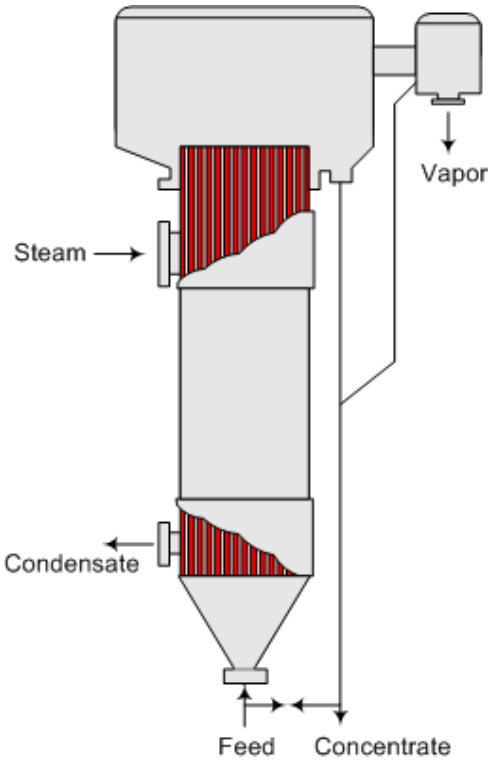

Figure 1.4: In a long-tube rising-film vertical evaporator, feed flows upwards through the tubes and heating medium flows downward on the shellside [28].

The dilute feed enters at the bottom of the tubesheet and flows upward through the tubes, with the heating medium on the shellside. The feed is heated to its boiling point in the lower portion of the tubes. Bubbles form on the tubes at some distance further up and boiling begins, increasing the linear velocity and the rate of convective heat transfer. Near the top of the tubes, bubbles grow rapidly. In this bubble zone, slugs of liquid and bubbles rise quickly through the tubes and are discharged at high velocity from the top, where they impinge on a liquid/vapor separator that tends to break any foam

that has formed. This allows the use of this type of evaporator for products that tend to foam [28].

1.3.2 Forced Circulation Evaporators

This evaporator is suitable for the largest variety of applications and is usually the most expensive type [90]. It usually consists of a shell-and-tube heat exchanger, a vapor-liquid separator, and a pump to circulate the liquor from the body through the heater and back to the body. The system is usually arranged so that there is no boiling in the heater. The heat input is therefore absorbed as sensible heat, and vapor liberation does not occur until the liquor enters the flash chamber. Absorption of the heat input as sensible heat results in a temperature rise that reduces the net temperature difference available for heat transfer. To keep this temperature rise to reasonable limits, usually on the order of 2–6 K, requires circulating large volumes of liquor relative to the amount evaporated. There is also an upper limit to temperature rise, usually about 10 K, beyond which flashing at the entry to the flash chamber becomes so violent that large masses of liquor are ejected with the vapor. This makes entrainment separation more difficult and may impose structural shock loads on the separator. The head requirements of the circulating pump are generally quite low, consisting primarily of conventional friction and acceleration and deceleration losses at heater and body inlet and outlet, plus vortex losses in the body.

Several configurations of forced circulation evaporators exist. The most

common arrangement is shown in Figure 1.5 having an external vertical single-pass heater and a tangential inlet to the body.

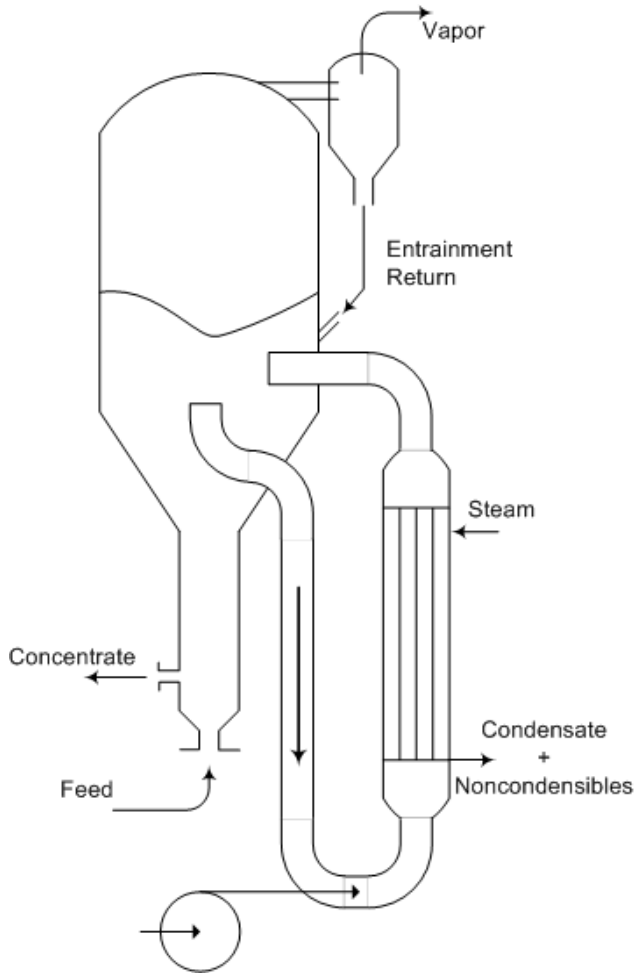

Figure 1.5: Submerged-tube forced circulation evaporator shown as circulating magma crystallizer [90].

1.3.3 Film-Type Evaporators

The long-tube falling film evaporator shown in Figure 1.6 is a variation of the long-tube rising-film evaporator, in which the equipment is turned upside down so the tubular heat exchanger is on top of the vapor/liquid separator section. Feed enters at the top of the evaporator, where specially designed distributors evenly distribute the feed into each of the tubes. Distribution of the feed is very critical and there are many designs for the distributors, but generally most are built around some type of perforated plate placed over the top tubesheet [28].

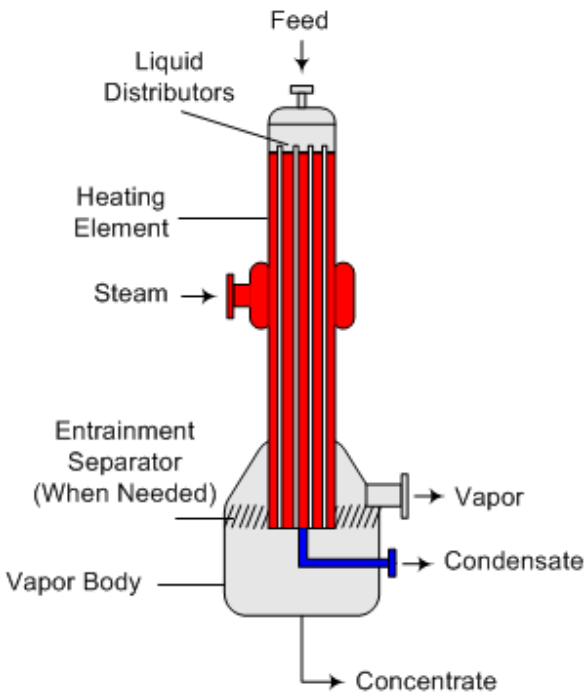

Figure 1.6: The falling-film evaporator is a variation of the long-tube rising-film design [28].

The principal advantages of the falling-film evaporator are good heat-transfer performance, even at low temperature and low temperature differences, low initial cost, and excellent vapor-liquid separation characteristics. Principal applications have been for citrus juices, where performance at low temperature and low holdup is important, and applications requiring low temperature differences, such as vapor compression or multiple-effect evaporators needing a large number of effects to be economical, e.q. for producing fresh water from saline waters.

1.3.3.1 Wiped Film Evaporator

The wiped film evaporator (WFE), also known as an agitated thin-film evaporator (ATFE) is a device often used to purify liquids with viscosities up to 10^5 poise [62], to separate temperature-sensitive mixtures, or in general to provide short residence times in heated zones. Unfortunately, the heat and mass transfer mechanisms involved in wiped film evaporators are poorly understood. Users of the technology must rely on equipment vendors and experience for guidance.

Wiped filmed evaporators are designed to spread a thin layer or film of liquid on one side of a metallic wall, with heat supplied to the other side. The unique feature of this equipment is not the thin film itself, but rather the mechanical wiping device for producing and agitating the film. This mechanical concept permits the processing of high-viscosity liquids, liquids with suspended solids, or situations requiring liquid rates too small to keep the

thermal surface of a falling-film evaporator uniformly wet [68].

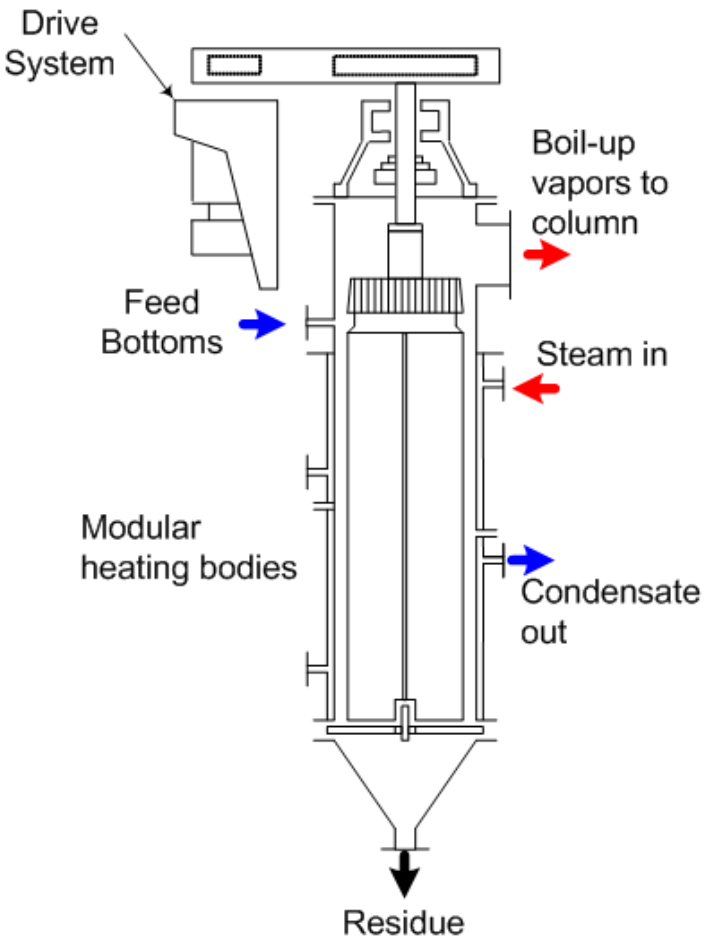

Figure 1.7: Diagram of a vertical thin-film vaporizer.

Most WFEs are vertical cylinders (see Figure 1.7) where the feed material is distributed to the inner surface. As the liquid flows downward, axially arranged blades or roller wipers distribute the liquid as a thin film, which is constantly mixed. This type of equipment can operate at very low pressure

and provides minimum pressure drop.

The double-walled evaporator jacket is heated continuously by a suitable medium. A vacuum system (often a combination of several individual pumps) reduces the pressure in the distillation chamber. Depending on the temperature and the pressure in the chamber, vapors leave through the vapor discharge nozzle and travel to an external condenser. Nonvolatile substances are discharged at the lower end of the evaporator. Table 1.1 shows the typical applications of WFEs and operating conditions.

Table 1.1: General Application Areas of Wiped Film Evaporators [6].

Areas of application	Operating Pressure		Concentration	Stripping	Deodorization
	1 mm Hg & above	Below 1 mmHg	Dehydration		
Organics, General	X	X	X	X	X
Pesticides & Herbicides	X	X			
Pharmaceuticals, General	X	X			
Vitamins	X	X			
Food, General	X		X	X	X
Tomato Paste	X		X–50% total solids		
Fats & Oil	X	X	X	X	X
Fatty Acids	X	X		X	X
Plastics & Resins	X	X	X	X	X
Radioactive Waste Conc.	X		X		
Rerefining Used Oils	X	X		X	
Solvent Recovery	X	X		X	

The WFE can function as a stand-alone unit (i.e., for purification) or as a part of another unit (e.g., as a reboiler in a distillation column). Two WFE

orientations are possible, horizontal or vertical. This study will concentrate on the commonly used vertically-aligned WFE.

An extensive literature review on wiped film evaporators indicates that heat transfer has been widely studied and several correlations for the prediction of the heat transfer coefficient exist: Abichandani and Sarma [1], Azzory and Bott [7], Bott and Romero [11], Bott and Sheikh [14], Miyashita and Hoffman [64], Miyashita et al. [65], Skelland [87], Skoczylas [88]. However, a correlation of the mass transfer coefficient for wiped film evaporators has not been published, and simultaneous heat and mass transfer have not been studied, thus providing a niche that the present study is trying to fulfill.

The fundamental heat and mass transfer characteristics of wiped film evaporators (WFEs) are poorly understood, and at present the technology is considered to be a "black art." In general, an equipment vendor, based on pilot plant data and general process experience, determines the design of a WFE. While the vendor may have a good understanding of the technology, the knowledge is well-guarded. In many cases, the end user prefers to limit any information shared with the vendor and does not have the capability to analyze the performance of the unit, in order to know if there is room for improvement (i.e., increase throughput).

1.4 Objective

The main objectives of the present work were to study WFE heat and mass transfer simultaneously and to develop a global model for the prediction

of heat and mass transfer coefficients as functions of system properties and contactor geometry in a vertical wiped film evaporator, and to verify if the assumption that a WFE can be treated as an isothermal flash in a process simulator. The global model was tested and validated with existing published data and additional experimental data obtained in this study. The sequence of the tasks followed are listed below:

1. Perform comprehensive literature review of wiped film evaporation and falling film evaporation technologies
2. Define research topic
3. Develop preliminary heat and mass transfer model
4. Test preliminary model with published data
5. Identify test systems for study
6. Obtain experimental WFE unit or access to a WFE unit
7. Develop experimental plan based on WFE equipment, test systems and preliminary model
8. Obtain experimental data
9. Compare experimental data with preliminary model
10. Modify preliminary model or develop new model based on additional experimental data
11. Develop Excel-based program for the design/rating of a WFE unit
12. Prepare dissertation.

The experimental systems that were tested cover a wide range of physical properties. Some papers with experimental data used water/glycerol as the system [1, 11, 14]. Water/ethylene glycol is another experimental system which has been used to measure heat transfer coefficients [1]. Water/sugar solutions have been used for heat transfer measurements [91] as well as for characteristic dimensions [25]. These three systems, water/glycerol, water/ethylene glycol, and water/sugar, were used to gather experimental data for this study.

These three well-characterized test systems were studied. Two of the systems present a wide variation in viscosity (water/sugar and water/glycerol) for different temperatures and concentrations, while the other (water/glycol) presents a slight variation on almost all physical properties.

The Excel-based program is called WFE-SRP. Because a lot of components are poorly characterized and in order to increase the usefulness of the program, it was necessary to include group contribution methods for the estimation of the vapor liquid equilibrium, as well as for the estimation of physical properties. Appendix A shows how to use the computer program, along with the available group contribution methods.

Chapter 2

Literature Review

2.1 Boiling Mechanisms in Evaporation

There are three mechanisms of heat transfer: conduction, convection, and radiation. In wiped film evaporators the important mechanisms are convection and conduction. The vaporization of liquids may result from various mechanisms of heat transfer. Figure 2.1 shows a physical interpretation of the boiling curve.

2.1.1 Pool Boiling

This refers to the type of boiling experienced when the heating surface is surrounded by a relatively large body of fluid which is not flowing at any appreciable velocity and is agitated only by the motion of the bubbles and by natural-convection currents. Two types of pool boiling are possible: subcooled pool boiling, in which the bulk fluid temperature is below the saturation temperature, resulting in collapse of the bubbles before they reach the surface, and saturated pool boiling, with bulk temperature equal to saturation temperature, resulting in net vapor generation [43].

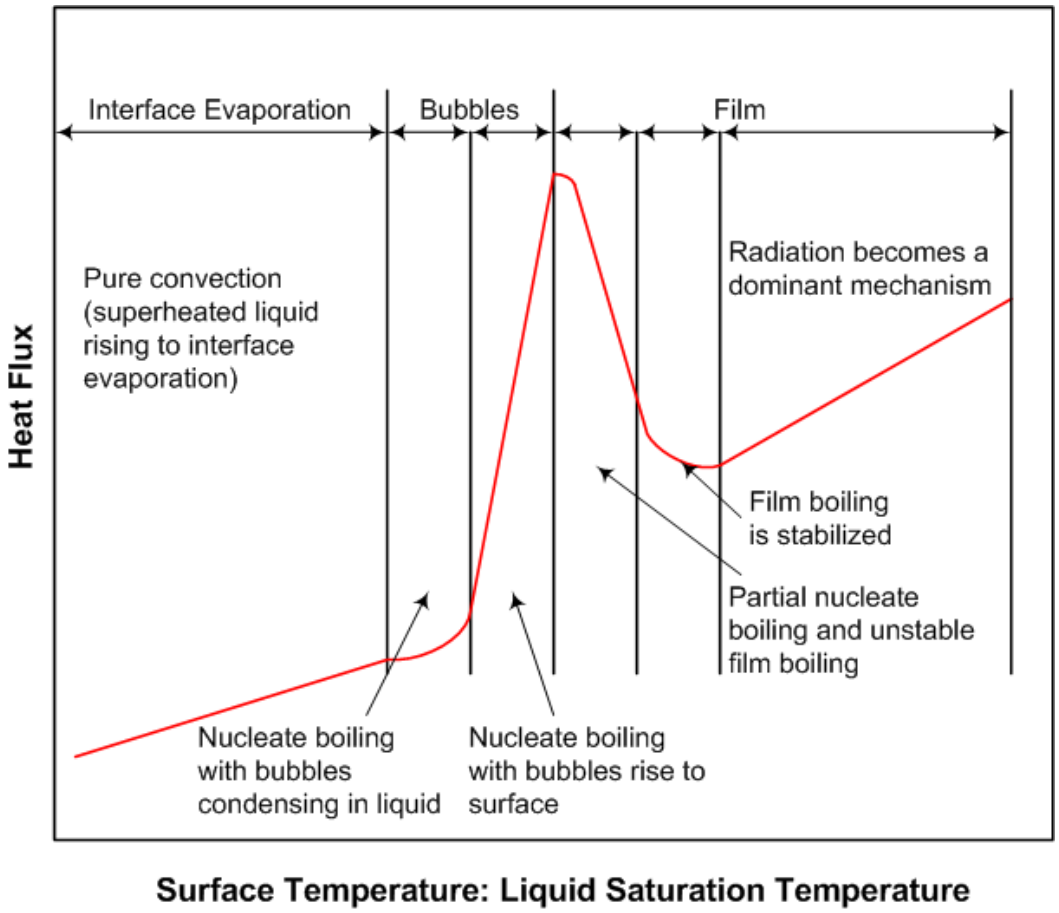

Figure 2.1: Interpretation of the boiling curve for water at atmospheric pressure [19].

2.1.2 Nucleate Boiling

Heat transfer by nucleate boiling is an important mechanism in the vaporization of liquids. It occurs in the vaporization of liquids in kettle-type and natural-circulation reboilers commonly used in the process industries. High rates of heat transfer per unit of area (heat flux) are obtained as a result of

bubble formation at the liquid-wall interface rather than from mechanical devices external to the heat exchanger. There are available several expressions from which reasonable values of the film coefficients may be obtained [43].

2.1.3 Film Boiling

In fully developed film boiling the vapor blankets the heating surface in a smooth continuous film except where the generated vapor escapes from the film in very large bubbles. If the heating surface is vertical and extends through the liquid level, the vapor can escape from the ends of the annular spaces and bubbles may not be generated.

2.2 Literature Review

An extensive literature review on wiped film evaporators indicates that heat transfer has been widely studied and several correlations for the prediction of the heat transfer coefficient exist. However, a correlation of the mass transfer coefficient for wiped film evaporators has not been published, and simultaneous heat and mass transfer have not been studied, thus providing a niche that the present study is trying to fulfill.

The fundamental heat and mass transfer characteristics of wiped film evaporators (WFEs) are poorly understood, and at present the technology is considered to be a "black art." In general, an equipment vendor, based on pilot plant data and general process experience, determines the design of a WFE. While the vendor may have a good understanding of the technology,

the knowledge is well-guarded. In many cases, the end user prefers to limit any information shared with the vendor and does not have the capability to analyze the performance of the unit, in order to know if there is room for improvement (i.e., increase throughput). In an earlier Separations Research Program (SRP) publication, Rocha-Uribe and Lopez-Toledo [76] provided a state-of-the-art review that includes a list of WFE vendors. Table 2.1 shows the updated information for several vendors of wiped film evaporators.

Table 2.1: Vendors of Wiped Film Evaporators [76].

Company	Address	Phone	Fax and e-mail
ChemTech Services (formerly UIC Inc)	P.O. Box 2097 Joliet, IL 60434	815-744-4696 800-343-5841	815-744-3938 shortpathdistillation @uicinc.com
Artisan Industries	73 Pond Street Waltham, MA 02451	781-893-6800	781-647-0143 info@artisanind.com
Pope Scientific, Inc	P.O Box 80018 Saukville, WI 53080	262-268-9300	262-268-9400 sales@popeinc.com
Aaron Equipment	735 E. Green St. Bensenville, IL 60106	630-350-2200	630-350-9047 sales@aaronequipment.com
LCI Coprporation (formerly Luwa)	P.O. Box 16348 Charlotte, NC 28297	704-394-8341	704-392-8507 info@lcicorp.com
Summit Process Tech	8 Hamilton Road Ridgefield, CT 06877	203-438-8915	203-431-4842 summitec@aol.com
Pfaudler, Inc.	1000 West Avenue P.O. Box 23600 Rochester, NY 14692	585-235-1000	
Gooch Thermal Systems Inc.	1221 Route 22 East Lebanon, NJ 08833	908-236-9350	908-236-9333 info@goochthermal.com

Rocha-Uribe and Lopez-Toledo provided a table with a classification of the papers by type of information presented. Table 2.2 includes an updated list with additional references that were found during this study.

Table 2.2: Technical papers on Wiped Film Evaporator Technology [76].

Modeling	Theory	Correlations	Vendor	Related
1. Kern and Karakas [39]	1. Godau [29]	1. Bott and Romero [11, 12]	1. Nadjer [69]	1. King [40, 41]
2. McKelvey and Sharps [61]	2. Nakamura and Watanabe [70*]	2. Bott and Sheikh [14]	2. Freese and Glover [26]	2. Mutzenberg and Giger [67]
3. Billet [8]	3. Komori et al. [44, 45, 46*]	3. Stankiewicz and Rao [91]	3. Tyzack [95, 96]	3. Cvengros [20]
4. Gruber and Rak [31]	4. Burrows and Beveridge [15]	4. Cvengros et al. [21]	4. Lavis [52]	4. Larson et al. [50]
5. McKenna [62]		5. Sangrame et al. [80]	5. Schurter [83]	5. Bott and Sheikh [13]
		6. Frank and Lutcha [25]	6. Arlidge [6]	6. Chawankul et al. [16]
			7. Mutzenburg [68]	7. Chuaprasert et al. [17]
			8. Parker [74]	8. Martinez-Chitoy [57]
			9. Eckles [23]	
			10. Bishop and Arlidge [10]	

*Horizontal WFEs

The earliest paper dealing with modeling of WFE is by Kern and Karakas [39] in 1959. In their paper, the authors attempted to combine principles of heat and mass transfer, hydrodynamics, and rheology (viscosity correlations) in order to find equations for the prediction of the WFE performance. An expression for calculating the required power for mechanical agitation was provided. While the authors stated that their model is a first step towards a more complex model (i.e., to take into account variations in physical properties), the follow-up rigorous model has not been published and is assumed to be proprietary.

McKelvey and Sharps [61] examined the velocity profile and flow structure of the bow waves[1] (see Figure 2.2) and their dependence on certain parameters (e.g. blade clearance and film thickness) and on throughput. Expressions for the velocity profile and power consumption were developed. However, mass transfer was not considered.

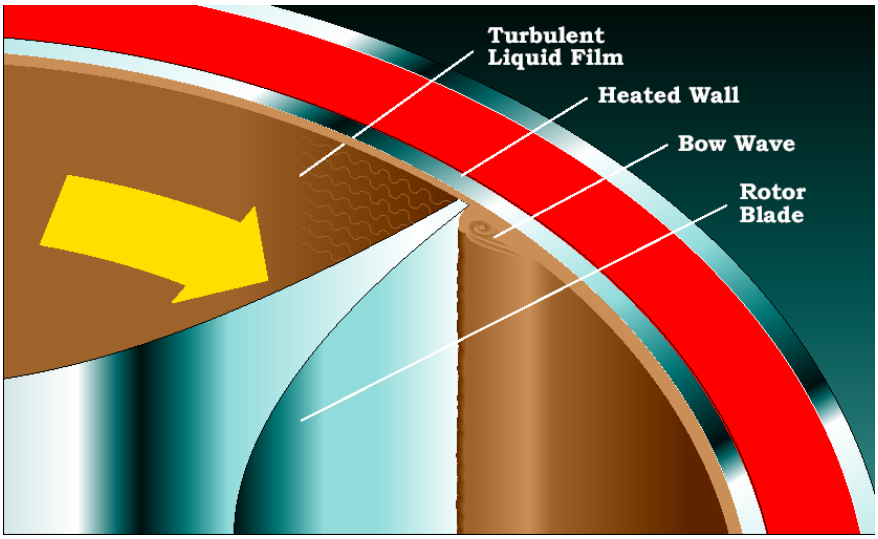

Figure 2.2: Cross section of a wiped fim evaporator showing the blade and bow wave formed in front of it.

Gouw and Jentoft [30] modeled a glass wiped-film still using the equations for batch distillation, and they mentioned the possibility of extrapolating the results to commercial-size film evaporators. They assumed that the concentration of the film is uniform (i.e., there is no gradient from the surface of

[1] A bow wave is formed in front of the wiping blades when the liquid flowrate is high enough to fill the clearance between the blades and the wall and it often presents turbulent flow.

the evaporating film to the wall). Dodecane-octadecene was the test system. Their results, on a small scale, agree with the results obtained by Kirschbaum and Dieter [42] on an industrial-scale wiped-film evaporator using ethanol-water as the test system.

Unterberg and Edwards [97] studied the evaporation of a saline solution wiped on the outside of a heated vertical copper tube at different salt concentrations. They noticed that free surface evaporation occurred with non-boiling feed. Film continuity was poor for pure water but better for the saline solutions.

Gruber and Rak [31] modeled the WFE as a series of co-current flashes, where the liquid from the first flash flows to the second and then to the third, and so on, until it leaves the WFE. The vapors from all the flashes form the exiting vapor from the unit. This rather simple model required experimental data to develop correlations for liquid entrainment as a function of vapor velocity, for the heat transfer coefficient for the jacket as a function of hot oil flowrate and temperature, and for heat loss as a function of ambient temperature. Data were inputted into a Fortran code and the WFE operation was simulated with AspenPlus[2].

Godau [29] developed approximate and exact solutions for the evaporator film thickness as a function of fluid density and viscosity, and evaporator throughput. He did not consider the influence of the wiper blades nor did he

[2]AspenPlus™ is a simulation/design program for chemical processes sold by Aspen Technologies http://www.aspentech.com

study mass transfer.

Komori et al. [44, 45] examined the flow structure and mixing mechanisms in the bow wave, both theoretically and experimentally in model wiped film devices with a limited number of blades. They looked at the degree of mixing between the film and the bow wave, and attempted to determine optimum device configuration for adequate mixing. They did not consider mass transfer.

A more rigorous WFE model was proposed by McKenna [62] and is the basis for the previous work of Rocha-Uribe and Lopez-Toledo [76]. The model focuses on analyzing the mass transfer phenomena and does not include a heat transfer analysis. It is also limited to a binary system (it was developed for a monomer-polymer solution). The model provides a tool to obtain order of magnitude estimates of device size, power requirements and throughput; uncertainties in parameter values can affect the design.

Bott and Romero [11] and Bott and Sheikh [14] presented experimental data and correlations for predicting the heat transfer rate coefficient. They studied different WFE column configurations (6, 12 and 24-in long by 1.0 in i.d.) using water and water/glycerol mixtures. They correlated their results using an expression of the following form:

$$Nu = f\left[Re_f^{a_1} Re_N^{a_2} Pr^{a_3} N_b^{a_4} (D/L)^{a_5}\right] \tag{2.1}$$

but they did not consider mass transfer in their calculations.

Other authors who used expressions similar to Equation 2.1 and who have also presented experimental heat transfer data are Stankiewicz and Rao [91], Abichandani et al. [2], and Skoczylas [88].

Expressions for the characteristic dimensions of WFEs are also available. Among them, the models of Bott and Romero [12] and Frank and Lutcha [25] are worth mentioning since they provide mass transfer data for different systems. Bott and Romero used a water/glycol system while Frank and Lutcha studied water and water/sugar mixtures.

Vendors (see Table 2.1) report characteristics and advantages of WFEs over other evaporators (i.e., falling film, rising film, etc.). Freese and Glover [26] mention the different types of rotors available for WFEs and the different configurations (horizontal and vertical) of the unit. Mutzenburg [68] explains how the WFE performs (flow patterns inside the unit, residence time, etc), as well as the characteristic overall heat transfer coefficient for particular applications. Parker [74] describes WFE design and associated costs based on fixed clearances and geometry, vertical or horizontal.

Eckles [23] recommends operating at vacuum when the purification cannot be achieved at atmospheric conditions and/or when the product is thermally unstable. The author also recommends WFE for the separation of medium-viscosity materials (up to 500 centipoises). Table 2.3 shows the advantages/disadvantages of vacuum evaporator systems (another advantage for the falling film evaporator not mentioned in Table 2.3 is that it does not have moving parts), while Fischer [24] provides a list of various WFE applications

(see Table 2.4).

Table 2.3: Advantages and Disadvantages of Vacuum Evaporator Systems [23].

Type	Advantages	Disadvantages
Falling-film evaporators	• Relatively simple design • High throughput per unit size (since it is a continuous process)	• Extremely poor separation efficiency • Not suitable for viscous feed materials • Laminar films can have large ΔTs through the film, which can lead to "hot areas" near the heating surface
Wiped-film evaporators	• High throughput per unit size (since it is a continuous process) • Can handle high viscosity materials • Can incorporate baffles to eliminate contamination of the product by the feed material	• Poor separation efficiency • Many designs do not allow operation at lower pressures
Short-path systems (in general)	• Run at the lowest possible operating pressure of any system • Capable of a high throughput per unit size (due to continuous operation) • A large body of operating and design correlations exists as a result of a considerable number of these systems currently in operation)	• Poor separation efficiency • Potential for direct contamination of the product by the entrained particles in the feed mixture • Have the shortest thermal history of any process

Table 2.4: Where Wiped Film Evaporators are Used [24].

	Concentration, Dehydration	Distillation		Fractionation	Stripping	Deodorization
		Steam Heated	High Temperature			
General chemicals	Fuels Formaldehyde Caprolactam recovery Urea Insecticides Ammonium nitrate Nitrochalk Pyrethrum extract Sodium isopropyl xanthate Dyes (water soluble) Phosphoric acid Aniline dye	Acetic derivatives Solvent recovery Cresylic acid Glycols Amines Cyclohexyl phthalate Ketones Isopropenyl acetone Fatty alcohols (to C_{16}) Insecticides Phenothiazine Herbicides Caprolactum Ethylene glycol recov. Lactic acid	Isocyanates Solvent recovery Acrylonitriles Amines (above C_{16}) Chlorinated hydrocarbons Dibutyl maleate Didecyl phthalate Sucrose ester Laural mercaptan Resorcinol Trixylne phosphate Hydroxquinoline Dibasic acids Rasin acids Naphthenic acids Fatty alcohols (from C_{16}) Triethanolamine Dimethyl tertiary amines	Isocyanates Caprolactam Solvent recovery Cresylic acids Glycols Cumene hydroperoxide Ethanolamines Hydrazine Nonyl phenol Isomers Rosin acid Fatty alcohols Amine solutions Anthracene oil recovery	Isocyanates Acetic derivatives Petroleum sulfonates Caprolactamum Acrylonitriles Chlorinated paraffins Cumene hydroperoxide Cyclohexyl phthalate Dibutyl maleate Laural mercaptan Resorcinol Trixylene phosphate Acetic acid Naptha oil solutions Insecticides Didecyl phthalate	Chlorinated paraffins Vaseline Petroleum jelly Naphtha oil solutions
Food	Tomato paste Coffe, tea Candies Beer malt Milk, whey Meat extracts Tannin extract Ketoglutamic acid		Benzoates	Recovery of volatile oils Flavor extract	Oleomargarine resins Spice extracts Flavor extract Peel oils	Peel oils
Pharmaceuticals	Vitamin A Sugal sol. Enzymes Ascorbic acid Amino acids Choline chloride Hormone and antibacterial sol. Dextran compounds	Undisclosed organic compounds Essential oils	Vitamin C Amino esters Flavors Essential oils	Saccharin extract Tocopherol	Liver extract	Amino acids
Fats and Oils	Glue Gelatine	Tallow nitrile	Glycerin Fatty acids Tall oil	Glycerin Fatty acids Tall oil	Silicone oils Olive oils Saccharin oil Edible oils	Olive oil Tallow Edible oils Vegetable oil plasticizers
Plastics, resins	Latex Urea-formaldehyde resin Liquid rubbers Water-soluble polymers	Tricresyl phosphate	Dioctyl phthalate Diisooctyl phthalate Phenolic resins	Styrene Adiponitrile	Phenolic resin Tricresyl phosphate Melamine resin Polystyrene Rubber polymers	Cumene resin Dioctyl phthalate Diisooctyl phthalate Latex (rubber) Polystyrene
Misc	Tobacco extract Atomic wastes				Varnish	Viscose rayon (degassing)

A review of the literature indicates that WFE heat and mass transfer characteristics have not been studied simultaneously. A few papers present experimental heat transfer data for different systems (water/sugar and water/glycerol) along with heat transfer coefficient correlations. However a WFE mass transfer coefficient correlation has not been published. Frank and Lutcha provide limited experimental data that can be used to calculate mass transfer coefficients. Their data were used primarily for the prediction of the thickness of the film inside a WFE with variable clearance.

Much work has been done regarding heat transfer for vertical and horizontal WFEs, but limited research for mass transfer is reported in the literature. There are equations to predict the velocity profiles for the gap between the wipers and the wall, and for the calculation of the heat transfer coefficient, but there are no equations for the calculation of the mass transfer coefficient. Mass transfer has not been studied simultaneously with heat transfer. Thus a significant gap of WFE knowledge is missing and we hope to fill this gap with the present dissertation.

Falling film evaporators (FFEs) can represent a base case of WFEs (i.e., WFEn = WFE without agitation). Much information has been published regarding FFE. A recent "state-of-the-art" study of falling film evaporation was conducted by Thome [92]. His studies will be useful because the existing models for FFEs can be used to predict a "base value" (i.e., heat transfer coefficient), and with the available models for WFEn, an "enhancement factor" can be calculated as a ratio of FFEn to WFEn. Because mass transfer models

for FFEs are also available, the mass transfer coefficient for WFEn will be predicted using the enhancement factor times the mass transfer coefficient for FFEn.

Al-Najeem et al. [4] present a semi-mechanistic model for the prediction of FFE heat transfer coefficients in vertical tube evaporators. They solved the governing energy equation and fitted the solution to an equation which is valid over wide ranges of Reynolds and Prandtl numbers.

Ahmed and Kaparthi [3] present a correlation for the calculation of the heat transfer coefficient as a function of the Reynolds and Prandtl numbers. It was developed from experiments that were carried out using water and aqueous solutions of glycerol.

Numrich [73] developed a FFE model, using a modification of the Prandtl analogy, to predict the heat transfer coefficient. This model shows good agreement with existing experimental data for Prandtl numbers up to 50.

Chapter 3

Modeling: Previous Work

As mentioned in Chapter 2, a lot of work has been done in the modeling of heat transfer in wiped-film evaporators. In the following paragraphs the available models for heat and mass transfer for falling film and wiped film evaporators will be discussed.

3.1 Heat Transfer

Heat transfer has been studied by several authors such as Ahmed and Kaparthi [3], Al-Najeem et al. [4], Alhusseini et al. [5], Krupiczka et al. [48], Numrich [73], Tsay and Lin [94], for falling film evaporators, and Abichandani and Sarma [1], Abichandani et al. [2], Bott and Romero [11, 12], Bott and Sheikh [13, 14], Kern and Karakas [39] for wiped film evaporators.

3.1.1 Falling Film Evaporators

Al-Najeem et al. [4] present a semi-mechanistic model for the prediction of heat transfer coefficients in vertical falling film evaporators. The case solved assumed steady turbulent flow of incompressible fluids having constant properties along a vertical plane surface or inside a vertical circular tube. The

following assumptions were made:

- Uniform film thickness.
- Fully developed hydrodynamic condition.

The resulting two-dimensional momentum equation and boundary conditions in dimensionless form are given by:

$$\frac{d}{dR}\left[(s-R)^n E_m(R)\frac{dW(R)}{dR}\right] + (\beta+\varphi)(s-R)^n = 0 \tag{3.1a}$$

$$W(R) = 0 \text{ at } R = 0 \tag{3.1b}$$

$$\frac{dW(R)}{dR} = \bar{\tau}_i \text{ at } R = 0 \tag{3.1c}$$

where $n = 0$ for a plane wall, and $n = 1$ for a circular tube.

The solution for the local dimensionless heat transfer coefficient is:

$$h^*(Z) = \frac{Q_2}{\dfrac{Z}{\int_0^1 (s-R)^n W(R)dR} + \displaystyle\int_0^1 \frac{[1-H(R)]^2}{(s-R)^n E_h(R)}dR - 2\sum_{i=1}^{\infty}\frac{e^{-\mu_i^2 Z}}{N\mu_i^2}} \tag{3.2a}$$

where

$$h^* = \frac{h\nu^{2/3}}{kg^{1/3}} \tag{3.2b}$$

$$Q_2 = \frac{\nu^{2/3}\delta u_m}{Q_0 L\alpha s^{2n} g^{1/3}} \tag{3.2c}$$

$$Q_0 = q_0 S/K\Delta T \tag{3.2d}$$

A more useful equation for the prediction of the local dimensionless heat transfer coefficient h^* in terms of Reynolds and Prandtl numbers was

developed:

$$h^*(Z) = C_1 Re_L^{C_2} Pr_L^{C_3} + C_4 Z^{C_5} Re_L^{C_6} \tag{3.3}$$

where h^* is defined by Equation 3.2b, Re_L is the liquid Reynolds number and Pr_L is the liquid Prandtl number. Constants C_1 to C_6 are given in Table 3.1.

Equation 3.3 is valid for the turbulent region defined by Al-Najeem et al. as $1.8 \leq Pr_L \leq 5.5$ and $4,000 \leq Re_L \leq 20,000$. Unfortunately, Equation 3.3 sometimes predicts negative Nusselt numbers (i.e., when the Pr numbers is greater than 5.5), and it will not be used.

Table 3.1: Correlation constants for Equation 3.3 [4].

	$Z \leq 0.2$	$0.2 < Z \leq 1.0$
C_1	$7.69400 \cdot 10^{-02}$	$1.0000 \cdot 10^{-06}$
C_2	$2.00100 \cdot 10^{-01}$	1.0000
C_3	$3.47240 \cdot 10^{-01}$	1.6477
C_4	$-8.31145 \cdot 10^{-01}$	$1.0100 \cdot 10^{-04}$
C_5	$2.43700 \cdot 10^{-01}$	-1.8195
C_6	$1.39580 \cdot 10^{-02}$	$4.9515 \cdot 10^{-01}$

Ahmed and Kaparthi [3] used a copper tube of 3.015 cm of internal diameter in their study. Their experiments were carried out using water and aqueous solutions of glycerol over a wide range of Reynolds and Prandtl numbers ($3 \leq Re \leq 10250$; $3.6 \leq Pr \leq 950$). The correlation is:

$$Nu_L = 6.92 \times 10^{-3} Re_L^{0.345} Pr_L^{0.4} \tag{3.4}$$

Numrich [73] developed a simpler model for the heat transfer coefficient in a turbulent falling film. He used a modification of the Prandtl analogy to

formulate a new expression for the prediction of the heat transfer coefficient. His model shows good agreement with existing experimental data for Prandtl numbers up of 50. The equation for the prediction of the heat transfer coefficient is:

$$Nu_L = 0.003 Re_L^{0.44} Pr_L^{0.4} \tag{3.5}$$

where the Nusselt number is defined as:

$$Nu_L = \frac{h\nu^{2/3}}{kg^{1/3}} \tag{3.6}$$

This equation is the same as Equation 3.2b, the equation that Al-Najeem et al. [4] define as the dimensionless heat transfer coefficient (h^*). Equation 3.5 is valid for the turbulent region, which Numrich defines as $Pr_L \geq 3$ and $1,200 \leq Re_L \leq 40,000$.

Other authors present similar correlations to Equation 3.5. Krupiczka et al. [48] provide the following correlation:

$$\frac{Nu_L}{Nu_{Lz}} = 1 + C(B_0 \cdot Ka^{1/11})^{1.6} \tag{3.7a}$$

$$\text{where for } B_0 \cdot Ka^{1/11} > 10^{-6}, \quad C = 7.05 \times 10^7 \tag{3.7b}$$

$$\text{and for } B_0 \cdot Ka^{1/11} \leq 10^{-6}, \quad C = 0 \tag{3.7c}$$

where Nu_{Lz} is given by the correlation of Chun and Seban [18]:

$$Nu_{Lz} = 0.0038 Re_L^{0.4} Pr_L^{0.65} \tag{3.8}$$

and Ka is the Kapitza number, B_0 is the boiling number, given by:

$$Ka = \frac{\mu^4 g}{\rho \sigma^3} \tag{3.9}$$

$$B_0 = \frac{\dot{q}}{m \Delta H} \tag{3.10}$$

If the flow regime is in the laminar region, Chun and Seban propose the following correlation:

$$Nu_L = 0.821 Re^{-0.22} \text{ if } Re < Re_c \tag{3.11}$$

where $Re_c = 5900 Pr^{-1.06}$

3.1.2 Wiped Film Evaporators

Heat transfer has been widely studied in wiped film evaporators for a wide range of applications and for different types of evaporators.

Skelland [87] developed one of the earliest correlations for a scraped-film Votator (horizontal evaporator). He used different systems for the experiments: glycerol, water, and two similar glyceride oils in four different Votators. His correlated equation is:

$$h_p = 4.9 \frac{k}{D_t} \left(\frac{D_t u \rho}{\mu} \right)^{0.57} \left(\frac{C_p \mu}{k} \right)^{0.47} \left(\frac{D_t N}{u} \right)^{0.17} \left(\frac{D_t}{L} \right)^{0.37} \tag{3.12}$$

The thermal performance of a heat exchanger is characterized by a heat transfer coefficient, particularly the inside film heat transfer coefficient, since in the majority of applications of WFE, the latter represents the limiting thermal resistance [56].

Maingonnat and Corrieu [56] present a discussion of the methods for calculating the heat transfer coefficient that have been used by several authors for scraped film heat exchangers. There are two theoretical methods (two-step and three-step mechanisms) as well as an empirical approach.

The film heat transfer coefficient can be determined experimentally. The measurement of flow rates of the two fluids and their temperatures at the inlet and outlet of the WFE will make it possible to calculate the overall heat transfer coefficient (U_{ov}). Once U_{ov} is determined using the expression

$$U_{ov} = \frac{Q}{A_{ln}\Delta T} \tag{3.13}$$

where A_{ln} is the logarithmic mean of the inside and outside surface areas of the wall:

$$A_{ln} = \frac{A_e - A_i}{ln\left(\frac{A_e}{A_i}\right)} \tag{3.14}$$

If the two fluids are considered to be in plug flow, the temperature difference is the logarithmic mean of the differences between the fluids at the entry and exit of the WFE. Figure 3.1 shows all the resistances present in a WFE. The three heat transfer coefficients (HTCs) involved in the calculation are:

- External HTC between heating fluid and the exchange surface (h_o).
- HTC of the heat exchange surface (λ_{wall}).
- Internal HTC between the process fluid and heat transfer surface (h_p).

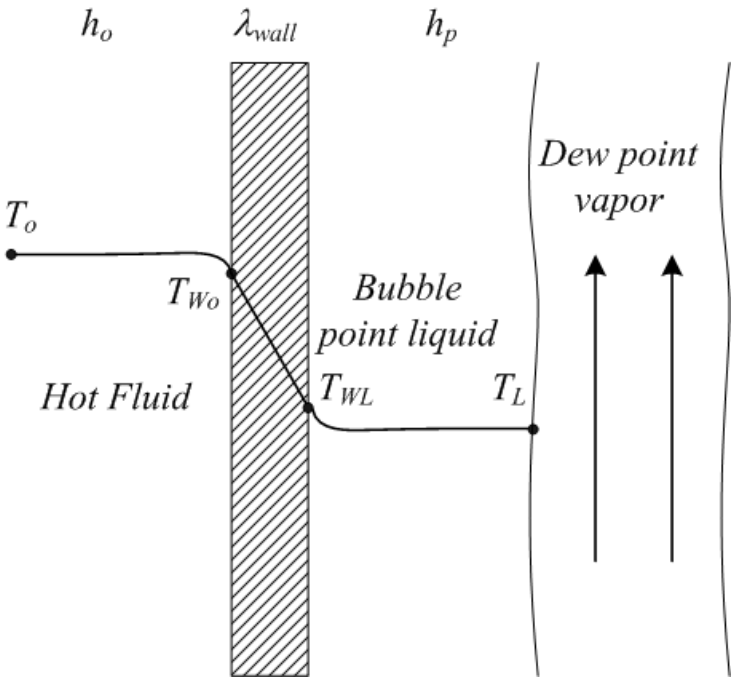

Figure 3.1: Heat transfer coefficient resistances in a wiped film evaporator

The expression for the calculation of h_p is:

$$\frac{1}{h_p} = \frac{1}{U_{ov}} - \frac{1}{\lambda_{wall}} - \frac{1}{h_o} \tag{3.15}$$

where λ_{wall} is the ratio $\frac{k_{wall}}{\delta_{wall}}$ (thermal conductivity divided by the thickness of the wall).

The value of h_o can be determined either experimentally or using a suitable correlation. When steam is used as the heating medium, h_o can be calculated with the equation for film condensation on vertical tubes or vertical

walls [9, 59]:

$$h_o = \frac{4}{3}\left(\frac{k_s^3 \rho_s^2 g}{3\mu_s \Gamma}\right)^{1/3} \tag{3.16}$$

where Γ is the rate of steam (mass flow) per unit length (kg/m).

When a different hot fluid is used, the correlation presented by McAdams [60] can be used if the flow is laminar (i.e., $Re \leq 2,000$):

$$\frac{h_o D}{\lambda} = \frac{2}{\pi}\frac{wC_p}{\lambda L}\frac{1-8\psi(n_1)}{1+8\psi(n_1)} \tag{3.17}$$

$$\psi(n_1) = 0.10238e^{-14.627n_1} + 0.01220e^{-89.22n_1} + 0.00237e^{-212n_1} + \ldots \tag{3.18}$$

$$n_1 = \frac{\pi\lambda L}{4wC_p} \tag{3.19}$$

For the transition region ($2,000 < Re < 10,000$), Knudsen et al. [43], recommend the equation from Hausen:

$$\frac{h_o D}{\lambda} = 0.116\left(Re^{2/3} - 125\right) Pr^{1/3}\left[1 + \left(\frac{D}{L}\right)^{2/3}\right]\left(\frac{\mu}{\mu_w}\right)^{0.14} \tag{3.20}$$

For turbulent flow ($Re > 10,000$), Knudsen et al. [43] suggest the use of the Dittus-Boelter equation:

$$\frac{h_o D}{\lambda} = 0.0243 Re^{0.8} Pr^{0.4}\left(\frac{\mu}{\mu_w}\right)^{0.14} \tag{3.21}$$

where the physical properties are evaluated at the bulk temperature.

3.1.2.1 Heat Transfer Models Based on Mechanism

There are two models for the mechanisms of heat transfer: two-step and three-step.

Two-step mechanism. This mechanism was discussed by Kool [47] and is described here:

First: Heat penetrates by molecular conduction into a thin layer of the product which is assumed to be immobile along the wall during the interval between two consecutive scrappings of the wall. The quantity of heat exchanged is calculated from Fourier's law for transient conduction.

Second: Heat is transmitted by convection. The layer of product is removed from the wall by the blade and is mixed radially with the rest of the product; simultaneously, "fresh" product is brought into contact with the wall.

The expression found by Kool is:

$$h_p = \frac{1.24}{h_{wo}^{0.03}} \left(\lambda_L C_{pL} \rho_L N N_b\right)^{0.515} \tag{3.22}$$

with the following condition:

$$2 < h_{wo} \frac{1}{\left(\lambda_L C_{pL} \rho_L N N_b\right)^{0.5}} < 30 \tag{3.23}$$

where h_{wo} is the HTC between the heating fluid and the internal surface of the heat exchange wall.

Latinen [51] and Harriot [34] presented a different expression for the internal HTC. They calculated the quantity of heat transferred between the internal surface of the exchange wall and the product. The simple expression is:

$$h_p = 2\sqrt{\frac{\lambda_L \rho C_{pL} N N_b}{\pi}} \tag{3.24}$$

Equation 3.24 can be written as a function of dimensionless numbers as [51]:

$$h_p = 2\sqrt{\frac{Re_N Pr N_b}{\pi}} \tag{3.25}$$

Three-step mechanism. Trommelen, Beek, and van de Westelaken [93] added an extra step between one and two. They noted that the perfect radial mixing assumed cannot truly occur. Between the stage of molecular conduction and radial heat convection, they describe an intermediate step where the film of product which has been separated from the wall and is on the blade, and only partly gives up its heat to the stream of product flowing between the blade and the rotor. The product which is brought back into contact with the wall after leaving the blade is at a higher temperature than would have occurred if the radial mixing had been perfect. Trommelen et al. [93] found that this partial equalization reduced the heat transfer by a factor less than unity. Their expression for the internal HTC is:

$$Nu = 1.13\varphi\sqrt{Re_N Pr N_b} \tag{3.26}$$

where

$$\varphi = 2.0 Pr^{-0.25} \text{ for } Re_N > Re_{cr} \tag{3.27}$$

and Re_{cr} is around 280.

Heat transfer in vertical wiped film evaporators was studied by other authors. Bott and Romero [11] and Bott and Sheikh [14] present correlations for the prediction of the inside HTC.

Bott and Romero used three experimental scraped surface falling film vertical heat exchanger tubes: 15.24 cm, 30.48 cm, and 60.96 cm by 2.54 cm diameter. Water and water-glycerol mixtures were used as test systems. Flowrates of 455 kg/hr-m (based on wetted perimeter) to 1,592 kg/hr-m were used, while the rate of rotation was varied from 370 to 1,600 rpm. The number of blades mounted on the shaft were also varied: from 1 to 4. They made 108 runs using pure water (83 runs) and water-glycerol (13 runs for 28.5%, 4 runs for 33.85%, 4 runs for 43.53%, and 4 runs for 61.85% in water content). They correlated their experimental data as a function of dimensionless parameters:

$$Nu = 0.018 Re_f^{0.46} Re_N^{0.6} Pr^{0.87} \left(\frac{D}{L}\right)^{0.48} N_b^{0.24} \tag{3.28}$$

This correlation was accurate within ±20% in the range of the variables studied.

Bott and Sheikh [14] later ran a similar series of experiments at atmospheric pressure using an evaporator with 3.81 cm ID by 45.72 cm long tubes, with the same experimental systems but with more data points for water-glycerol mixtures (45%, 62%, and 85% in glycerol content). For the 45% glycerol system, different numbers of blades were used: 2, 6, and 8. The range of flowrate was from 258 kg/hr-m to 1,482 kg/hr-m. The speed of rotation was varied from 600 to 1400 rpm.

Their results for boiling water show that h_p is weakly dependent on the film Reynolds number (Re_f), even at low speed rotations (6000 rpm). An increase in the rotational speed N increases the HTC. The effect of N was

varied as $h_p \propto N^{0.37}$. Kirschbaum and Dieter [42] found the dependence to be $h_p \propto N^{0.33}$, in close agreement to the value found by Bott and Sheikh [14]. Their correlation is:

$$Nu = 0.65 Re_f^{0.25} Re_N^{0.43} Pr^{0.30} N_b^{0.33} \tag{3.29}$$

Azzory and Bott [7] studied the heat transfer coefficient in a vertical scraped surface evaporator. They found an expression similar to the one found by Trommelen et al. [93], Equation 3.26. Azzory and Bott also found that the HTC is independent of the flow rate above a certain rotational speed (180 rpm). Their correlation is:

$$h_p = \frac{8.74}{f} \sqrt{C_p \rho k N N_b} \tag{3.30}$$

where f is defined as

$$f = \frac{Pr}{500} + 3.5 \tag{3.31}$$

3.2 Mass Transfer

Whereas heat transfer in falling and wiped film evaporators has been thoroughly studied, the same cannot be said for mass transfer. There are several papers for falling film evaporators Hoke and Chen [35], Krupiczka et al. [49], Nielsen et al. [71], Salvagnini and Taqueda [79], Spedding and Jones [89], Yüksel and Schlünder [99, 100]. Just a few authors present studies for wiped film evaporators: McKenna [62], Miyashita and Hoffman [64], Miyashita et al. [65].

3.2.1 Falling Film Evaporators

Hoke and Chen [35] present the formulation of the governing equations and boundary conditions that describe the evaporation of two-component liquid films falling down a vertical surface. They solve the equations numerically.

Spedding and Jones [89] present mass and heat transfer data for humidification of air in a glass wetted-wall column with a 4.04 cm inside diameter and the length varied between 0.72 m and 3.54 m. Their only correlation is for the thickness of the theoretical film, given by:

$$\frac{d_i}{\delta} = 0.016 \pm 0.002 Re_f^{0.83 \pm 0.015} \tag{3.32}$$

Gilliland and Sherwood [27] studied gas-side mass transfer in a wetted-wall column, evaporating water and eight different organic liquids into air flowing over a wetted surface with an inside diameter of 2.54 cm and 117 cm long. Air was flowing cocurrent and countercurrent at different pressures (0.1 to 3 atm). Their correlation is:

$$\frac{k_c d}{D_{AB}} \frac{p_{BM}}{P} = 0.023 \left(\frac{du\rho}{\mu} \right)^{0.83} \left(\frac{\mu}{\rho D} \right)^{0.44} \tag{3.33}$$

This correlation is valid for gas-phase Reynolds numbers from 2,000 to 27,000.

Nielsen et al. [71] measured the rate of gas and liquid phase mass transport in a pilot scale wetted-wall column with an internal diameter of 3.26 cm and a length of 5 m, developing empirical correlations for the physical liquid

and gas phase mass transfer coefficient. The correlations are:

$$Sh_L = 0.01613 Re_G^{0.664} Re_L^{0.426} Sc_L^{0.5} \tag{3.34}$$

$$Sh_G = 0.00031 Re_G^{1.05} Re_L^{0.207} Sc_G^{0.5} \tag{3.35}$$

Which are valid for gas-phase Reynolds numbers from 7,500 to 18,300 and liquid-phase Reynolds numbers from 4,000 to 12,000.

Yih and Chen [98] used a a long wetted-wall column for absorption of CO_2 and O_2 into falling water films on the outside of a stainless steel pipe 2.72 cm OD and 183 cm absorption length. The studied range of Reynolds number was from 129 to 10500. Their correlations is:

$$k_L^{FFE} = a \cdot Re_f^b \cdot Sc_L^{1/2} \frac{D \rho_L^{2/3} g^{1/3}}{\mu_L^{2/3}} \tag{3.36}$$

where:

$a = 1.099 \times 10^{-2}$, $b = 0.3955$ for $49 < Re_f < 300$

$a = 2.995 \times 10^{-2}$, $b = 0.2134$ for $300 < Re_f < 1600$

$a = 9.777 \times 10^{-4}$, $b = 0.6804$ for $1600 < Re_f < 10500$

These values of a, b, and Re_f were correlated by Yih and Chen [98] using their experimental values as well as the data from 10 other authors.

3.2.2 Wiped Film Evaporators

Only a few papers analyze mass transfer in wiped film evaporators. McKenna [62] developed a model for the devolatilization (removal of monomer) of polymer solutions in a WFE. He considered fluid transport (velocity profile)

and mass transfer in the evaporator, but not heat transfer. Another conclusion was that the capacity of the WFE increases as the rotational speed increases, up to a limit where the gain in mass transfer is overshadowed by the increase in power consumption.

Miyashita and Hoffman [64] used an electrochemical technique, described by Mizushina [66], in a scraped-film heat exchanger with a 78.7 mm ID by 457.2 mm in length and two blades. They measured mass transfer coefficients, later converted to heat transfer coefficients using the heat and mass transfer analogy. The expression is:

$$Nu = 0.15 \left(Re_N Pr\right)^{0.5} Re_f^a \tag{3.37}$$

where

$$a = \frac{1 - 3.74 \times 10^{-2} N}{9} \tag{3.38}$$

Later, Miyashita et al. [65] extended the range of the Schmidt (Prandtl) number, using the same technique as in the earlier paper [64]. Their correlation for mass transfer is:

$$Sh = 1.53 Re_f^{0.51} Sc^{0.33} \left(\frac{d_i}{d_i - d_s}\right)^{0.44} \tag{3.39}$$

with the following restrictions

$$1320 < Sc < 5810 \tag{3.40}$$

$$2.94 < \frac{d_i}{d_i - d_s} < 7.2 \tag{3.41}$$

Transforming the equation for heat transfer:

$$Nu = 1.53 Re_f^{0.51} Pr^{0.33} \left(\frac{d_i}{d_i - d_s} \right)^{0.44} \tag{3.42}$$

which has the same restrictions for the Schmidt number in Equation 3.39.

3.3 Flash Calculation

As mentioned in Chapter 2, a wiped film evaporator can also be modeled as an isothermal flash or series of isothermal flashes [31]. Figure 3.2 shows the variables involved in the calculation of a single-stage two-phase flash at a specified pressure (P) and temperature (T). The equations to solve are [84]:

$$f(\psi) = \sum_i^n \frac{z_i(1 - K_i)}{1 + \psi(K_i - 1)} \tag{3.43}$$

$$x_i = \frac{z_i}{1 + \psi(K_i - 1)} \tag{3.44}$$

$$y_i = \frac{K_i z_i}{1 + \psi(K_i - 1)} \tag{3.45}$$

$$Q = V H_V + L h_L - F H_F \tag{3.46}$$

where $\psi = \dfrac{V}{F}$ is the fraction of generated vapor with respect to the feed, K_i is the equilibrium constant calculated as $K_i = \dfrac{\gamma_i P^{vap}}{P}$, and H_V, h_L, H_F are the enthalpies of the vapor, liquid, and feed respectively.

When solving the previous equations, information about the heat duty, vapor and liquid flowrates, and the distribution of components in the liquid and vapor are obtained. From these equations, it can be seen that several parameters for the wiped film evaporator (i.e., number of blades, rotational

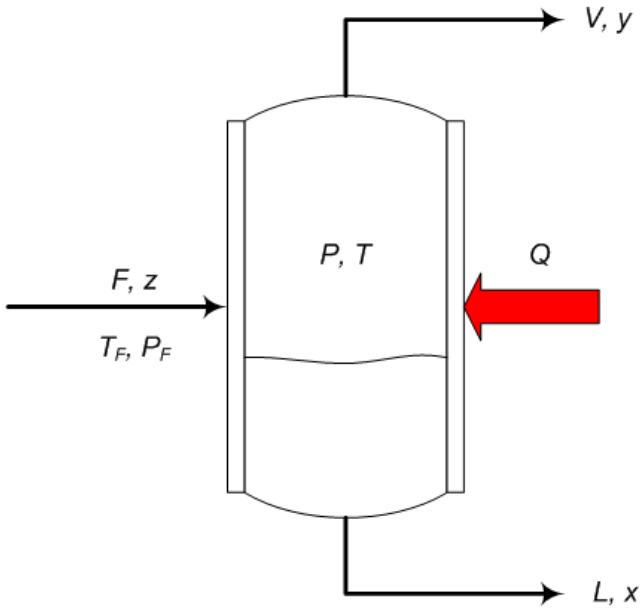

Figure 3.2: Two phase flash model for a wiped film evaporator.

speed) are not included. In order to take into account their impact, a more rigorous model is needed. This model is presented in Chapter 4.

Chapter 4

Model Development

4.1 Heat and Mass Transfer Model for Vertical Wiped Film Evaporators

A vertical wiped film evaporator (WFE) is a countercurrent vapor-liquid contactor (see Figure 4.1) and is closely related to the well-studied falling film evaporator (FFE). Relative to the FFE, the WFE has the ability to renew the vapor-liquid surface through mechanical wiping. The wiping action may also induce waves (i.e., turbulence) that enhance the mass transfer area. Thus the efficiency of a WFE should be greater than that of a FFE.

Unfortunately, as noted in Chapter 3, little information has been published on the subject of wiped film evaporation. In particular, very little fundamental experimental WFE mass transfer data, and no WFE mass transfer models, have been reported. In contrast, the literature contains a significant amount of data and fundamental models on heat transfer within wiped film evaporators. Likewise, numerous studies on falling film evaporators have been reported.

4.2 Proposed Design Model

The relationship between the overall heat transfer coefficient U_{ov} and the individual heat transfer resistances (Figure 4.2) is derived from heat bal-

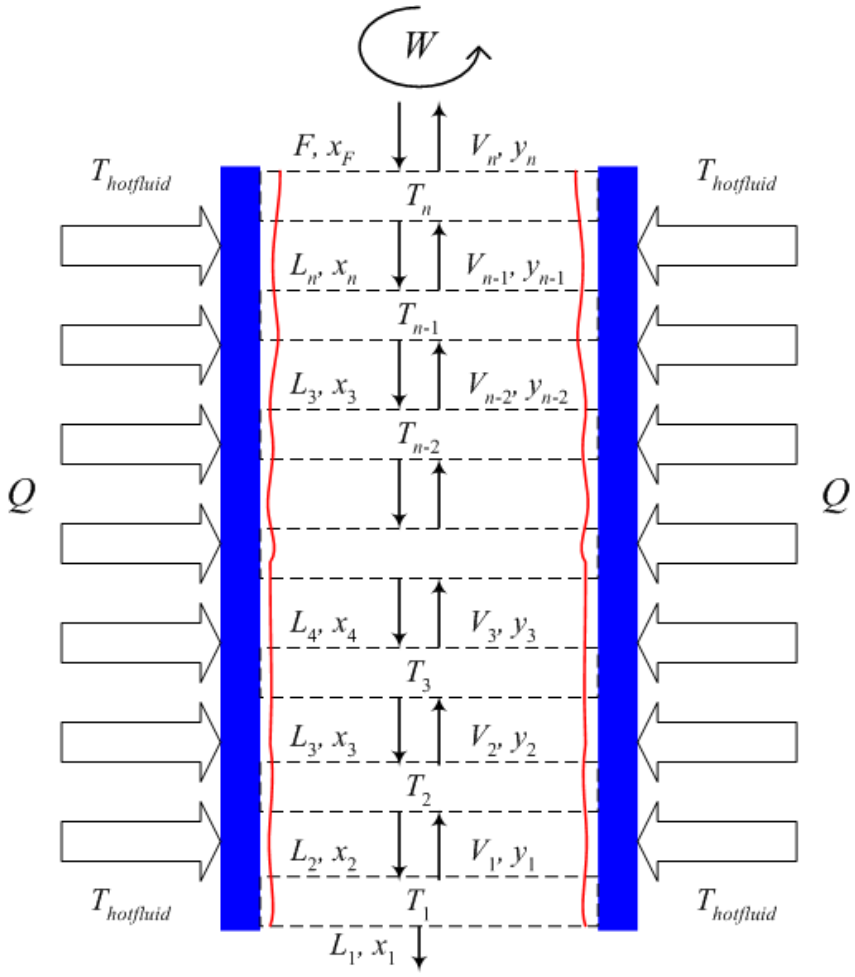

Figure 4.1: Sketch of a Vertical Wiped Film Evaporator. The heat added to the system generates evaporation at the surface of the falling liquid and the rotating blades generate turbulence at the surface.

ances around the heating medium, the wall, and liquid.

$$q = h_o \left(T_o - T_{Wo}\right)$$
$$q = \frac{\delta_{wall}}{k_{wall}} \left(T_{Wo} - T_{WL}\right)$$
$$q = h_p \left(T_{WL} - T_L\right)$$

where q is the heat flux per unit area at each interface.

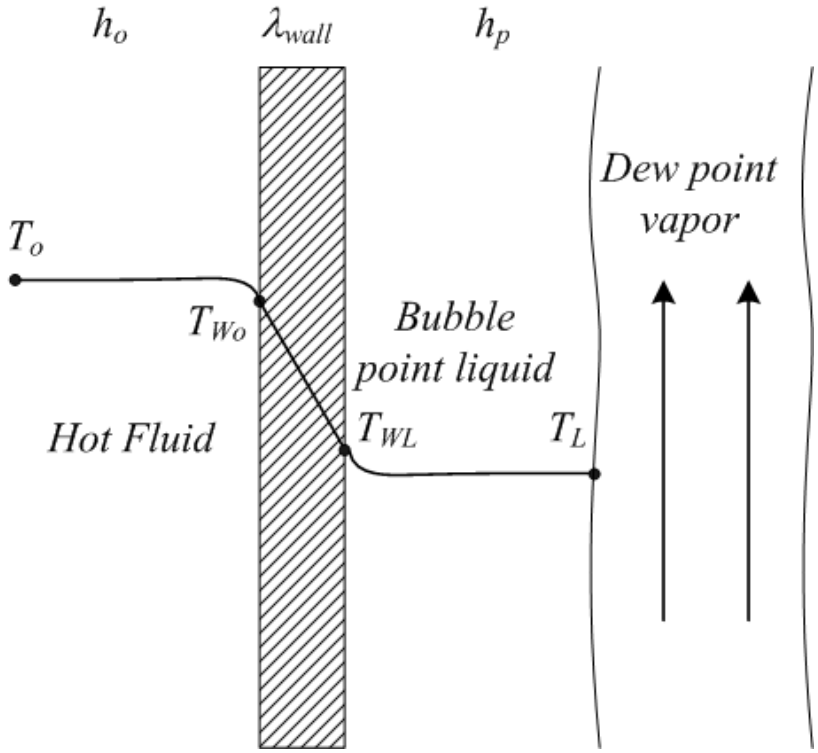

Figure 4.2: Heat transfer resistances in a wiped film evaporator.

The previous equations state that the amount of heat transferred from the medium to the wall must be equal to the amount passing through the wall

and the amount transferred to the liquid. Equating all the heat terms and solving for q, the following expression for the overall heat transfer coefficient results:

$$\frac{1}{U_{ov}} = \frac{1}{h_o} + \frac{\delta_{wall}}{k_{wall}} + \frac{1}{h_p} \tag{4.1}$$

where U_{ov} is the overall heat transfer coefficient (W/m^2-K), h_o is the heat transfer coefficient for the heating medium (W/m^2-K), k_{wall} is the thermal resistance of the wall (W/m-K), δ_{wall} is the thickness of the wall (m), and h_p is the heat transfer coefficient for the liquid film (W/m^2-K).

As mentioned in Chapter 3, the process side HTC, h_p, can be calculated from experimental data. Equation 3.13 is used to calculate U_{ov}, then Equation 3.16 (steam) or 3.17 (other fluid) is used to calculate the hot fluid side HTC, h_o. The wall resistance is readily calculated using the thermal conductivity of the wall as well as it thickness. Finally, Equation 3.15 is used to calculate the process side HTC, h_p.

The present research was focused on modeling h_p (the heat transfer coefficient inside the WFE) and k_L^{WFE} (mass transfer coefficient inside the WFE). Preliminary studies had indicated that h_p in WFEs is a function of the number of blades, the speed of rotation, and the physical properties of the system (i.e., viscosity, thermal conductivity, etc.)

Considering the WFE as a stage-wise unit (i.e., dividing the length into small "stages", see Figure 4.1) and assuming plug flow (i.e., no backmixing), the performance of a WFE can be predicted using the equations below.

Applying mass balance, energy balance, and equilibrium considerations to the stage, the amount of generated vapor (ΔV, kg/s) can be calculated.

Mass balance:

$$L_n + V_n = F + V_{n-1} \tag{4.2}$$

$$L_n x_n + V_n y_n = F x_F + V_{n-1} y_{n-1} \tag{4.3}$$

Equilibrium:

$$K_n = \frac{y_n}{x_n} \tag{4.4}$$

Energy balance:

$$\begin{aligned} L_n h_{L,n} + V_n h_{V,n} &= F h_{L,F} + V_{n-1} h_{V,n-1} + q \\ V_{n-1} &= \frac{L_n h_{L,n} + V_n h_{V,n} - F h_{L,F} - q}{h_{V,n-1}} \end{aligned} \tag{4.5}$$

where $q = U_{ov} A \Delta T_{lm}$

The possibility of correcting correlations for falling film evaporator and applying them to wiped film evaporators was analyzed, and was found that it can be used. Additional experimental data were needed in order to verify this approach.

The initial approach was to use an enhancement factor β, defined as the ratio of the WFE heat or mass transfer coefficient to the FFE heat or mass transfer coefficient. Since little information has been reported on WFE mass

transfer, the enhancement factor was initially evaluated based on reported WFE and FFE heat transfer information.

The heat transfer enhancement factor, β_h, is defined as follows:

$$\beta_h = \frac{h_p^{WFE}}{h_p^{FFE}} \tag{4.6}$$

where h_p^{WFE} is the heat transfer coefficient for the WFE, and h_p^{FFE} is for the FFE.

Since wiped film evaporation is generally used in liquid phase controlled systems (e.g. viscous mixtures), our models are based on the prediction of liquid phase coefficients for heat and mass transfer. From the published models for the prediction of the heat transfer coefficient for WFE, two were selected: Bott and Romero [11], Bott and Sheikh [14]. These correlations are of the form:

$$Nu = f\left(Re_f^{a_1} Re_N^{a_2} Pr^{a_3} N_b^{a_4} (D/L)^{a_5} N_b^{a_6}\right) \tag{4.7}$$

where the parameters a_1 to a_6 were correlated using heat transfer coefficient data. N_b is the number of blades, D is the diameter, L is the length, N is the rotational speed, and the dimensionless numbers are:

$Nu = \dfrac{h_p D}{k}$ is the Nusselt number

$Re_f = \dfrac{4F}{\pi D \mu}$ is the film Reynolds number

$Re_N = \dfrac{D^2 N \rho}{\mu}$ is the rotational Reynolds number

$Pr = \dfrac{C_p \mu}{k}$ is the Prandtl number.

The expression for each particular WFE heat transfer coefficient model is as follows.

Bott and Romero [11]:

$$Nu = 0.018 Re_f^{0.46} Re_N^{0.6} Pr_L^{0.87} \left(D/L\right)^{0.48} N_b^{0.24} \tag{4.8}$$

Bott and Sheikh [14]:

$$Nu = 0.65 Re_f^{0.25} Re_N^{0.43} Pr_L^{0.3} N_b^{0.33} \tag{4.9}$$

Two FFE heat transfer coefficient models for different Nu values were used: Ahmed and Kaparthi [3], and Numrich [73]. The expression for each model is as follows.

Ahmed and Kaparthi [3]

$$Nu = 6.92 \times 10^{-3} Re_f^{0.345} Pr_L^{0.4} \tag{4.10}$$

Numrich [73]

$$Nu = 0.003 Re_f^{0.44} Pr_L^{0.4} \tag{4.11}$$

In these models, the Nusselt number is defined as:

$$Nu = \frac{h\delta_L}{k} \tag{4.12}$$

where $\delta_L = \left(\frac{\mu^2}{\rho^2 g}\right)^{1/3}$ = the characteristic length.

Figures 4.3, 4.4, and 4.5 show the variation of the heat transfer enhancement factor (β_h) with the film Reynolds number, rotational Reynolds

number, and Prandtl number using the four possible combinations of models for the heat transfer coefficient (two for WFEs and two for FFEs).

Figure 4.3 shows that as the film Reynolds number (Re) increases, the heat transfer enhancement factor decreases, having a high value at low Re. This means that the performance of the equipment will be expected not to change significantly after a critical Re is achieved. For this particular case, the value is around 2000.

Figure 4.4 shows that as the rotational Reynolds number (Re_N) increases, the heat transfer enhancement factor increases. This is due to the increase in the speed of rotation, which also increases the HTC for the wiped film evaporator. This is consistent with what other authors have found [14, 42, 64]. There is a region of the rotational speed where the evaporator is operated typically, highlighted by the square box.

Figure 4.5 presents a sharp increase in the enhancement factor as a function of the Prandtl number (Pr). This is because as the Prandtl number increases, usually the viscosity increases, and the HTC in a falling film evaporator will decrease, while in a wiped film evaporator, the HTC will increase.

4.3 Comparison of Preliminary Model With Experimental Data

The set of Equations 4.1-4.3 and 4.5 can be applied to a given set of experimental data. Considering the starting point as the top of the unit (see

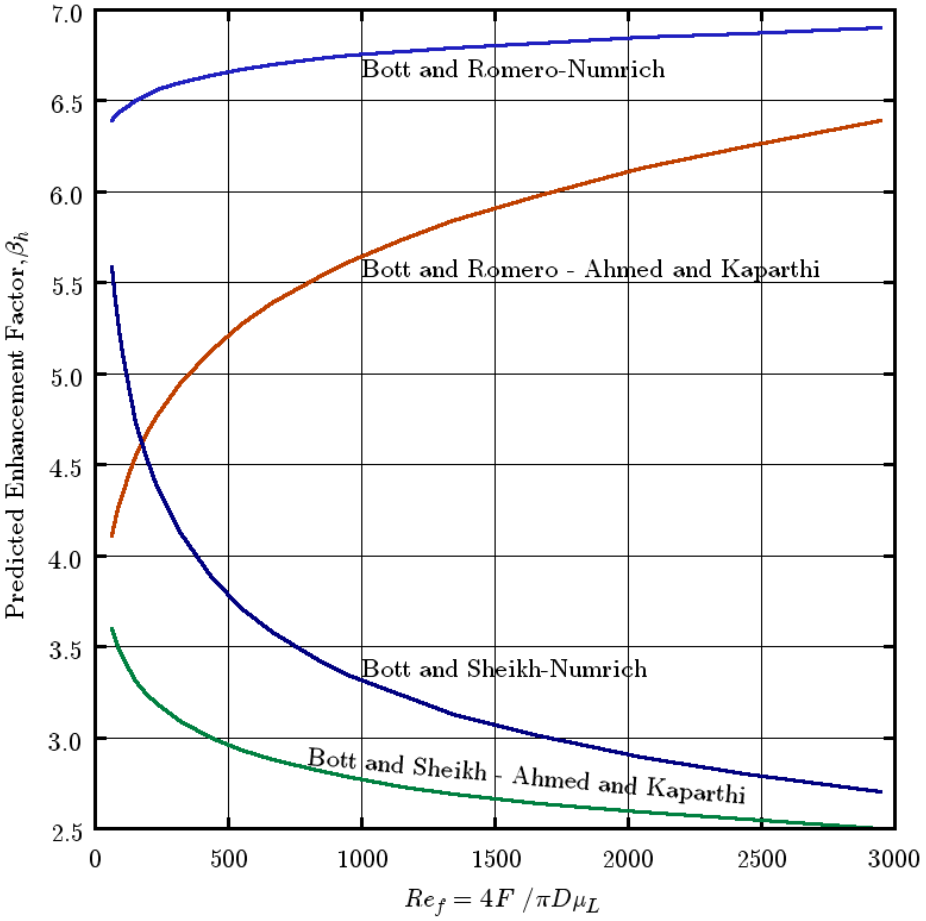

Figure 4.3: Heat Transfer Enhancement Factor (β_h) as a function of the film Reynolds number. D=0.21 m; L=1.521 m; μ_L=4.73 cP; k_L=0.468 W/m-K; ρ_L=1222 kg/m^3; C_{pL}=4179.6 J/kg-K; N=13.66 1/s; N_b=2; Re_N=constant; Pr=constant.

Figure 4.1, Page 52), from the mass and energy balance:

$$Fx_F + V_{n-1}y_{n-1} = L_n x_n + V_n y_n$$

$$F + V_{n-1} = L_n + V_n$$

$$Fh_{L,F} + V_{n-1}h_{V,n-1} + q = L_n h_{L,n} + V_n h_{V,n}$$

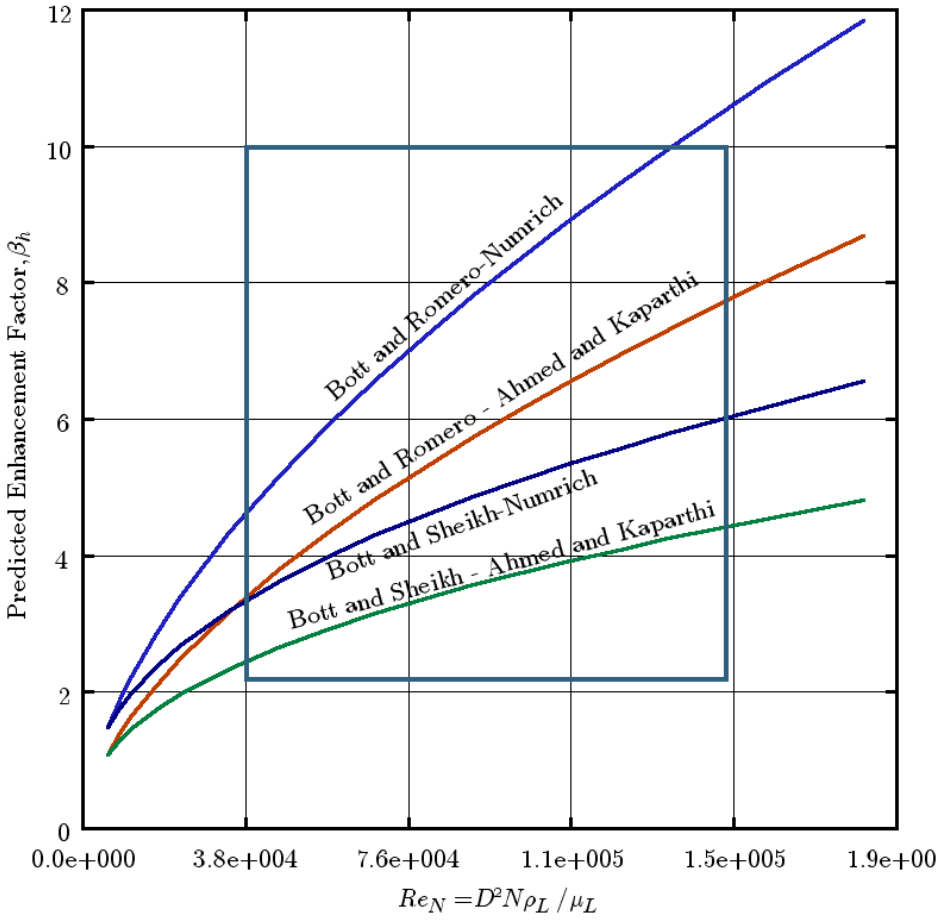

Figure 4.4: Heat Transfer Enhancement Factor (β_h) as a function of the rotational Reynolds number. D=0.21 m; L=1.521 m; μ_L=4.73 cP; k_L=0.468 W/m-K; ρ_L=1222 kg/m^3; C_{pL}=4179.6 J/kg-K; N_b=2; Re_f=constant; Pr=constant.

From the experimental data, the feed flowrate (F) and its composition (x_F), the amount of vapor (V_n) and its composition (y_n), and the amount of heat transferred are known, and the temperature of the stage can be calculated (using the bubble point equation). Knowing the temperature, the amount of

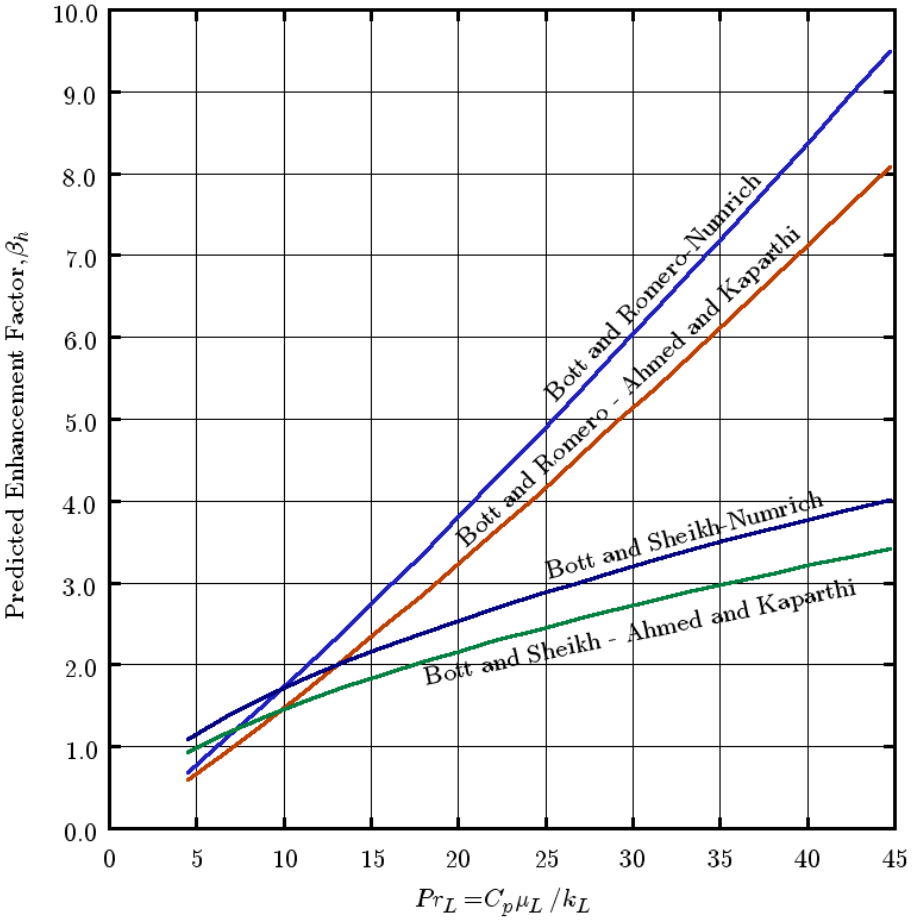

Figure 4.5: Heat Transfer Enhancement Factor (β_h) as a function of the Prandtl number. D=0.21 m; L=1.521 m; k_L=0.468 W/m-K; ρ_L=1222 kg/m^3; C_{pL}=4179.6 J/kg-K; N_b=2; Re_f=constant; Re_N=constant.

vapor (V_{n-1}) and its composition (y_{n-1}) can be calculated. From this, the amount of liquid entering the next stage (L_n) and its composition (x_n) can be calculated. The same procedure can be applied until the last segment (i.e., bottom of the unit) is solved.

A set of experimental data from Frank and Lutcha [25] for sugar solutions is available and shown in Table 4.1. These data were originally used to find an expression for the film thickness but we can use them in order to verify the proposed model. Figure 4.6 shows the results for the exit concentration of water, when the proposed approach is applied.

Figure 4.7 shows the variation of the liquid mass fraction of the more volatile component (water) from the top (i.e., the feed point) to the bottom of the WFE, while Figure 4.8 shows the variation of liquid and vapor flow rates.

As shown in Figures 4.9 and 4.10, the prediction of the process side heat transfer coefficient and the overall heat transfer coefficient using the model of Bott and Sheikh [14] is better than the prediction using Bott and Romero [11].

4.4 Simultaneous Heat and Mass Transfer

In this section, the simultaneous heat and mass transfer in wiped film evaporators will be analyzed [85]. Figure 4.11 shows a differential section of the WFE. The mass, components, and energy balances are as follows:

$$L_{in} + V_{in} = L_{out} + V_{out} \tag{4.13}$$

$$L_{in}x_{in} + V_{in}y_{in} = L_{out}x_{out} + V_{out}y_{out} \tag{4.14}$$

$$L_{in}h_{L,in} + V_{in}h_{V,in} + q_{in} = L_{out}h_{V,out} + V_{out}h_{V,out} \tag{4.15}$$

Overall, component, and energy balances on each stream for an element of contact area ΔA gives the differential conservation equations. The mass

Table 4.1: Set of experimental data from Frank and Lutcha [25]. D=0.21 m; L=1.521 m

N (1/s)	F (kg/s)	V_N (kg/s)	x_F (%)[a]	x_1 (%)	T_v (°C)	T_p (°C)	q (W/m^2)
13.66	0.1614	0.0354	96.49	94.77	60	105.0	82617.2
6.08	0.1624	0.0270	96.49	95.09	60	105.0	62658.2
6.08	0.1125	0.0239	96.49	95.21	60	105.0	56396.4
13.66	0.1135	0.0301	96.49	94.52	60	105.0	71068.4
13.66	0.0654	0.0274	96.49	88.39	60	105.0	64995.4
6.00	0.0655	0.0191	96.49	93.48	60	105.0	45325.7
13.66	0.1739	0.0294	93.84	90.23	60	105.0	68459.0
6.03	0.1655	0.0242	93.60	91.02	59	105.0	55248.4
6.03	0.1149	0.0212	93.60	89.69	59	105.0	48412.5
13.66	0.1203	0.0265	93.60	87.65	60	105.0	61597.5
13.66	0.1147	0.0262	93.60	86.24	60	105.0	60852.4
13.66	0.1645	0.0373	98.36	97.78	60	105.0	86264.1
6.00	0.1588	0.0297	98.36	97.88	60	105.0	68500.1
6.00	0.1204	0.0274	98.49	97.84	60	105.0	64298.3
13.66	0.1202	0.0330	98.49	97.60	60	105.0	77864.4
13.66	0.0610	0.0294	98.59	96.60	60	105.0	69035.3
6.00	0.0705	0.0251	98.59	97.21	60	105.0	58481.1
6.00	0.1142	0.0283	98.59	97.82	60	105.0	65594.6
13.66	0.1192	0.0353	98.59	97.67	60	105.0	82058.2
6.66	0.1426	0.0152	90.81	87.26	60	95.0	31963.4
6.66	0.1110	0.0150	90.81	85.71	60	95.5	32317.4
13.33	0.1515	0.0172	90.81	86.73	60	95.0	38117.6
13.33	0.1008	0.0150	90.81	84.95	60	95.0	33445.6
6.66	0.1881	0.0161	90.73	88.08	60	95.0	32816.8
6.66	0.0970	0.0122	88.73	81.77	60	95.0	27691.2
6.66	0.1446	0.0107	88.73	85.55	60	95.0	23250.0
13.33	0.1945	0.0158	88.54	84.80	60	96.0	34660.8
13.33	0.1526	0.0139	88.54	84.12	60	95.0	30754.7

[a]mol concentration of water

balance on an element of the gas stream shown in Figure 4.11 gives:

$$V|_A + N_1 \Delta A = V|_{A+\Delta A} \tag{4.16}$$

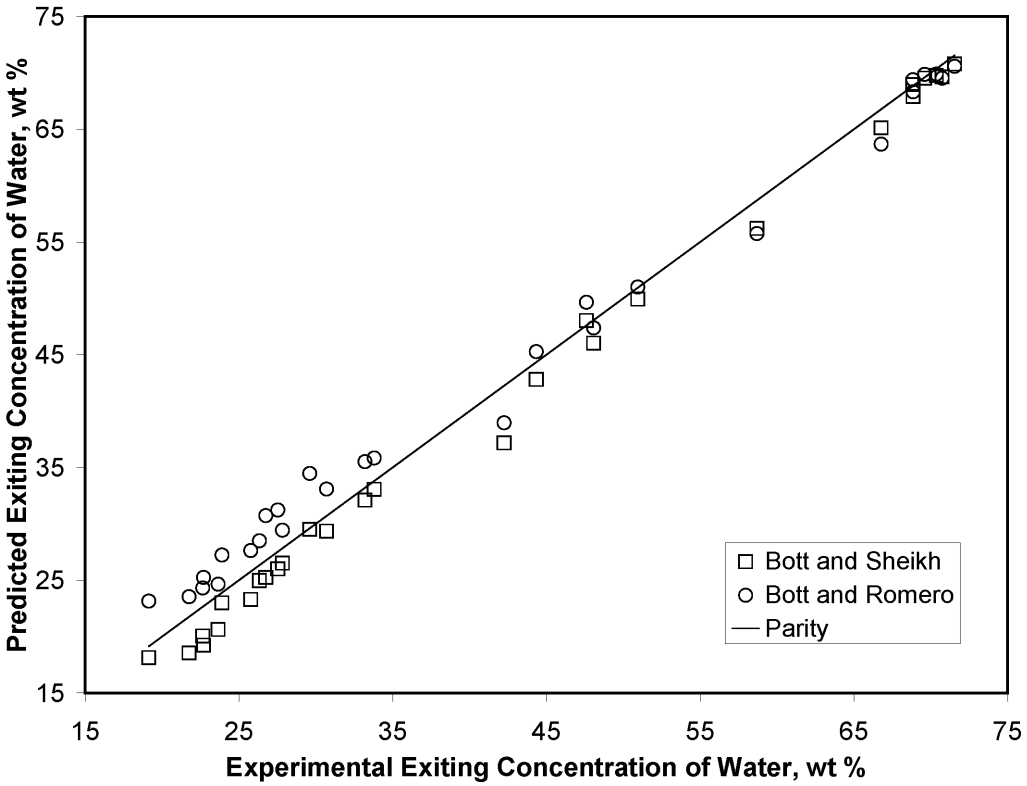

Figure 4.6: Predicted vs. Experimental weight fraction for concentrate using data from Frank and Lutcha [25]. $D = 0.21$ m, $L = 1.521$ m, $\delta_{wall} = 0.004$ m. No mass transfer considered.

Dividing by ΔA and letting $\Delta A \to 0$,

$$\frac{dV}{dA} = N_1 \tag{4.17}$$

And similarly for the liquid

$$\frac{dL}{dA} = N_1 \tag{4.18}$$

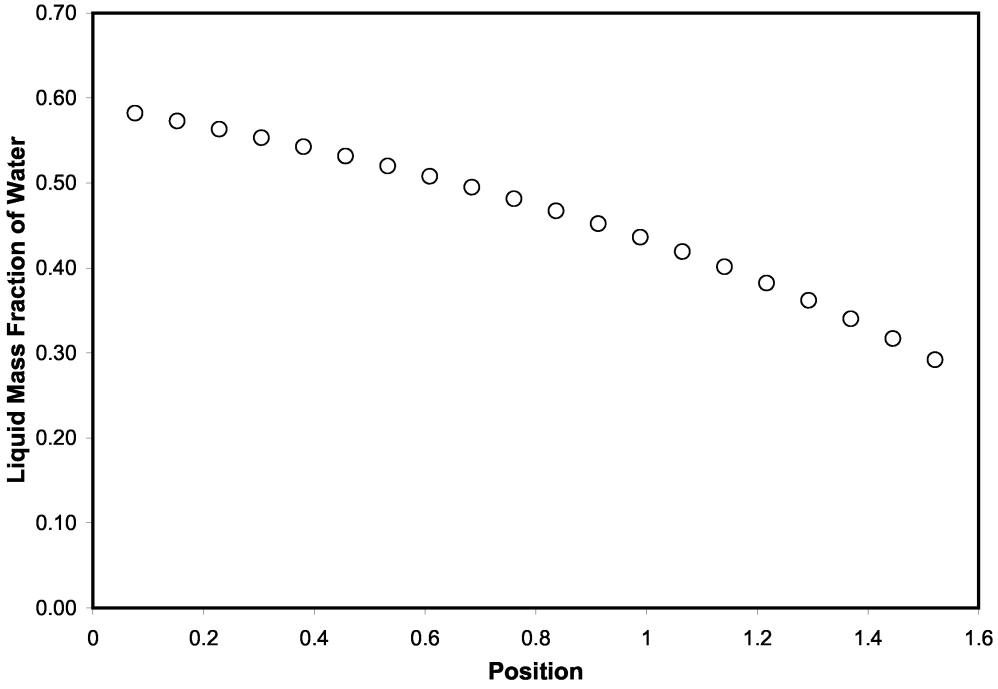

Figure 4.7: Liquid mass fraction variation along the WFE. 0=Top of the Unit.

The energy balance on the gas stream is:

$$q\Delta A = Vh_V|_{A+\Delta A} - Vh_V|_A - N_1 h_1 \Delta A \tag{4.19}$$

where the last term on the right-hand side accounts for the enthalpy added to the control volume by the evaporated component. Dividing by ΔA and letting $\Delta A \to 0$:

$$\frac{d(Vh_V)}{dA} = q + N_1 h_1 \tag{4.20}$$

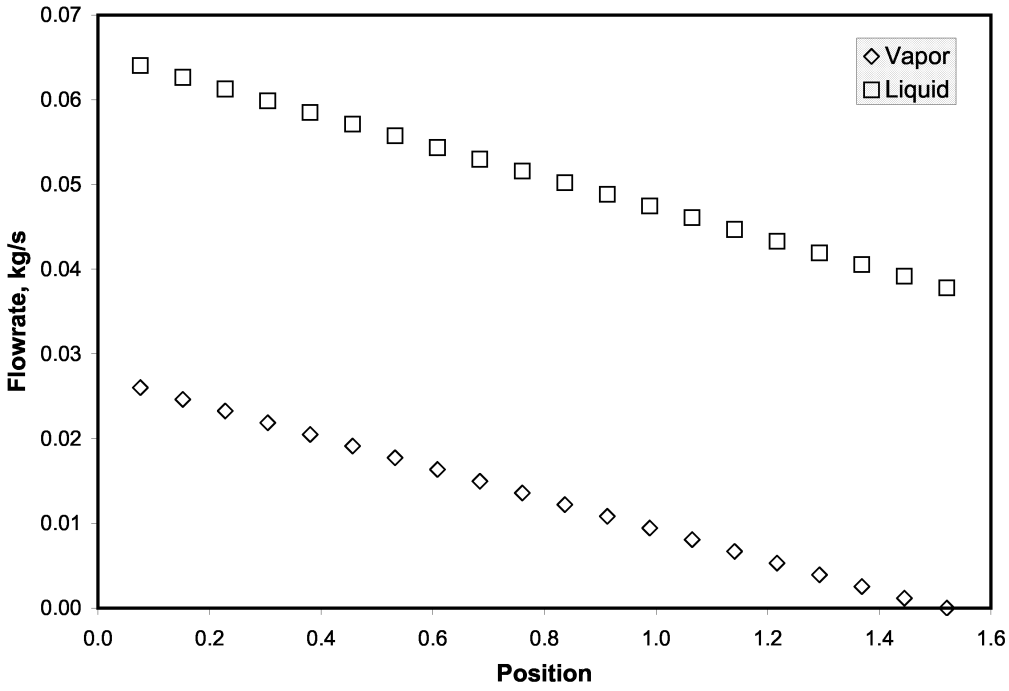

Figure 4.8: Liquid and vapor flowrate variation along the WFE. 0=Top of the Unit.

And similarly for the liquid

$$\frac{d(Lh_L)}{dA} = q + N_1 h_1 \tag{4.21}$$

From Figure 4.11 the total flux of enthalpy into a differential element of thickness dy is made up of two parts:

- The conduction heat flux: $-k\dfrac{dt}{dy}$
- The flux of enthalpy due to diffusion: $N_A C_{pA}(t - t_0) + N_B C_{pB}(t - t_0)$

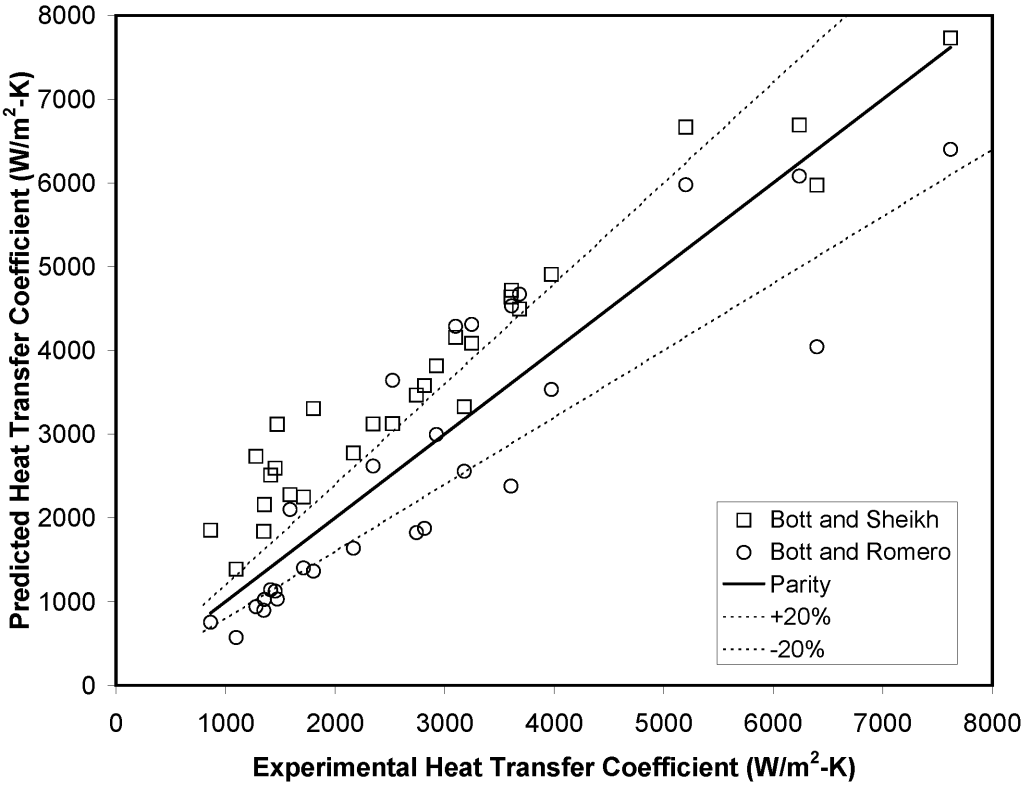

Figure 4.9: Predicted vs. Experimental heat transfer coefficient using data from Frank and Lutcha [25]. $D = 0.21$ m; $L = 1.521$ m, $\delta_{wall} = 0.004$ m. No mass transfer considered.

where t_0 is a standard state temperature.

Evaluating these quantities for the flux entering and leaving the differential element and setting their difference equal to zero, the temperature distribution in the film must satisfy

$$k\frac{d^2t}{dy^2} - (N_A C_{pA} + N_B C_{pB})\frac{dt}{dy} = 0 \tag{4.22}$$

The solution that satisfies the conditions that $t = t_1$ at the interface (wall)

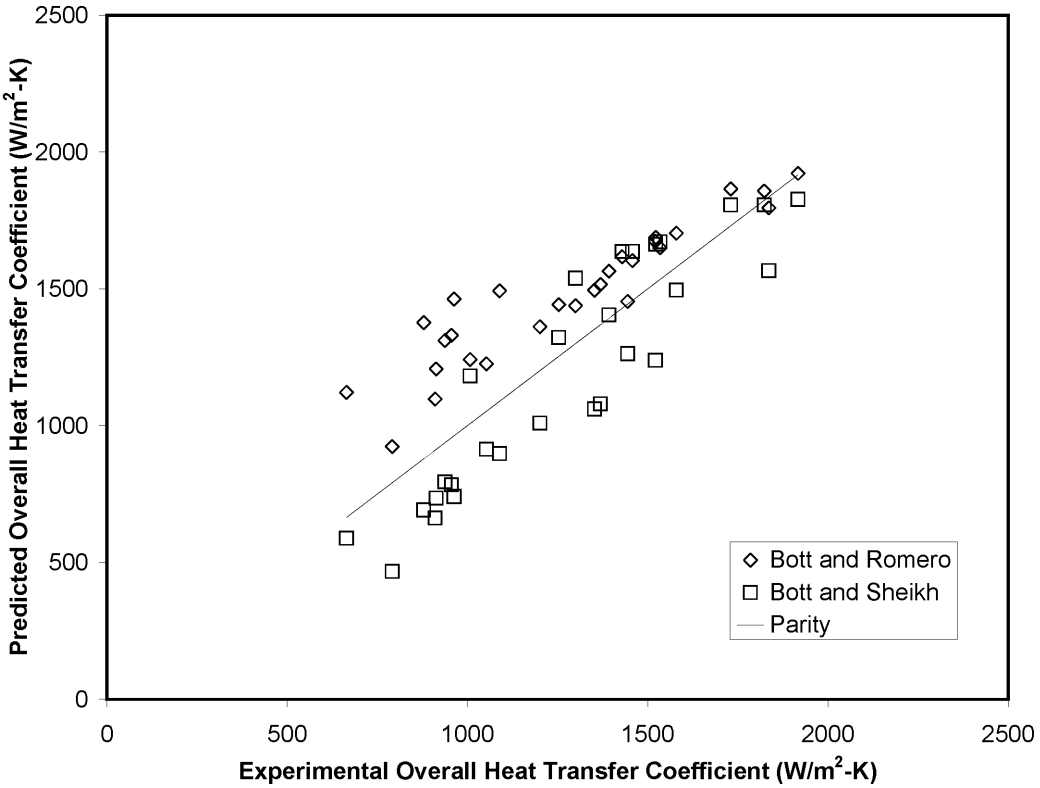

Figure 4.10: Predicted vs. Experimental overall heat transfer coefficient using data from Frank and Lutcha [25]. $D = 0.21$ m; $L = 1.521$ m, $\delta_{wall} = 0.004$ m. No mass transfer considered.

where $y = 0$ and $t = t_2$ at the bulk-gas boundary of the film is

$$t(y) = t_1 + (t_2 - t_1)\frac{\exp\left(C_0\frac{y}{\delta}\right) - 1}{\exp\left(C_0\right) - 1} \tag{4.23}$$

where C_0 is the Ackerman correction factor defined by

$$C_0 = \left(N_A C_{pA} + N_B C_{pB}\right)/h_p \tag{4.24}$$

and $h_p = k/\delta$. The conduction flux of heat at the interface is found from this

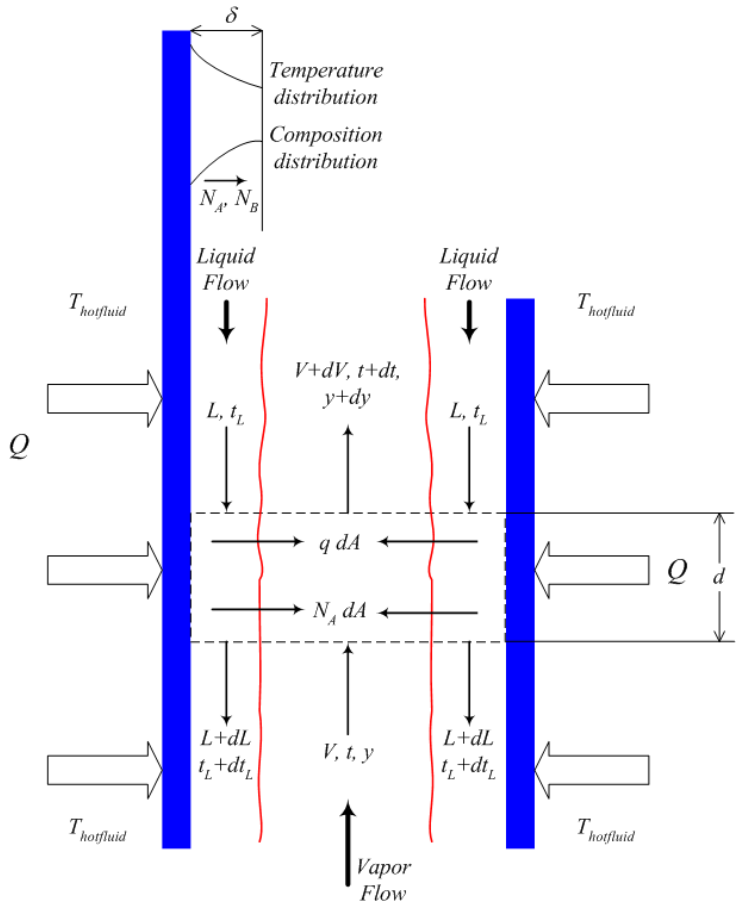

Figure 4.11: Differential section of a Wiped Film Evaporator.

result as

$$q_c = -k \left. \frac{dt}{dy} \right|_0 = h_p(t_1 - t_2) \frac{C_0}{\exp(C_0) - 1} \tag{4.25}$$

And the total heat flux is equal to the heat flux by conduction and the flux of enthalpy due to diffusion:

$$q = h_p(t - t_i) \frac{C_0}{1 - \exp(-C_0)} \tag{4.26}$$

The interface temperature lies between T_p, the temperature of the heating medium and the bulk temperature of the liquid, and it can be found from an energy balance at the interface.

$$\begin{aligned} U(T_p - t_i) &= q + \lambda_A N_A \\ &= h_p(t - t_i)\frac{C_0}{1 - \exp(-C_0)} + \lambda_A N_A \end{aligned} \tag{4.27}$$

The equation to calculate the rate of mass transfer is:

$$N_A = k_L^{WFE}\rho_L(x_A - x_A^*) \tag{4.28}$$

where x_A is the mole fraction of the component in the liquid and x_A^* is the equilibrium concentration.

In order to predict k_L^{WFE}, the value of β_h is needed (see Equation 4.6), and the heat and mass transfer analogy is assumed. The FFE mass transfer model of Yih and Chen [98] (based on its fit with previous data) is used to predict the mass transfer coefficient for FFE:

$$k_L^{FFE} = \left(a \cdot Re_f^b \cdot Sc_L^{1/2}\right)\left(\frac{D\rho_L^{2/3}g^{1/3}}{\mu_L^{2/3}}\right) \tag{3.36}$$

The equation to predict the mass transfer coefficient, assuming heat and mass transfer analogy is:

$$k_L^{WFE} = \beta_h \cdot k_L^{FFE} \tag{4.29}$$

When the heat and mass transfer effects are considered (i.e., using the previous equations) the results are shown in Figures 4.12 to 4.14. It can

be seen that the prediction of the exiting concentration of water and heat transfer coefficient improves over the calculated values when no mass transfer is considered.

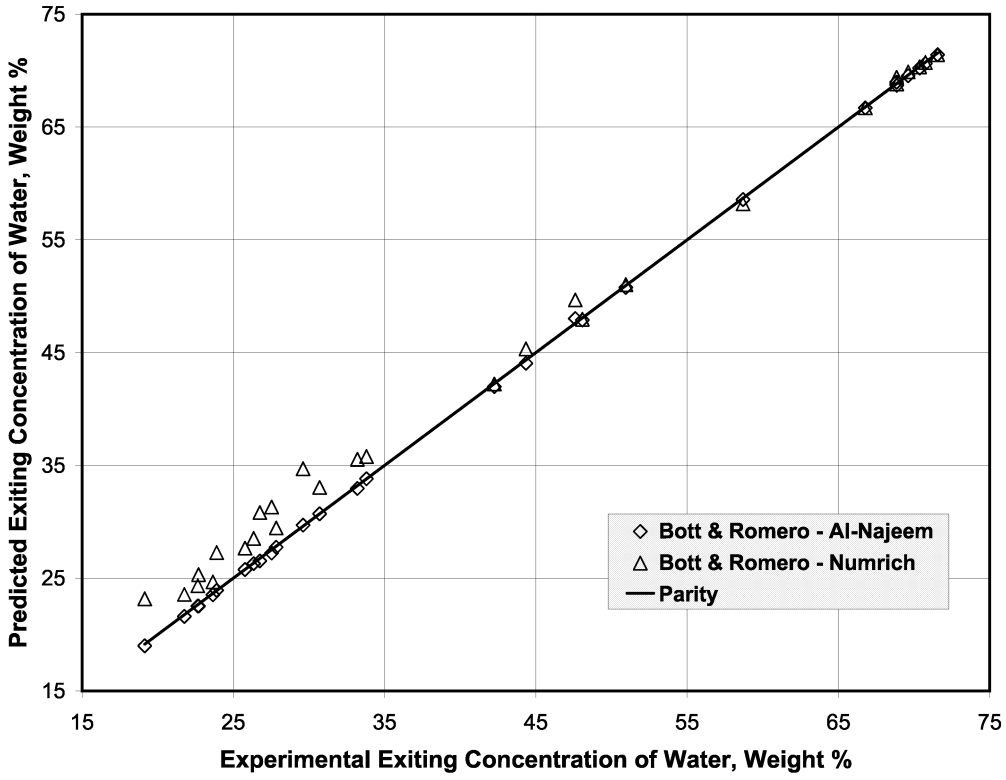

Figure 4.12: Predicted vs. Experimental weight fraction for concentrate using data from Frank and Lutcha [25]. $D = 0.21$ m, $L = 1.521$ m, $\delta_{wall} = 0.004$ m. Mass transfer considered.

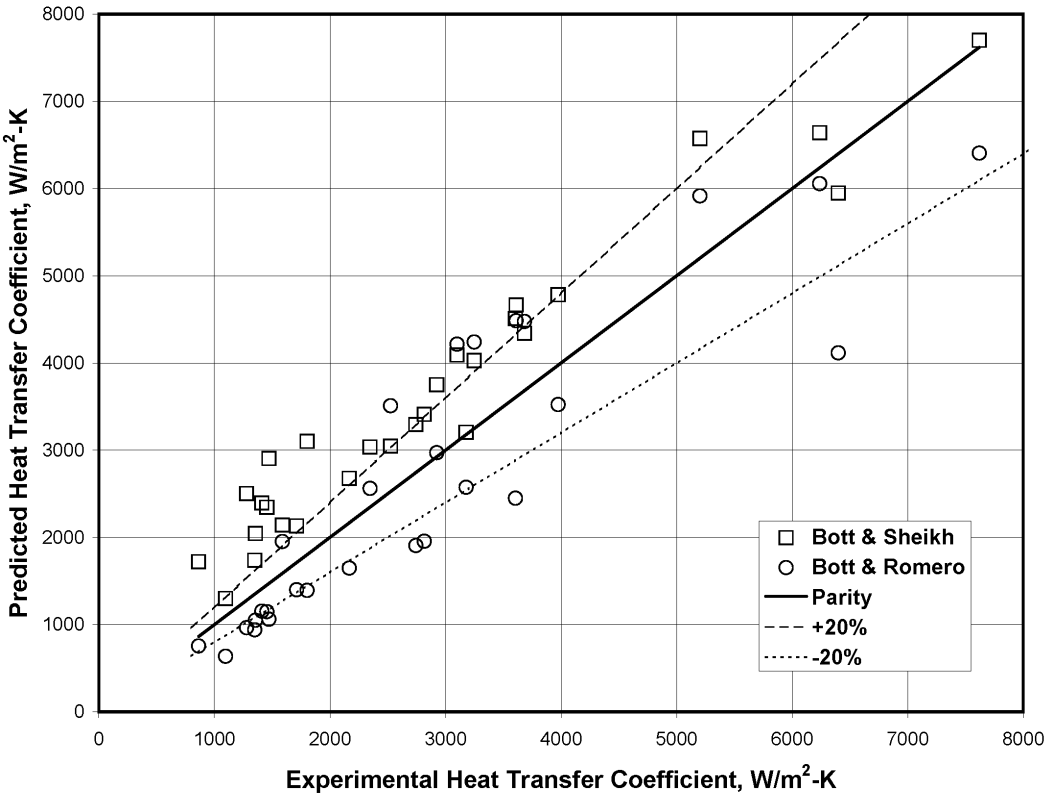

Figure 4.13: Predicted vs. Experimental heat transfer coefficient using data from Frank and Lutcha [25]. $D = 0.21$ m; $L = 1.521$ m, $\delta_{wall} = 0.004$ m. Mass transfer considered.

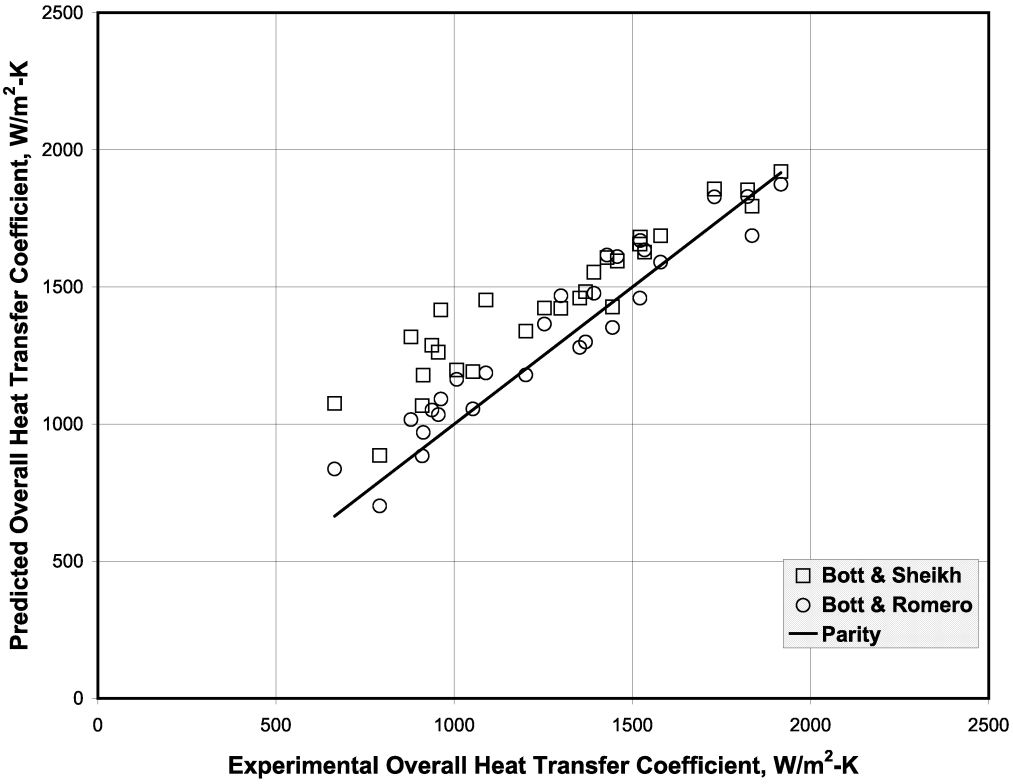

Figure 4.14: Predicted vs. Experimental overall heat transfer coefficient using data from Frank and Lutcha [25]. $D = 0.21$ m; $L = 1.521$ m, $\delta_{wall} = 0.004$ m. Mass transfer considered.

Chapter 5

Experimental System and Procedures

The experimental work for the present research was conducted at the Blair, Nebraska, plant of Cargill Inc. An excellent wiped film evaporator (WFE) was made available to the Separations Research Program (SRP) as part of Cargill's membership support. Cargill Inc. facilitated their staff for helping in the operation of the equipment.

5.1 Test Systems

The following test systems were selected: water-glycerol, water-sucrose, and water-ethylene glycol. These systems cover a wide range of physical properties.

5.1.1 Water/Glycerol

Earlier papers on WFE heat transfer used the system water/glycerol. The system is well-characterized and its physical properties do not change dramatically over a small change in concentration and/or pressure (P) and/or temperature (T) (except for viscosity which shows a moderate variation). Table 5.1 gives physical properties for different water-glycerol mixtures. The

system has been used for heat transfer studies by other authors in wiped film evaporators [1, 11, 14]. Their results will be utilized for comparison with data obtained in this work.

Table 5.1: Physical properties for several mixtures of glycerol and water at 5.3 kPa and 36 °C), calculated using AspenPlus version 11.1 with the UNIQUAC thermodynamics option. Composition is based on wt% glycerol. The balance is water.

Property	**38 wt%**	**58 wt%**	**75 wt%**
MW, kg/kmol	25.95	33.77	45.41
ρ_L, kg/m^3	1,092.2	1,158.8	1,214.8
μ_L, cP	1.42	2.56	5.49
λ_L, W/m-K	0.407	0.358	0.328
$C_{p,L}$, J/kg-K	3,258.3	2,920.2	2,644.2
$D_L \times 10^{12}$, m^2/s	9.55	11.60	17.24
σ, N/m	0.0697	0.0684	0.0663
h_L, kJ/kg	-12,530.6	-10,800.0	-9,327.5

Expressions for the calculation of physical properties (i.e., viscosity, density, thermal conductivity) exist in the literature. The DIPPR equations [22] will be used to predict physical properties as follows:

$$\rho_L = \frac{0.92382}{0.24386^{\left[1+\left(1-\frac{T}{850}\right)^{0.22114}\right]}} \tag{5.1}$$

$$C_{p,L} = 78468 + 480.71T \tag{5.2}$$

$$\lambda_L = 0.258 + 1.1340 \times 10^{-4}T \tag{5.3}$$

$$\mu_L = \exp\left(120.62 - \frac{15959}{T} - 17.118\ln T + \frac{2.693 \times 10^6}{T^2}\right) \tag{5.4}$$

$$P^{vap} = \exp\left(99.986 - \frac{13808}{T} - 10.088\ln T + 3.5712 \times 10^{-19}T^6\right) \tag{5.5}$$

where T is the temperature in K, ρ_L is the liquid density in kmol/m^3, $C_{p,L}$ is the liquid heat capacity in J/kmol-K, λ_L is the liquid thermal conductivity in W/m-K, and μ_L is the viscosity of the liquid in Pa-s.

5.1.2 Water/Sucrose

Another good experimental system for heat and mass transfer analysis is water/sucrose solutions. Table 5.2 shows physical properties for this system at different weight fractions of sucrose. Although it has a wide variation in viscosity and other properties (e.g., density) several authors have used the system (e.g., Frank and Lutcha [25] for characteristic dimension and Stankiewicz and Rao [91] for heat transfer analysis) and analytical expressions for the calculation of physical properties of the mixture are available in the literature.

Table 5.2: Physical properties for several mixtures of sucrose and water at 40 °C. Composition is based on wt% sucrose. The balance is water.

Property	**36 wt%**	**48 wt%**	**55 wt%**	**65 wt%**
MW, kg/kmol	27.34	33.04	37.61	46.89
ρ, kg/m^3	1,147.6	1,209.1	1,247.6	1,305.9
μ, cP	2.56	5.91	11.51	43.84
λ, W/m-K	0.507	0.466	0.442	0.408
C_p, J/kg-K	3,391.2	3,126.0	2,971.3	2,750.3
$D \cdot 10^{12}$, m^2/s	$3.18{\cdot}10^{-10}$	$2.08{\cdot}10^{-10}$	$1.52{\cdot}10^{-10}$	$0.85{\cdot}10^{-10}$
σ, N/m	0.0720	0.0733	0.0742	0.0757
h, kJ/kg	133.5	122.2	115.6	106.1
P^{vap}, kPa	30.54	30.52	30.50	30.46

For instance, the viscosity of the solution can be calculated with the

following equation [58]:

$$\begin{aligned}\mu_L &= 10^{\left(22.46\eta - 0.114 + \phi\left(1.1 + 43.1\eta^{1.25}\right)\right)} \\ \phi &= \frac{30 - t}{91 + t} \\ \eta &= \frac{wt}{19 - 18wt}\end{aligned} \tag{5.6}$$

where wt is the mass fraction of sucrose in the solution, t is the temperature in °C, and μ_L is the viscosity of the solution in mPa·s. One advantage of this system is that the vapor phase will consist of water only which leads to more reliable methods for the prediction of physical properties.

The expressions for other properties of water in sucrose, are as follows [58]. For density of the sucrose solution, ρ_L in kg/m^3:

$$\begin{aligned}\rho_L = &\frac{\sum_{i=1}^{6} A_i t^{i-1}}{1 + 1.6887 \cdot 10^{-2} t} + \sum_{i=1}^{6} B_i wt^i \\ &+ \left[\sum_{i=1}^{5} C_i wt^i\right]\left(\frac{t-20}{100}\right) + \left[\sum_{i=1}^{4} D_i wt^i\right]\left(\frac{t-20}{100}\right)^2 \\ &+ \left[\sum_{i=1}^{3} E_i wt^i\right]\left(\frac{t-20}{100}\right)^3 + \left[\sum_{i=1}^{2} F_i wt^i\right]\left(\frac{t-20}{100}\right)^4\end{aligned} \tag{5.7}$$

For the heat capacity, $C_{p,L}$ in J/kg-K:

$$C_{p,L} = 4186.8 - 2510wt + 7.5wt \cdot t \tag{5.8}$$

For the thermal conductivity, λ_L in W/m-K:

$$\begin{aligned}\lambda_L = &(5.466 \cdot 10^{-6} t^2 - 1.176 \cdot 10^{-3} t - 0.3024)wt + \\ &0.563 + 1.976 \cdot 10^{-3} t - 7.847 \cdot 10^{-6} t^2\end{aligned} \tag{5.9}$$

Table 5.3: Constants for Equation 5.7 [58].

i	A	B	C	D	E	F
1	999.8395	385.1761	-46.2720	59.7712	-47.2207	18.3184
2	16.9526	135.3705	-7.1720	7.2491	-21.6977	12.3081
3	$7.9905 \cdot 10^{-3}$	40.9299	1.1597	12.3630	27.6301	
4	$4.6242 \cdot 10^{-5}$	-3.9646	5.1126	-35.4791		
5	$1.0585 \cdot 10^{-7}$	13.4853	17.5254			
6	$2.8103 \cdot 10^{-10}$	-17.2890				

For the diffusion coefficient, D_L in m^2/s:

$$D_L = \exp\left[-21.2176 - 14.9109\left(1 + 18.9998\frac{1-wt}{wt}\right)^{-0.75}\right] \times \exp\left[\frac{17144.76 + 1046.46e^{2.89439wt}}{8.31432}\left(\frac{1}{298.15} - \frac{1}{273.15+t}\right)\right] \quad (5.10)$$

The thermodynamic equilibrium is predicted using the equations from Peres and Macedo [75]. The equations are:

$$\ln(\gamma_i) = \ln\left(\gamma_i^C\right) + \ln\left(\gamma_i^R\right) \quad (5.11)$$

where:

$$\ln\left(\gamma_i^C\right) = \ln\left(\frac{\varphi_i}{x_i}\right) + 1 - \frac{\varphi_i}{x_i} \quad (5.12)$$

$$\ln\left(\gamma_i^R\right) = 5q_i\left(1 - \ln\left(\theta_i + \theta_j\tau_{ji}\right) - \frac{\tau_{ji}}{\theta_i + \theta_j\tau_{ji}} - \frac{\tau_{ij}\theta_j}{\theta_i\tau_{ij} + \theta_j}\right) \quad (5.13)$$

$$\varphi_i = \frac{x_i r_i^{2/3}}{\sum_j x_j r_j^{2/3}} \quad (5.14)$$

$$\theta_i = \frac{q_i x_i}{\sum_i q_i x_i} \quad (5.15)$$

$$a_{ij} = a_{ij,0} + a_{ij,1}(T - T_0) + a_{ij,2}\left(T \ln \frac{T_0}{T} + T - T_0\right) \tag{5.16}$$

$$\tau_{ij} = \exp\left(-\frac{a_{ij}}{T}\right) \tag{5.17}$$

5.1.3 Water/Ethylene Glycol

The system water/ethylene glycol has also been used for heat transfer studies in falling film evaporators by Leuthner et al. [53] and Hameed and Muhammed [32]. Table 5.4 shows the physical properties for a mixture of 75% weight fraction of ethylene glycol in water. While the test system does not have a large variation in physical properties, some properties are in the low end of the range, thermal conductivity and heat capacity are lower for this system compared to the other two. Thus the three systems provide a wide range of variation in physical properties.

Table 5.4: Physical properties for 75 wt% ethylene glycol and water at 4.3 kPa and 42 °C, calculated using AspenPlus version 11.1 with the UNIQUAC thermodynamic option.

Property	**75 wt%**
MW, kg/kmol	38.52
ρ, kg/m^3	1,074.2
μ, cP	2.20
λ, W/m-K	0.288
C_p, J/kg-K	2,805.2
$D \cdot 10^{10}$, m^2/s	3.518
σ, N/m	0.0587
h, kJ/kg	-9,467.8
P^{vap}, kPa	8.25

As for the water/glycerol system, the DIPPR equations [22] will be

used to predict physical properties as follows:

$$\rho_L = \frac{1.315}{0.25125^{\left[1+\left(1-\frac{T}{720}\right)^{0.21868}\right]}} \tag{5.18}$$

$$C_{p,L} = 35540 + 436.78T - 0.18486T^2 \tag{5.19}$$

$$k_L = 0.088067 + 9.4712 \times 10^{-4}T - 1.3114 \times 10^{-6}T^2 \tag{5.20}$$

$$\mu_L = \exp\left(-20.515 + \frac{2468.5}{T} + 1.2435 \ln T + \frac{2.4998 \times 10^{12}}{T^5}\right) \tag{5.21}$$

$$P^{vap} = \exp\left(84.09 - \frac{10411}{T} - 8.1976 \ln T + 1.6536 \times 10^{-18}T^6\right) \tag{5.22}$$

where T is the temperature in K, ρ_L is the liquid density in kmol/m^3, $C_{p,L}$ is the liquid heat capacity in J/kmol-K, k_L is the liquid thermal conductivity in W/m-K, and μ_L is the viscosity of the liquid in Pa-s.

5.2 Experimental Setup

Figure 5.1 shows a schematic of a representative experimental installation, similar to the one used by Stankiewicz and Rao [91]. Liquid is pumped from the feed tank to the heat exchanger where it is preheated to the boiling temperature. The feed temperature is controlled to maintain a value within a specified variation (e.g., ±1 °C) using a temperature controller. The feed solution entering the WFE is spread with a distributor mounted on the shaft, providing complete circumferential coverage of the surface by the liquid. Evaporation takes place under vacuum in the vertical WFE. Vapors are separated from the concentrate in the glass separation chamber and condensed in tubular water coolers. Condensate is pumped out and collected for measurements.

Concentrated liquid is pumped out to a collecting tank. After volumetric measurements, condensate and concentrate are remixed and the solution is returned to the feed tank.

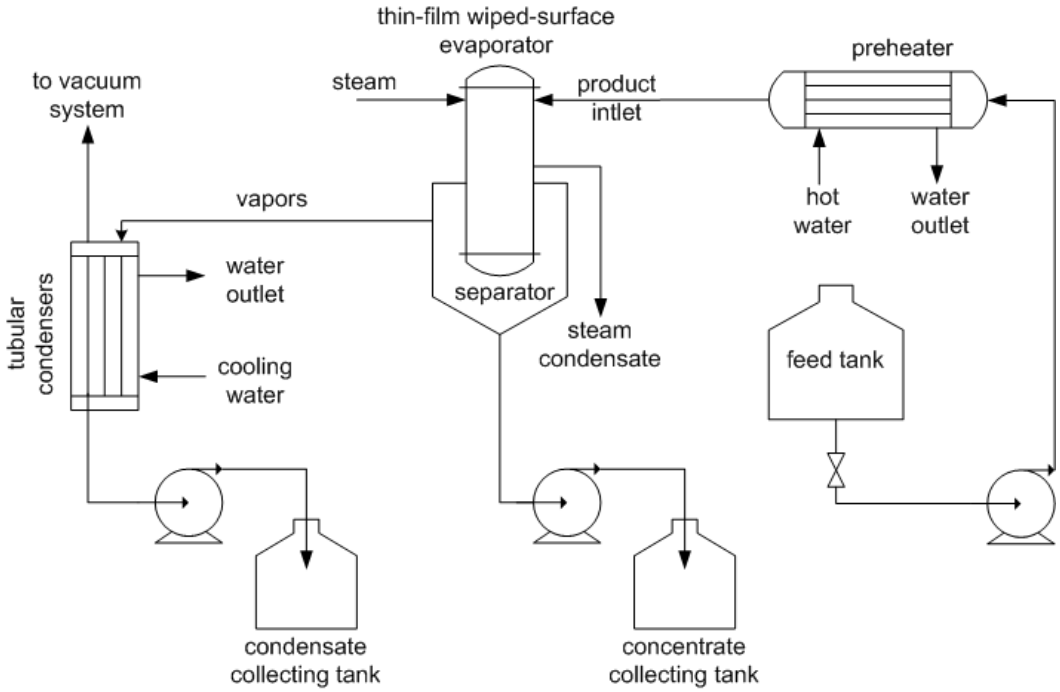

Figure 5.1: Simplified flow diagram of experimental installation for a wiped fim evaporator [91]

5.3 Error Analysis

Laboratory experiments involve taking measurements of physical quantities. No measurement of any physical quantity is ever perfectly accurate, except possibly the counting of objects. The discrepancy between the measured value and the true value of the quantity may arise from different sources. No

matter how much effort is put into refinement of technique or into improvement of the instruments, the error can be decreased in magnitude but never eliminated entirely. The statement of the result of a measurement is not complete without an indication of how much error the measurement might contain.

To obtain an experimental result with an estimate of the degree of uncertainty in the measurements, the types of errors, the ways to reduce the errors, and how to treat the data properly need to be known.

For the calculation of the heat transfer coefficient for the liquid film (h_p), Equation 4.1 (page 54) will be used. In order to calculate h_p, the overall heat transfer coefficient U_{ov}, needs to be known. The following equations provide a way to calculate it when using hot oil for heating purposes:

$$Q = w_h C_{p,h} \left(T_{h,i} - T_{h,o}\right) \tag{5.23}$$

$$Q = U A \Delta T_{lm} \tag{5.24}$$

$$U_{ov} = \frac{w_h C_{p,h} \left(T_{h,i} - T_{h,o}\right)}{A \Delta T_{lm}} \tag{5.25}$$

$$\Delta T_{lm} = \frac{\left(T_{h,i} - T_L\right) - \left(T_{h,o} - T_L\right)}{\ln\left(\dfrac{T_{h,i} - T_L}{T_{h,o} - T_L}\right)} \tag{5.26}$$

where ΔT_{lm} is the logarithmic mean temperature difference between the inlet and outlet conditions.

Thus the experimental h_p is calculated using the equation:

$$h_p = \left[\frac{A \Delta T_{lm}}{w_h C_{p,h} \left(T_{h,i} - T_{h,o}\right)} - \frac{1}{h_o} - \frac{\delta_w}{k_{wall}}\right]^{-1} \tag{5.27}$$

From Equation 5.27, the measured variables that can influence the value of h_p are:

- Temperature of the evaporating liquid (T_L)
- Flowrate of the hot oil (w_h)
- Temperature of the hot oil at inlet ($T_{h,i}$) and outlet ($T_{h,o}$)

In order to know the experimental error associated with these parameters, the following equations will be used.

Error associated with T_L:

$$\Delta h_p = \frac{A(T_{h,i} - T_{h,o})}{h_p^2 w_h C_{p,h} \left(\ln T_R\right)^2 (T_{h,i} - T_L)(T_{h,o} - T_L)} \cdot \Delta T_L \tag{5.28}$$

Error associated with w_h:

$$\Delta h_p = \frac{A}{h_p^2 w_h^2 C_{p,h} \ln T_R} \cdot \Delta w_h \tag{5.29}$$

Error associated with $T_{h,i}$:

$$\Delta h_p = \frac{A}{h_p^2 w_h C_{p,h} \left(\ln T_R\right)^2 (T_{h,i} - T_L)} \cdot \Delta T_{h,i} \tag{5.30}$$

Error associated with $T_{h,o}$:

$$\Delta h_p = -\frac{A}{h_p^2 w_h C_{p,h} \left(\ln T_R\right)^2 (T_{h,o} - T_L)} \cdot \Delta T_{h,o} \tag{5.31}$$

In all the previous equations, T_R is defined as follows:

$$T_R = \frac{T_{h,i} - T_L}{T_{h,o} - T_L}$$

Equations 5.28 to 5.31 were derived using the equation:

$$\Delta(variable) = \frac{\partial\,[variable]}{\partial\,[measurement]} \cdot \Delta(measurement) \tag{5.32}$$

Table 5.5 shows the effect of the error in measured variables to be taken in the experiments and its effect on the experimental process side heat transfer coefficient, based on the proposed model.

Table 5.5: Effect of measurement errors in operational parameters over the experimental process side heat transfer coefficient.

Variable	**3% error**	**5% error**	**10% error**
T_L, °C	5.9	10.2	22.7
$T_{h,i}$, °C	29.9	50.9	n.c.
$T_{h,o}$, °C	12.6	10.4	n.c.
M_h, kg/s	5.9	9.9	19.9

5.4 Experimental Conditions

A full range of operating conditions was run, and is shown on Table 5.6

Table 5.6: Operational Parameters for Experimental Measurements

Parameter	**Range**
Liquid rate	8-58 kg/hr-m^2
Inlet Concentration (weight fraction %)	35-75
Speed of Rotation (rpm)	180-540
Number of Blades	3
Film Reynolds Number	0.1-6.0

Table 5.7: Main dimensions of the Cargill evaporator

Diameter (m)	0.08
Length (m)	0.2141
Wall thickness (mm)	2.5
Number of blades	3
Jacket clearance (m)	0.012

5.5 Equipment

The experimental equipment for this research was made available by Cargill Inc. at their Blair, Nebraska, plant. The experimental data were taken in summer 2003. The WFE was manufactured by UIC Inc. (now ChemTech Services Inc), model KDL-6. The unit was modified to allow the measurement of process conditions (i.e., temperature of vapor and liquid). The heat was provided by a hot oil. Marlotherm® SH [81] was used for this purpose. Appendix B describes the characteristics of this heating medium.

Figure 5.2 represents a diagram of the modified experimental equipment. In Figure 5.3 a picture of the evaporator and condenser is shown. In Table 5.7 the main dimensions of the WFE are displayed, and Figure 5.4 depicts these dimensions.

5.6 Curves Calibration

Before running the experiments it was necessary to have a method for reading the concentration of each component in water. The refractive index method was used. For this purpose, the Mettler/Toledo RA-510M Refrac-

tometer was available.

Solutions of known weight percent were prepared for each system and were read using the refractometer. For the water-sucrose system, the solutions were prepared up to 65% only because the maximum solubility of sucrose at 20 °C is 66.7%. Table 5.8 shows the refractive index for this system, and Figure 5.5 shows a plot of the refractive index versus the weight concentration. At the beginning of each reading, the refractive index of pure water was read in order to check for consistency of the measurements.

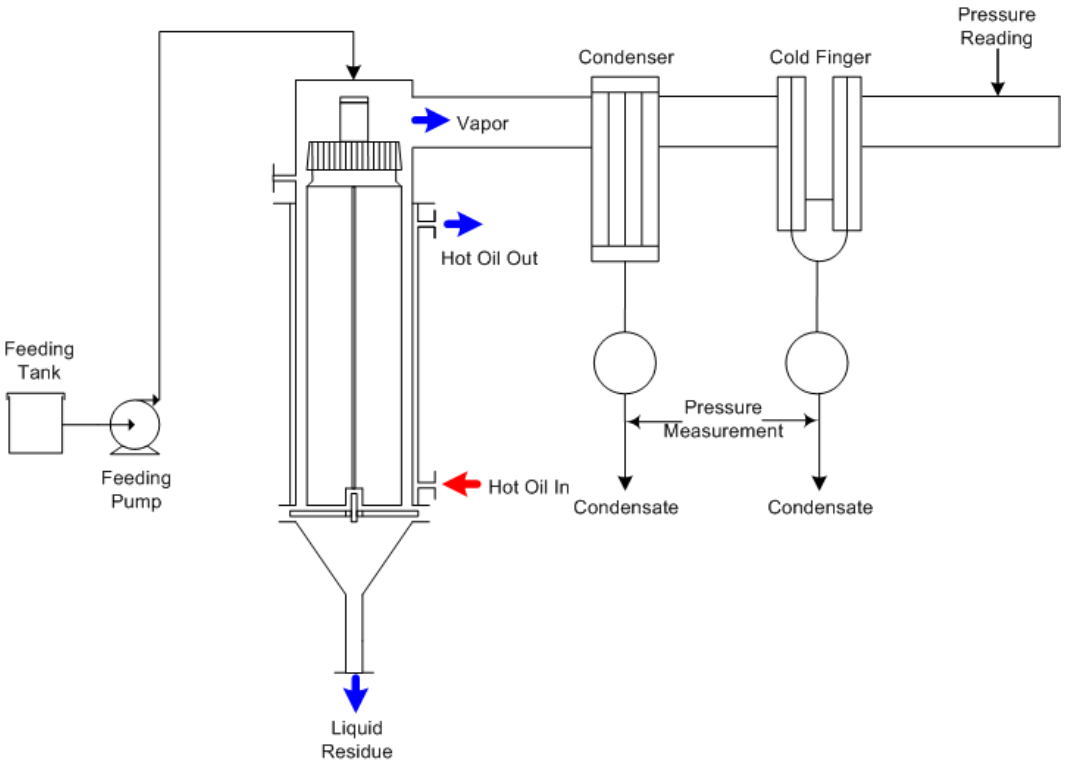

Figure 5.2: Diagram of the original Wiped Film Evaporator from Cargill.

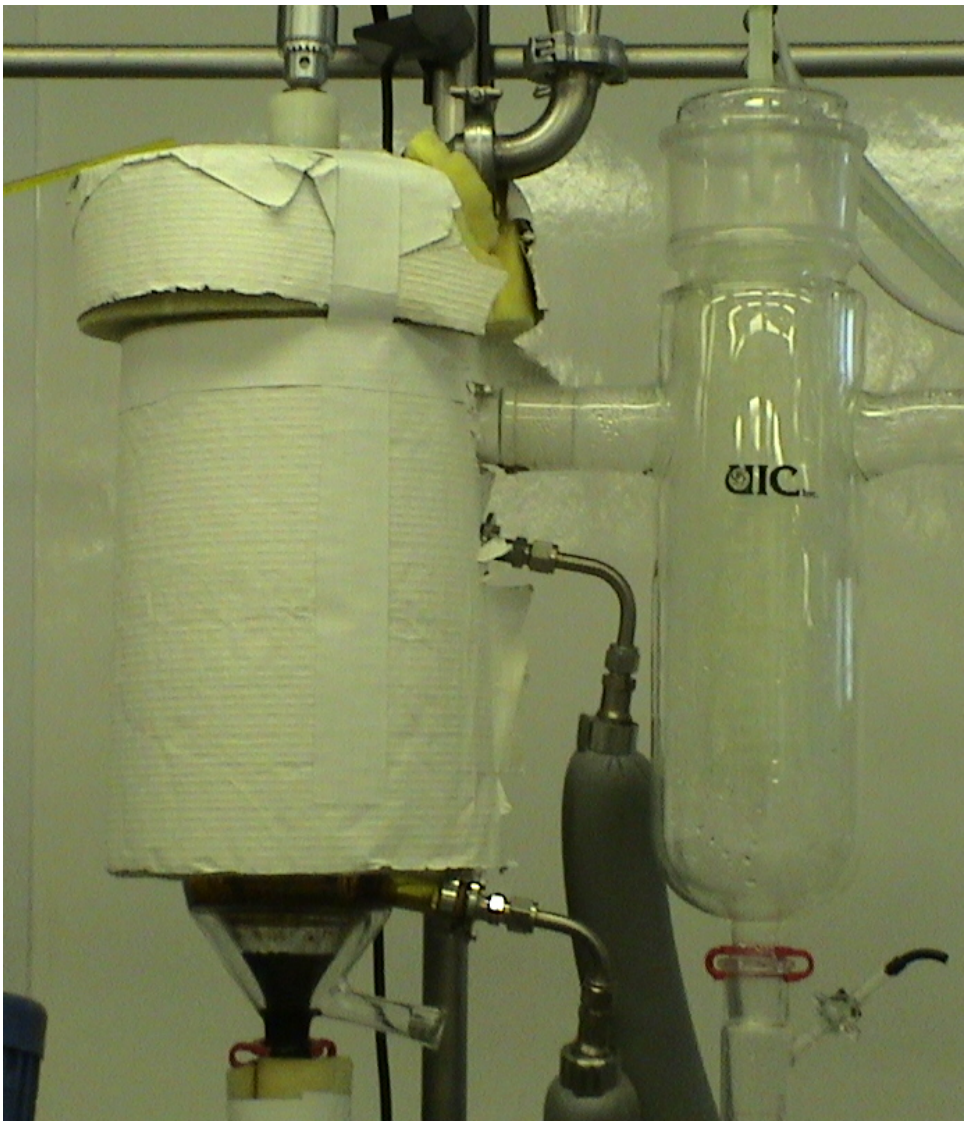

Figure 5.3: Photo of the UIC Inc. Wiped Film Evaporator and condenser from Cargill.

For the system water-glycerol, the solutions were prepared up to 90%, and the refractive index for pure glycerol was also recorded. Table 5.9 presents

the refractive index for the solutions at 20 °C, and Figure 5.6 presents a plot of the refractive index versus the composition in weight percent.

For the system water-ethylene glycol, the solutions were also prepared up to 90%, and the refractive index for pure ethylene glycol was also recorded. Table 5.10 presents the refractive index for the solutions at 20 °C, and Figure 5.7 presents a plot of the refractive index versus the composition in weight

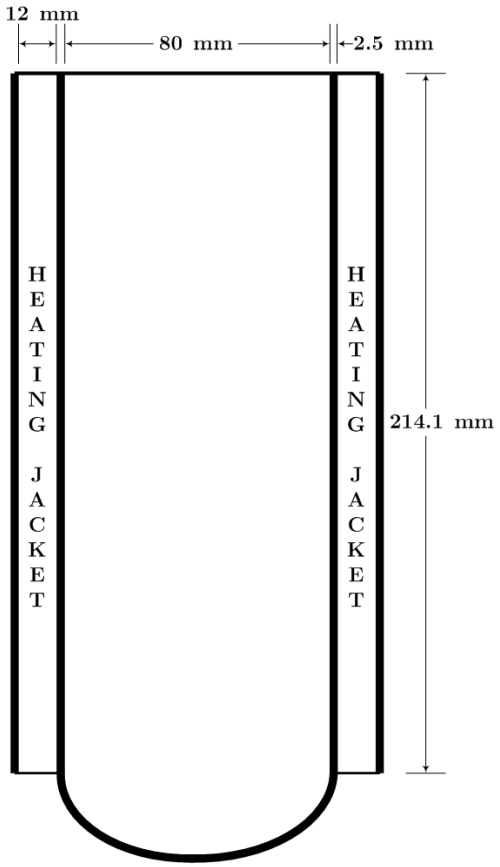

Figure 5.4: Dimensions of the ChemTech Services Wiped Film Evaporator from Cargill.

Table 5.8: Refractive index for different solutions of sucrose in water at 20 °C

Weight %	RI
4.99	1.3403
9.99	1.3478
20.05	1.3639
30.00	1.3811
39.96	1.3997
49.76	1.4196
54.81	1.4303
59.95	1.4418
65.05	1.4536

Table 5.9: Refractive index for glycerol in water at 20 °C

Weight %	RI
0.00	1.3331
10.01	1.3426
20.00	1.3525
30.00	1.3627
39.90	1.3728
49.87	1.3831
59.99	1.3935
69.92	1.4034
80.00	1.4133
90.03	1.4228
100.00	1.4319

percent.

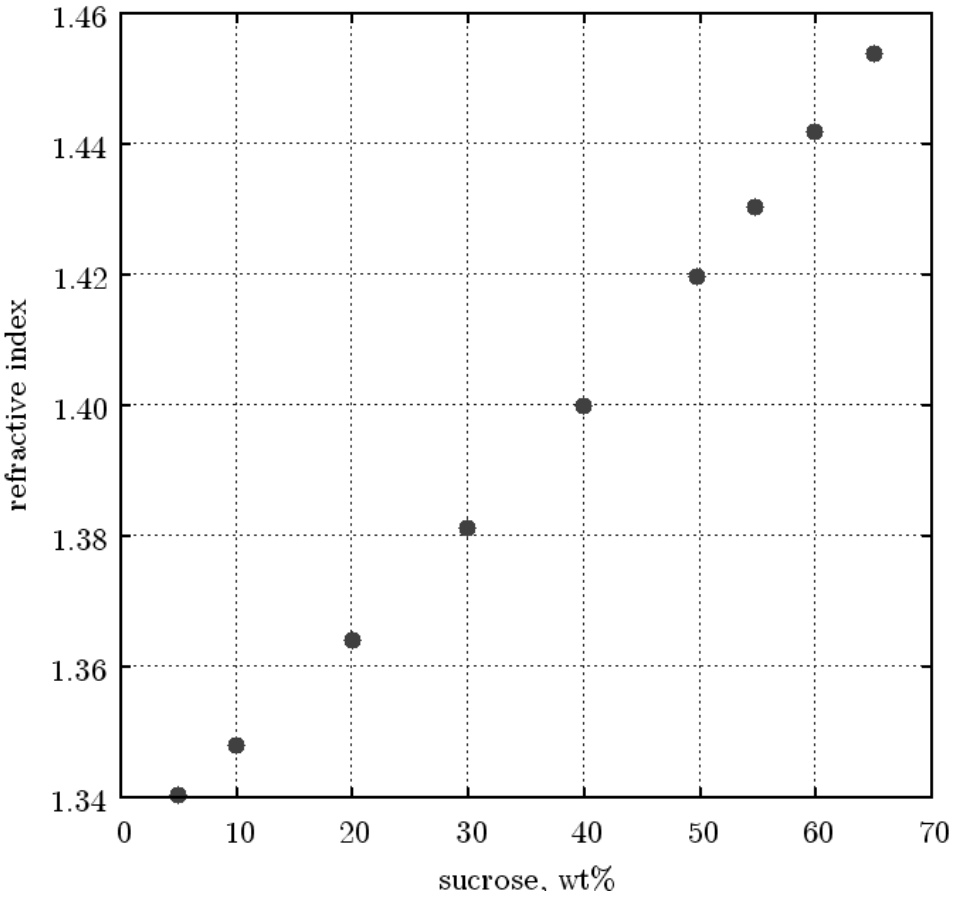

Figure 5.5: Refractive index variation with weight percent for the water-sucrose system at 20°.

5.7 Run Procedure

Before collecting experimental data, several tests were run using pure water as the feeding material. This was done for three reasons:

1. Cleaning the equipment: the WFE was used sporadically by Cargill during the period when the data were collected.

2. Training for running the equipment: using water only as feed allowed learning the operation of the unit.

3. Heat balance and troubleshooting: during the first week, several problems with the evaporator were corrected (i.e., original pressure gauge was replaced to allow the correct reading of the high vacuum conditions).

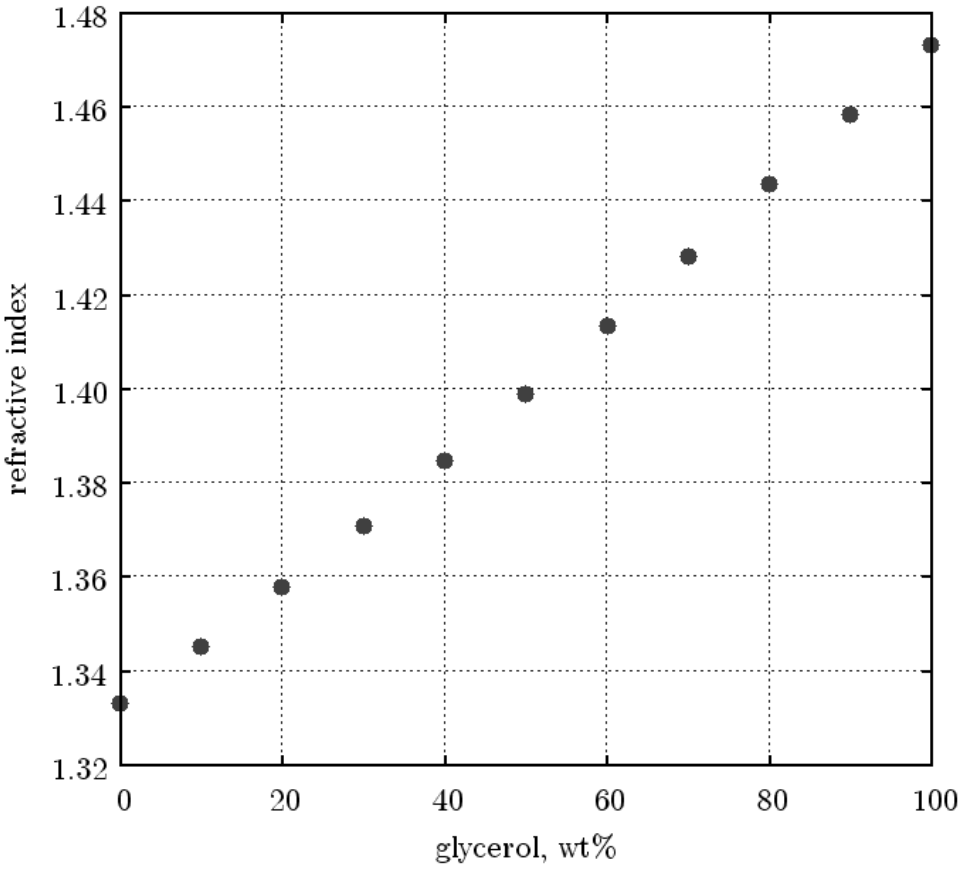

Figure 5.6: Refractive index variation with weight percent for the water-glycerol system at 20°.

Table 5.10: Refractive index for ethylene glycol in water at 20 °C

Weight %	RI
0.00	1.3331
10.01	1.3452
19.99	1.3577
30.02	1.3708
39.99	1.3846
50.06	1.3987
60.09	1.4134
70.02	1.4282
80.00	1.4434
90.03	1.4584
100.00	1.4730

The steps to follow for the experiments were:

1. Start cooling system (this was used to condensate the vapor generated in the WFE).
   1.1. Turn on cooling refrigerator.
   1.2. Turn on cooling pump.
2. Start vacuum system (in order to set the desired operating pressure).
   2.1. Pre-heat oil in vacuum pump using the heat gun.
   2.2. Put dry ice in alcohol mixture, inside cold finger, to prevent any vapor to affect the pressure reading.
   2.3. Turn on vacuum pump.
   2.4. Pull off vacuum to desired operating conditions.

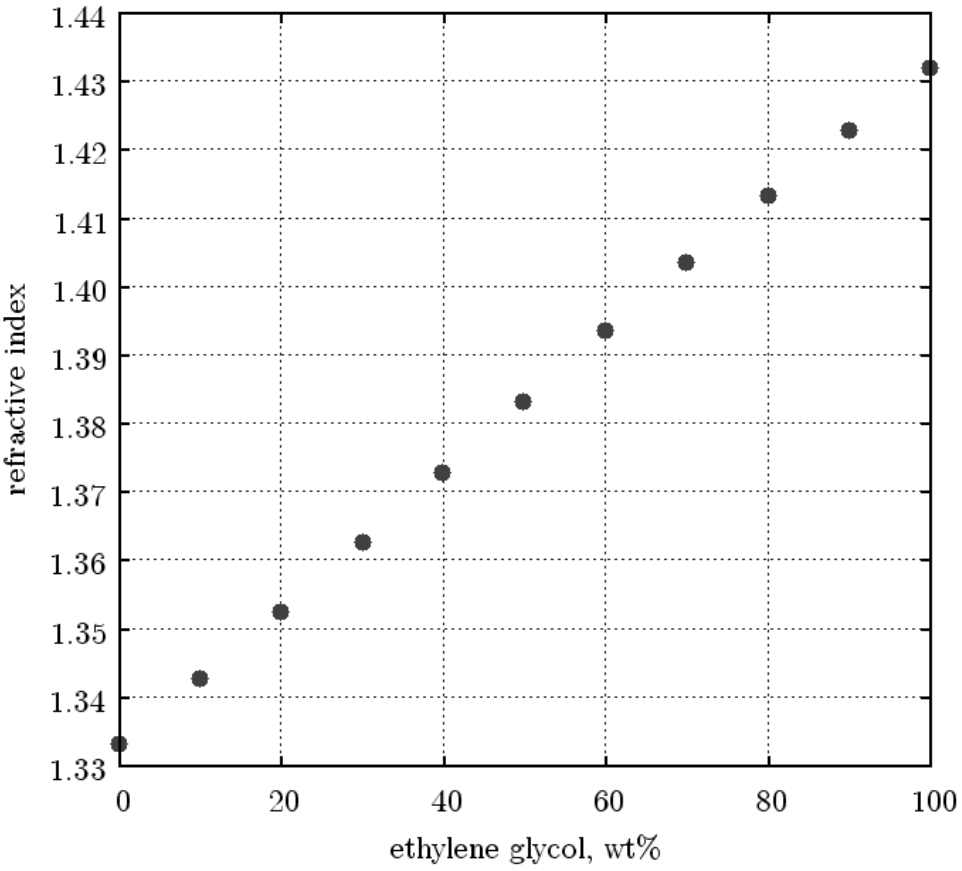

Figure 5.7: Refractive index variation with weight percent for the water-ethylene glycol system at 20°.

3. Set the temperature of the hot oil bath and turn on bath.

4. Set feeding pump to desired volumetric flow rate and turn on.

5. Start the agitator (rotor) and set speed of the wipers.

6. Take samples after "steady state" is reached (it was determined that

steady state was reached after 1 hour of making a change to an operating condition).

6.1. Start stopwatch and close bottom valves (to collect the liquid residue).

6.2. Record initial weight, temperatures (vapor and liquid), and rotational speed.

6.3. Close valves when about 500 grams are fed to the evaporator, and record time.

6.4. Weight vapor and liquid streams.

6.5. Take samples and read refractive index.

5.8 Experimental Data

In this section, the collected experimental data are presented. During the experiments with water-sucrose, crystals of sugar were formed due to the low feed rate and high rate of evaporation. Pure water was needed to clean up the evaporator.

When using water-glycerol, the silicone-based sealant for the glass junctions was being dissolved.

5.8.1 Operating Conditions

Table 5.11 presents the ranges of experimental conditions studied during these experiments. As can be seen, wide variations of liquid viscosity,

density, and flowrates were studied. The three systems include these parameters.

Table 5.11: Range of experimental conditions

Liquid rate	$8 - 58$ kg/hr-m^2
Vapor velocity	$0.2 - 0.4$ m/s
Rotational speed	$180 - 540$ rpm
Inlet concentration (weight%)	$35 - 75$
Liquid density	$895 - 1280$ kg/m^3
Liquid viscosity	$3 - 50$ cp
Liquid Reynold number	$0.1 - 6.0$

5.8.2 Collected Data

Data were collected for the three systems at different conditions. Tables 5.12 (for water-sucrose), 5.13 (for water-glycerol), and 5.14 (for water-ethylene glycol) show the experimental data collected using the steps mentioned before.

Table 5.12: Experimental data for water-sucrose at different operating conditions.

Sucrose						**Evaporator**				**Hot Oil**		
Feed kg/hr	T_{feed} °C	x_{in} %	x_{out} %	Vapor kg/hr	Liquid kg/hr	P torr	T_{top} °C	T_{bot} °C	Speed rpm	T_{in} °C	T_{out} °C	Flow L/min
1.648	29.0	46.94	56.61	0.275	1.374	55.0	39.8	42.8	300	94.3	90.4	1.548
1.640	30.0	46.92	56.47	0.277	1.363	55.0	39.8	40.0	420	94.3	90.4	1.529
1.638	30.0	46.97	57.04	0.281	1.354	54.9	39.9	40.0	540	94.3	90.3	1.542
3.321	31.8	47.29	51.56	0.264	3.052	54.1	39.8	40.0	540	94.3	90.3	1.534
2.472	29.7	47.68	53.59	0.262	2.196	54.3	39.5	40.0	180	94.3	90.3	1.521
2.470	31.6	47.87	53.90	0.273	2.200	54.5	40.0	40.0	360	94.3	90.4	1.596
2.468	31.8	47.84	53.99	0.272	2.189	54.5	39.9	40.0	540	94.3	90.4	1.565
2.464	32.5	47.87	53.77	0.268	2.197	54.5	39.8	40.0	180	94.3	90.5	1.577
1.645	30.0	47.89	57.18	0.267	1.377	54.9	39.9	40.0	180	94.3	90.4	1.514
1.640	30.2	47.96	58.08	0.278	1.360	54.9	39.9	40.0	360	94.3	90.3	1.521
1.636	31.0	47.96	58.24	0.281	1.354	54.9	39.9	40.0	539	94.3	90.3	1.526
2.494	28.7	48.22	54.94	0.306	2.183	41.2	34.9	35.0	182	94.4	90.1	1.524
2.488	29.0	48.30	55.33	0.312	2.174	41.3	34.9	35.0	360	94.3	90.1	1.524
2.483	29.0	48.41	55.74	0.316	2.156	41.2	35.0	35.0	540	94.3	90.1	1.584
3.330	28.0	48.59	53.37	0.294	3.030	41.2	35.0	35.0	180	94.3	90.2	1.548
3.327	29.0	48.61	53.62	0.306	3.018	41.2	35.1	35.0	360	94.3	90.2	1.575
3.325	29.5	48.55	53.60	0.307	3.013	40.8	35.0	35.0	540	94.3	90.1	1.529
3.382	29.5	50.48	54.74	0.246	3.115	54.8	39.8	40.0	181	94.3	90.3	1.518
3.365	30.5	49.62	53.87	0.253	3.097	54.8	40.0	40.0	360	94.3	90.2	1.513
1.659	27.0	49.25	60.09	0.309	1.350	40.2	35.1	35.0	180	94.3	90.3	1.573
1.664	27.5	49.85	62.03	0.325	1.337	40.0	34.2	35.0	360	94.3	90.1	1.601

Continued on next page

Table 5.12 – continued from previous page

Sucrose						Evaporator				Hot Oil		
Feed kg/hr	T_{feed} °C	x_{in} %	x_{out} %	Vapor kg/hr	Liquid kg/hr	P torr	T_{top} °C	T_{bot} °C	Speed rpm	T_{in} °C	T_{out} °C	Flow L/min
1.662	27.8	49.76	62.19	0.332	1.330	40.0	33.8	35.0	540	94.3	90.1	1.539
2.557	29.6	55.21	61.59	0.263	2.288	55.2	38.1	40.0	360	94.3	90.4	1.527
1.703	28.7	55.39	65.82	0.266	1.431	56.1	38.5	40.0	360	94.3	90.4	1.505
1.692	30.0	53.66	64.21	0.272	1.412	55.9	38.7	40.0	540	94.3	90.5	1.563
2.578	27.5	53.98	61.26	0.306	2.271	41.9	33.8	35.0	360	94.3	90.0	1.514
2.571	28.0	54.02	61.58	0.312	2.256	41.9	34.0	35.0	539	94.3	90.0	1.519
1.705	28.8	53.98	66.32	0.313	1.389	42.0	34.9	35.0	360	94.3	90.1	1.507
3.430	29.2	54.16	59.57	0.309	3.117	41.8	33.1	35.0	540	94.3	90.1	1.549
2.486	30.4	47.56	53.22	0.271	2.216	55.7	37.8	40.0	540	94.3	90.4	1.576
2.483	30.5	47.52	53.33	0.273	2.213	55.7	38.7	40.0	540	94.3	90.4	1.542
1.568	25.5	36.31	43.91	0.269	1.299	59.1	39.0	40.0	361	94.3	90.3	1.528
0.780	27.2	36.31	57.01	0.284	0.496	59.1	38.0	40.0	360	94.3	90.4	1.527
2.350	29.4	36.27	40.85	0.257	2.087	59.1	39.9	40.0	360	94.3	90.3	1.527
1.564	30.0	36.27	45.86	0.327	1.237	42.1	33.8	35.0	360	94.3	90.0	1.520

Table 5.13: Experimental data for water-glycerol at different operating conditions.

Glycerol					**Evaporator**			**Hot Oil**		
Feed kg/hr	x_{in} %	x_{out} %	Vapor kg/hr	Liquid kg/hr	Pressure torr	T_{evap} °C	Speed rpm	T_{in} °C	T_{out} °C	Flow L/min
1.556	57.85	70.90	0.277	1.279	40.4	40.6	360	94.3	89.4	1.464
1.555	58.01	71.04	0.278	1.277	39.8	40.3	540	94.3	89.5	1.488
0.775	58.00	85.16	0.245	0.530	39.8	40.3	360	94.3	89.9	1.469
1.552	58.47	69.36	0.238	1.313	39.8	40.5	180	94.3	89.7	1.438
0.774	58.40	75.57	0.175	0.599	39.8	40.4	180	94.3	90.8	1.451
1.162	58.62	76.80	0.269	0.893	39.7	40.5	360	94.3	89.4	1.438
1.549	58.66	71.49	0.270	1.279	39.7	40.5	540	94.3	89.3	1.441
0.770	58.41	89.78	0.266	0.504	29.1	34.7	360	94.3	88.9	1.425
1.158	58.53	79.50	0.300	0.858	29.1	34.7	360	94.3	89.0	1.421
1.545	58.53	73.38	0.306	1.239	29.1	34.7	360	94.3	89.5	1.386
1.156	58.42	79.28	0.299	0.857	29.1	34.7	360	94.3	89.3	1.384
0.733	38.28	65.65	0.300	0.433	38.9	36.2	360	94.3	88.9	1.436
0.732	38.05	66.09	0.303	0.429	38.7	36.0	540	94.3	89.2	1.436
1.100	38.14	53.38	0.306	0.793	38.8	36.1	360	94.3	89.0	1.447
1.467	38.11	48.60	0.307	1.160	38.8	36.1	360	94.3	89.0	1.450
1.467	38.18	50.16	0.343	1.124	29.1	31.0	360	94.3	88.7	1.443
0.731	38.23	70.71	0.329	0.402	29.0	30.9	360	94.3	88.9	1.432
1.598	74.22	85.83	0.216	1.383	38.3	46.3	360	94.3	90.0	1.438
1.203	75.02	90.06	0.203	1.000	38.3	46.8	360	94.3	90.2	1.444
2.010	74.98	84.13	0.218	1.793	38.3	46.8	360	94.3	89.8	1.437
1.605	74.96	86.59	0.217	1.389	38.3	46.8	360	94.3	90.0	1.440

Table 5.14: Experimental data for water-ethylene glycol at different operating conditions.

Ethylene Glycol						**Evaporator**			**Hot Oil**		
Feed kg/hr	x_{in} %	Vapor kg/hr	y %	x_{out} %	Liquid kg/hr	Pressure torr	T_{evap} °C	Speed rpm	T_{in} °C	T_{out} °C	Flow L/min
1.125	72.78	0.209	1.99	88.70	0.916	32.0	45.1	360	94.3	90.1	1.448
1.495	73.62	0.211	1.57	85.37	1.284	35.1	43.5	361	94.3	89.9	1.444
1.871	73.89	0.217	1.87	83.34	1.654	35.0	44.3	359	94.3	89.9	1.497
1.121	73.98	0.202	2.30	89.66	0.920	32.0	44.4	360	94.3	90.2	1.464
1.118	74.16	0.207	2.12	90.47	0.911	32.0	43.9	540	94.3	90.2	1.467
1.498	73.73	0.359	4.15	95.71	1.139	31.8	48.8	538	119.2	113.5	1.666

Chapter 6

Experimental Results and Model Validation

6.1 Isothermal Flash

A wiped film evaporator can be simulated sometimes as an isothermal flash to calculate the heat duty and composition distribution of the vapor and liquid streams.

6.1.1 Water-Sucrose

When applying the flash Equations 3.43-3.46 to the water-sucrose system, the results, as shown in Figure 6.1, are consistent with the experimental compositions for the wiped film evaporator when Equations 5.6-5.10 are used to predict the physical properties, and the modified UNIQUAC equations from Peres and Macedo [75] are used to predict the activity coefficients (Equations 5.11-5.17). When using group contribution methods (GCM) for this system, the predicted concentration of water deviates from the experimental results. This is because the GCM for this particular system does not work very well. The prediction of liquid enthalpy and viscosity are off with respect to the real values, specially the viscosity (i.e., predicted viscosity was off by an order of magnitude of 10). Figure 6.2 presents the relative error for the compositions when using the two methods for physical properties.

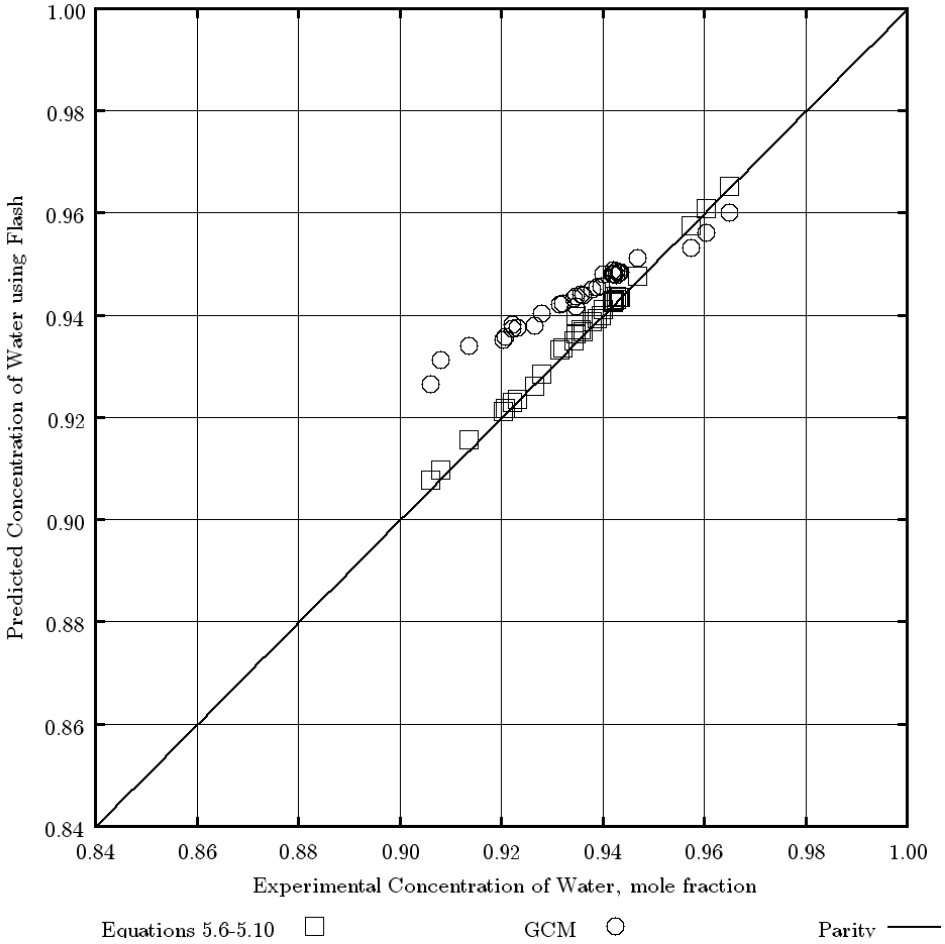

Figure 6.1: Predicted concentration of water when simulating the wiped film evaporator as an isothermal flash for the water-sucrose system.

The good agreement between the experimental concentrations of water when simulating the wiped film evaporator (WFE) as an isothermal flash and using the special equations for the prediction of physical properties and activity coefficient is because this system presents an almost constant temperature profile (i.e., top and bottom temperature difference was around a maximum of

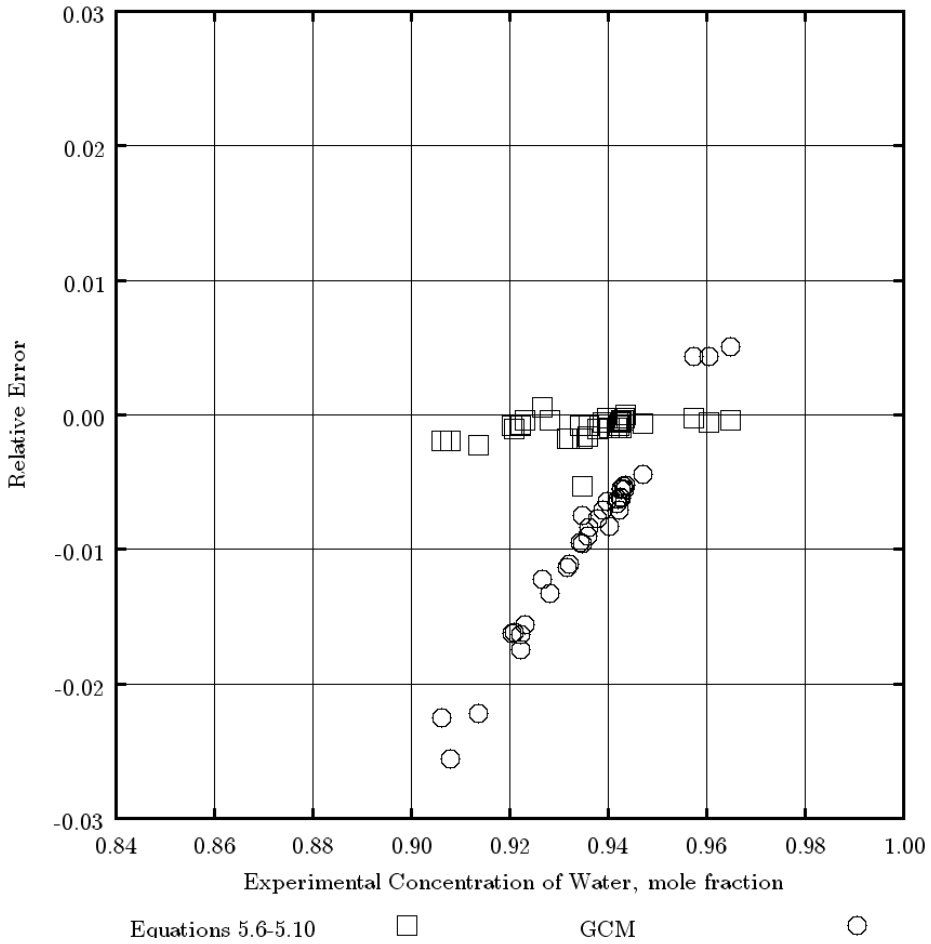

Figure 6.2: Relative error when simulating the wiped film evaporator as an isothermal flash for the water-sucrose system.

0.5 °C), approaching the conditions of a flash at constant temperature. The next two systems do not show the same behavior.

6.1.2 Water-Glycerol

When applying the flash equations to the water-glycerol system, the results, as shown in Figure 6.3, are somewhat consistent with the experimental compositions for the wiped film evaporator for both DIPPR and GCM predictions when the experimental composition of water is high (i.e., $> 60\%$). When the concentration of the exiting water is low, the deviations from the flash calculations are higher. This is because as the evaporation rate is low (i.e., high concentration of water in the liquid stream), the temperature gradient in the WFE is small, approaching the conditions that exist in an isothermal flash. However, when the evaporation rate is high, the remperature gradient in the WFE increases, deviating from the conditions of an isothermal flash.

The average error is shown in Figure 6.4 for this system, and it presents greater errors as the concentration of water is $> 60\%$, as stated before.

6.1.3 Water-Ethylene Glycol

The experimental data for this system only has 6 data points. The obtained results, as shown in Figure 6.5 when applying the flash equations to this system do not show a good agreement with the experimental values. This is because the conditions of the evaporator when using the water-ethylene glycol system are not close to an isothermal flash. A temperature profile between the top and bottom of the evaporator was always present when running the experiments. Figure 6.6 shows the relative error between the predicted and experimental concentration of water in the ethylene glycol liquid stream.

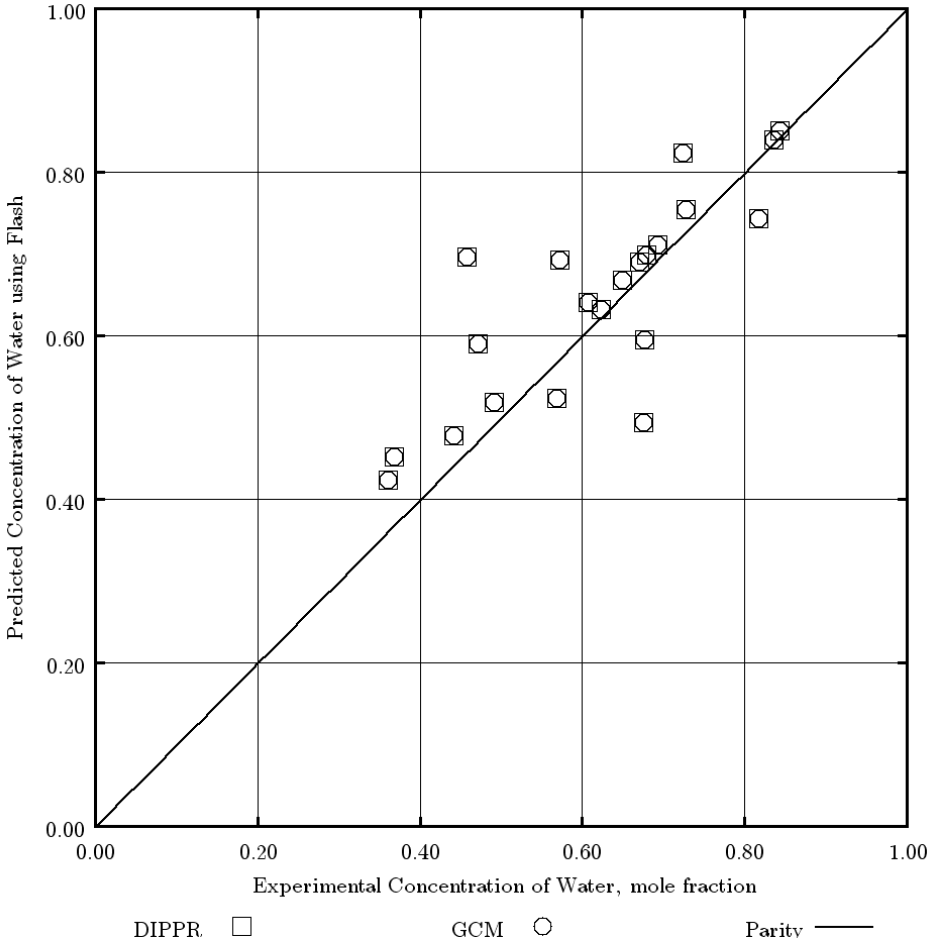

Figure 6.3: Predicted concentration of water when simulating the wiped film evaporator as an isothermal flash for the water-glycerol system.

6.1.4 WFE as an Isothermal Flash

As can be seen from the previous plots (Figures 6.1, 6.3, and 6.5), an isothermal flash can sometimes represent the product distribution of a wiped film evaporator. This is true when the temperature gradient in the evaporator is small (i.e., in the order of $1 - 2$ °C). When the gradient is significant (i.e.,

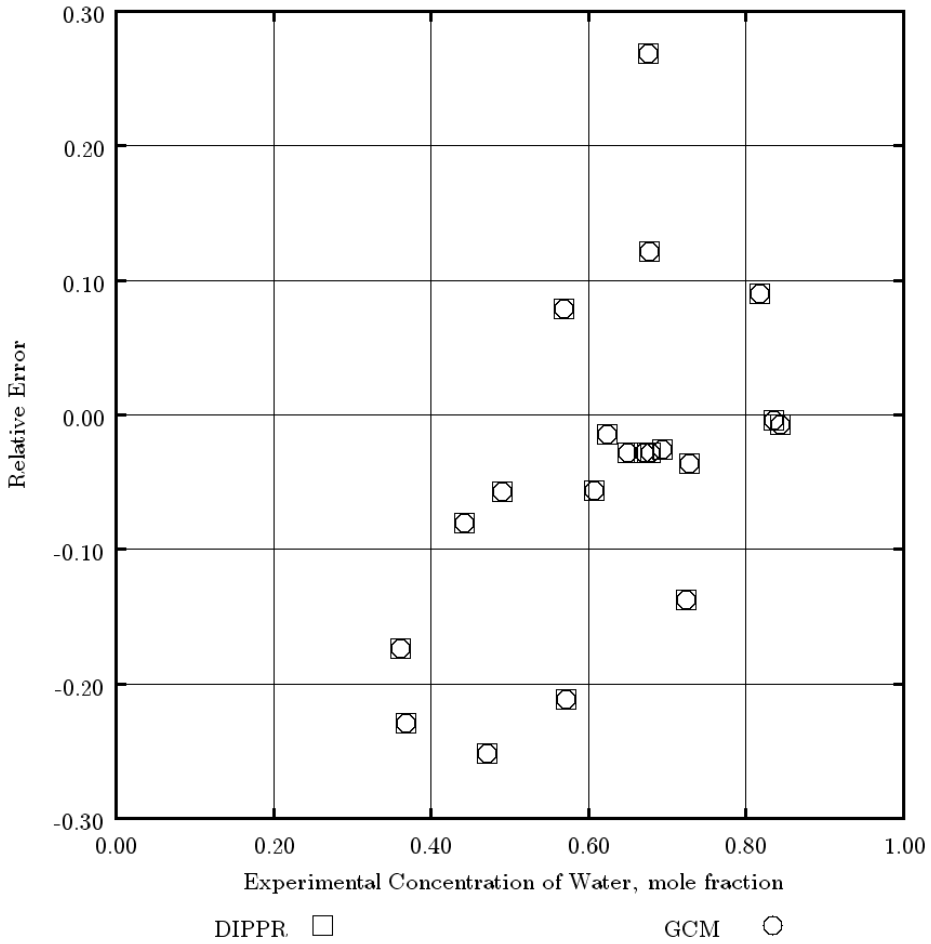

Figure 6.4: Relative error when simulating the wiped film evaporator as an isothermal flash for the water-glycerol system.

$>$ 4 °C), an isothermal flash is less likely to represent the results of a wiped film evaporator.

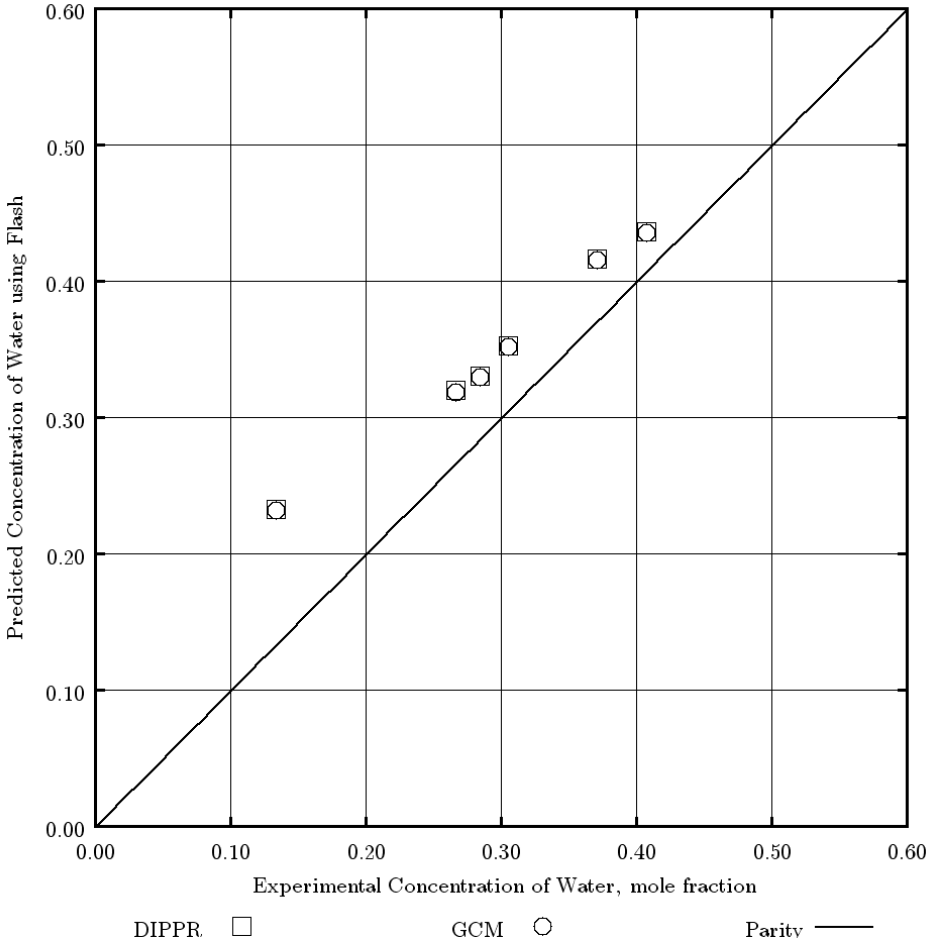

Figure 6.5: Predicted concentration of water when simulating the wiped film evaporator as an isothermal flash for the water-ethylene glycol system.

6.2 Heat and Mass Transfer Coefficient

In this section, the back-calculation of the process-side heat transfer coefficient (h_p) and the prediction of the mass transfer coefficient (k_L^{WFE}) from the experimental data for the three systems is presented.

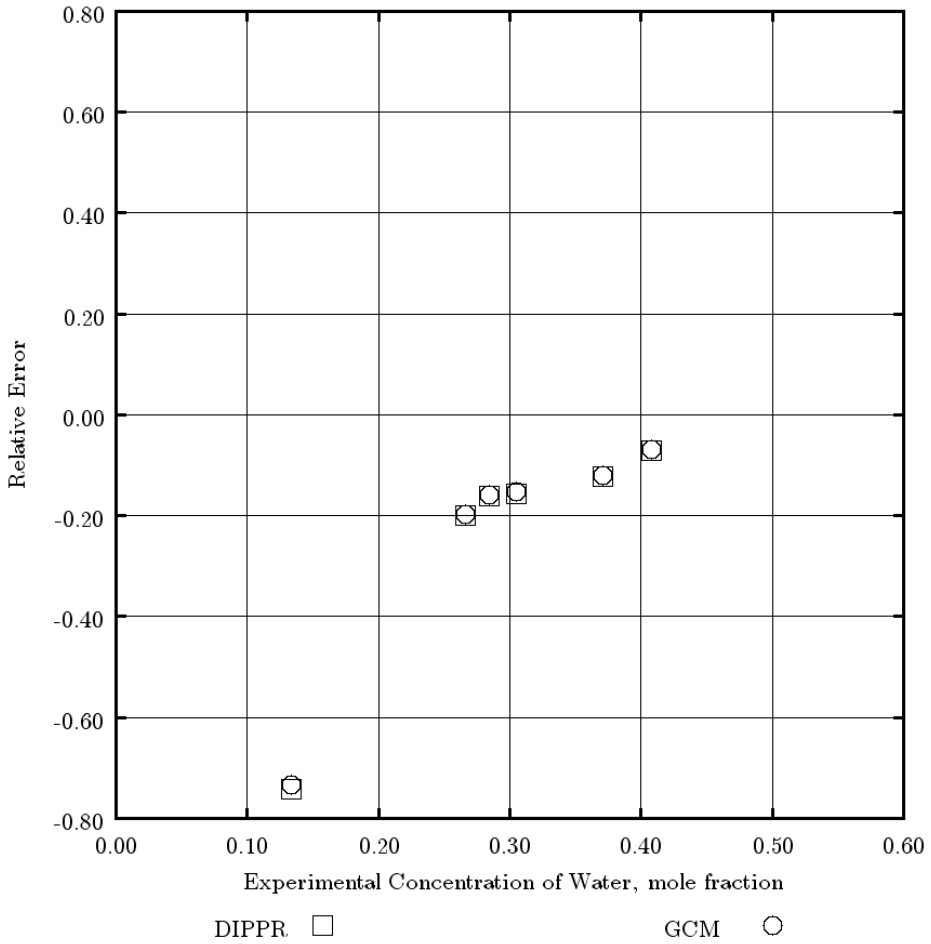

Figure 6.6: Relative error when simulating the wiped film evaporator as an isothermal flash for the water-ethylene glycol system.

6.2.1 Experimental Heat Transfer Coefficient

From the experiments described in Chapter 5 using the Cargill wiped film evaporator and the three experimental systems (water-sucrose, water-glycerol, and water-ethylene glycol), the process-side heat transfer coefficient

(h_p) can be calculated. Starting with Equation 4.1:

$$\frac{1}{U_{ov}} = \frac{1}{h_o} + \frac{\delta_{wall}}{k_{wall}} + \frac{1}{h_p} \tag{4.1}$$

Solving for $\frac{1}{h_p}$, Equation 3.15 is obtained:

$$\frac{1}{h_p} = \frac{1}{U_{ov}} - \frac{1}{\lambda_{wall}} - \frac{1}{h_o} \tag{3.15}$$

where the wall resistance can be calculated as $\lambda_{wall} = \frac{k_{wall}}{\delta_{wall}}$, the heat transfer coefficient for the hot fluid side (h_o) is calculated using a model [60], and the overall heat transfer coefficient (U_{ov}) can be calculated from the experiments as:

$$U_{ov} = \frac{Q_{used}}{A \times \Delta T_{lm}} \tag{6.1}$$

where:

$$Q_{used} = V \times \Delta H_{vap,water} \tag{6.2}$$

$$\Delta T_{lm} = \frac{(T_{h,i} - T_{bot}) - (T_{h,o} - T_{top})}{\ln\left(\frac{T_{h,i} - T_{bot}}{T_{h,o} - T_{top}}\right)} \tag{6.3}$$

$$A = \pi D L \tag{6.4}$$

A sample calculation using the first point from Table 5.12 is presented below. The wall resistance will be constant and equal to $\lambda_{wall} = \frac{1.2 \text{ W/m-K}}{0.0025 \text{ m}} = 480 \text{ W/m}^2\text{-K}$.

The external resistance h_o is calculated using Equations 3.17-3.19 [60]. The physical properties for the hot fluid are calculated at the average temperature $\frac{T_{h,i} + T_{h,o}}{2}$ using equations provided in the Appendix B, and shown in Table 6.1

Table 6.1: Equations for the calculation of physical properties for Marlotherm® SH. Temperature in °C

Property	**Equation**	**Units**
Thermal conductivity	$\lambda = 0.1333 - 0.00013T$	W/m-K
Heat capacity	$C_p = 1.4745 + 0.003726T$	J/kg-K
Density	$\rho = 1058.4 - 0.7184T$	kg/m^3
Kinematic viscosity	$\frac{\mu}{\rho} = 12294T^{-1.792}$	mm^2/s

$$T_{avg} = \frac{T_{h,i} + T_{h,o}}{2} = \frac{94.3 + 90.4}{2}$$

$$T_{avg} = 92.35$$

$$\lambda = 0.1333 - 0.00013T = 0.1333 - 0.00013(92.35)$$

$$\lambda = 0.1213 \text{ W/m-K}$$

$$C_p = 1.4745 + 0.003726T = 1.4745 + 0.003726(92.35)$$

$$C_p = 1,818.6 \text{ J/kg-K}$$

$$\rho = 1058.4 - 0.7184T = 058.4 - 0.7184(92.35)$$

$$\rho = 992.06 \text{ kg/m}^3$$

$$\mu = \rho \left[12294T^{-1.792}\right] = 992.06 \left[12294(92.35)^{-1.792}\right]$$

$$\mu = 0.00367 \text{ kg/m-s}$$

$$w = (1.5293 \text{ liter/min}) \left(992.06 \text{ kg/m}^3\right) \left(\frac{1}{1000}\right) \left(\frac{1}{60}\right)$$
$$w = 0.0253 \text{ kg/s}$$

The equations from McAdams [60] are used to calculate the hot fluid side heat transfer coefficient h_o:

$$\frac{h_o D}{\lambda} = \frac{2}{\pi} \frac{wC_p}{\lambda L} \frac{1 - 8\psi(n_1)}{1 + 8\psi(n_1)}$$
$$\psi(n_1) = 0.10238e^{-14.627n_1} + 0.01220e^{-89.22n_1} + 0.00237e^{-212n_1} + \ldots$$
$$n_1 = \frac{\pi\lambda L}{4wC_p} \tag{3.19}$$

Substituting values in these equations:

$$n_1 = \frac{\pi\lambda L}{4wC_p} = \frac{\pi(0.1213)(0.2141)}{4(0.0253)(1,818.6)}$$
$$n_1 = 4.43 \times 10^{-4}$$
$$\psi(n_1) = 0.10238e^{-14.627n_1} + 0.01220e^{-89.22n_1} + 0.00237e^{-212n_1} + \ldots$$
$$\psi(n_1) = 0.10238e^{-14.627(4.43\times10^{-4})} + 0.01220e^{-89.22(4.43\times10^{-4})} + 0.00237e^{-212(4.43\times10^{-4})}$$
$$\psi(n_1) = 0.1156$$

$$\frac{h_o D}{\lambda} = \frac{2}{\pi}\frac{wC_p}{kL}\frac{1-8\psi(n_1)}{1+8\psi(n_1)}$$
$$\frac{h_o D}{\lambda} = \frac{2}{\pi}\frac{(0.0253)(1,818.6)}{(0.1213)(0.2141)} \times \frac{1-8(0.1156)}{1+8(0.1156)} = 44.065$$
$$h_o = 44.065\frac{0.1213}{0.024}$$
$$h_o = 222.7 \text{ W/m}^2\text{-K}$$

It can be assumed that all the vapor stream is water, allowing one to calculate the theoretical amount of heat to vaporize the stream. The heat of vaporization of water is calculated using the DIPPR [22] equation:

$$\lambda_w = \frac{52053}{18.01528}\left[1-\frac{T}{T_c}\right]^{\left(0.3199-0.212\frac{T}{T_c}+0.25795\left(\frac{T}{T_c}\right)^2\right)} \text{ kJ/kg} \tag{6.5}$$

Then the necessary amount of heat to vaporize an amount of water is:

$$Q_{req} = V \times \lambda_w \tag{6.6}$$

Then the required heat for this case is:

$$\lambda_w = \frac{52053}{18.01528}\left[1-\frac{313.05}{647.096}\right]^{\left(0.3199-0.212\frac{313.05}{647.096}+0.25795\left(\frac{313.05}{647.096}\right)^2\right)}$$
$$\lambda_w = 2404.68 \text{ kJ/kg}$$
$$Q_{req} = \frac{0.2765}{3600} \times 2404.57 \times 10^3$$
$$Q_{req} = 184.7 \text{ W}$$

The next to last step to calculate h_p is to calculate the overall heat transfer coefficient U_{ov}:

$$\Delta T_{lm} = \frac{(94.3 - 40) - (90.4 - 39.8)}{\ln\left(\frac{94.3 - 40}{90.4 - 39.8}\right)} \tag{6.7}$$

$$\Delta T_{lm} = 52.43 \tag{6.8}$$

$$U_{ov} = \frac{184.7}{\pi(0.08)(0.2141) \times 52.43} \tag{6.9}$$

$$U_{ov} = 65.47 \text{ W/m}^2\text{-K} \tag{6.10}$$

Finally, h_p is calculated:

$$\frac{1}{h_p} = \frac{1}{U_{ov}} - \frac{1}{\lambda_{wall}} - \frac{1}{h_o}$$

$$\frac{1}{h_p} = \frac{1}{65.47} - \frac{1}{480} - \frac{1}{227.7} = 0.015274 - 0.002083 - 0.004392$$

$$\frac{1}{h_p} = 0.008799$$

$$\boxed{h_p = 113.7 \text{ W/m}^2\text{-K}}$$

The above procedure is applied to all the experimental data from Tables 5.12, 5.13, and 5.14. The results are presented in Tables 6.2, 6.3, and 6.4.

Table 6.2: Experimental data for water-sucrose at different operating conditions with the experimental heat transfer coefficients.

Sucrose						**Evaporator**				**HTC**		
Feed kg/hr	T_{feed} °C	x_{in} %	x_{out} %	Vapor kg/hr	Liquid kg/hr	P torr	T_{top} °C	T_{bot} °C	Speed rpm	U_{ov} W/m^2-K	h_o W/m^2-K	h_p W/m^2-K
1.648	29.0	46.94	56.61	0.275	1.374	55.0	39.8	42.8	300	65.0	224.9	113.1
1.640	30.0	46.92	56.47	0.277	1.363	55.0	39.8	40.0	420	65.4	222.6	114.6
1.638	30.0	46.97	57.04	0.281	1.354	54.9	39.9	40.0	540	66.5	224.1	117.8
3.321	31.8	47.29	51.56	0.264	3.052	54.1	39.8	40.0	540	62.4	223.2	105.5
2.472	29.7	47.68	53.59	0.262	2.196	54.3	39.5	40.0	180	61.7	221.6	103.9
2.470	31.6	47.87	53.90	0.273	2.200	54.5	40.0	40.0	360	64.8	230.9	110.8
2.468	31.8	47.84	53.99	0.272	2.189	54.5	39.9	40.0	540	64.3	227.1	110.3
2.464	32.5	47.87	53.77	0.268	2.197	54.5	39.8	40.0	180	63.2	228.5	106.8
1.645	30.0	47.89	57.18	0.267	1.377	54.9	39.9	40.0	180	63.3	220.7	108.8
1.640	30.2	47.96	58.08	0.278	1.360	54.9	39.9	40.0	360	65.9	221.5	116.5
1.636	31.0	47.96	58.24	0.281	1.354	54.9	39.9	40.0	539	66.6	222.2	118.7
2.494	28.7	48.22	54.94	0.306	2.183	41.2	34.9	35.0	182	66.6	221.9	118.6
2.488	29.0	48.30	55.33	0.312	2.174	41.3	34.9	35.0	360	67.9	221.9	122.9
2.483	29.0	48.41	55.74	0.316	2.156	41.2	35.0	35.0	540	68.9	229.4	123.8
3.330	28.0	48.59	53.37	0.294	3.030	41.2	35.0	35.0	180	64.1	224.8	110.3
3.327	29.0	48.61	53.62	0.306	3.018	41.2	35.1	35.0	360	66.7	228.2	117.3
3.325	29.5	48.55	53.60	0.307	3.013	40.8	35.0	35.0	540	67.0	222.5	119.8
3.382	29.5	50.48	54.74	0.246	3.115	54.8	39.8	40.0	181	58.3	221.2	94.8
3.365	30.5	49.62	53.87	0.253	3.097	54.8	40.0	40.0	360	60.2	220.6	100.0
1.659	27.0	49.25	60.09	0.309	1.350	40.2	35.1	35.0	180	67.3	228.0	119.0

Continued on next page

Table 6.2 – continued from previous page

Sucrose						Evaporator				HTC		
Feed kg/hr	T_{feed} °C	x_{in} %	x_{out} %	Vapor kg/hr	Liquid kg/hr	P torr	T_{top} °C	T_{bot} °C	Speed rpm	U_{ov} W/m^2-K	h_o W/m^2-K	h_p W/m^2-K
1.664	27.5	49.85	62.03	0.325	1.337	40.0	34.2	35.0	360	69.9	231.5	126.6
1.662	27.8	49.76	62.19	0.332	1.330	40.0	33.8	35.0	540	70.9	223.8	132.5
2.557	29.6	55.21	61.59	0.263	2.288	55.2	38.1	40.0	360	60.2	222.3	99.8
1.703	28.7	55.39	65.82	0.266	1.431	56.1	38.5	40.0	360	61.3	219.6	103.5
1.692	30.0	53.66	64.21	0.272	1.412	55.9	38.7	40.0	540	62.9	226.7	106.2
2.578	27.5	53.98	61.26	0.306	2.271	41.9	33.8	35.0	360	65.6	220.7	115.8
2.571	28.0	54.02	61.58	0.312	2.256	41.9	34.0	35.0	539	67.0	221.2	120.1
1.705	28.8	53.98	66.32	0.313	1.389	42.0	34.9	35.0	360	68.0	219.8	124.0
3.430	29.2	54.16	59.57	0.309	3.117	41.8	33.1	35.0	540	65.4	225.0	114.2
2.486	30.4	47.56	53.22	0.271	2.216	55.7	37.8	40.0	540	61.9	228.4	103.1
2.483	30.5	47.52	53.33	0.273	2.213	55.7	38.7	40.0	540	63.2	224.2	107.7
1.568	25.5	36.31	43.91	0.269	1.299	59.1	39.0	40.0	361	62.7	222.4	106.7
0.780	27.2	36.31	57.01	0.284	0.496	59.1	38.0	40.0	360	65.1	222.6	113.9
2.350	29.4	36.27	40.85	0.257	2.087	59.1	39.9	40.0	360	61.0	222.3	101.8
1.567	30.0	36.27	45.86	0.327	1.237	42.1	33.8	35.0	360	70.1	221.4	130.3

Table 6.3: Experimental data for water-glycerol at different operating conditions with the experimental heat transfer coefficients.

Glycerol					**Evaporator**			**HTC**		
Feed kg/hr	x_{in} %	x_{out} %	Vapor kg/hr	Liquid kg/hr	Pressure torr	T_{evap} °C	Speed rpm	U_{ov} W/m^2-K	h_o W/m^2-K	h_p W/m^2-K
1.556	57.85	70.90	0.277	1.279	40.4	40.6	360	69.7	214.5	131.6
1.555	58.01	71.04	0.278	1.277	39.8	40.3	540	69.6	217.5	130.0
0.775	58.00	85.16	0.245	0.530	39.8	40.3	360	69.1	214.6	129.5
1.552	58.47	69.36	0.238	1.313	39.8	40.5	180	59.1	211.2	98.9
0.774	58.40	75.57	0.175	0.599	39.8	40.4	180	44.3	213.0	63.3
1.162	58.62	76.80	0.269	0.893	39.7	40.5	360	69.6	211.3	132.5
1.549	58.66	71.49	0.270	1.279	39.7	40.5	540	67.9	211.6	126.1
0.770	58.41	89.78	0.266	0.504	29.1	34.7	360	72.5	209.6	144.2
1.158	58.53	79.50	0.300	0.858	29.1	34.7	360	71.2	209.1	139.5
1.545	58.53	73.38	0.306	1.239	29.1	34.7	360	69.5	204.8	134.8
1.156	58.42	79.28	0.299	0.857	29.1	34.7	360	70.6	204.6	138.9
0.733	38.28	65.65	0.300	0.433	38.9	36.2	360	70.5	211.0	135.9
0.732	38.05	66.09	0.303	0.429	38.7	36.0	540	71.0	211.0	137.7
1.100	38.14	53.38	0.306	0.793	38.8	36.1	360	69.7	212.3	132.3
1.467	38.11	48.60	0.307	1.160	38.8	36.1	360	69.1	212.6	130.2
1.467	38.18	50.16	0.343	1.124	29.1	31.0	360	71.4	211.8	138.9
0.731	38.23	70.71	0.329	0.402	29.0	30.9	360	72.0	210.4	141.6
1.598	74.22	85.83	0.216	1.383	38.3	46.3	360	64.7	211.3	115.7
1.203	75.02	90.06	0.203	1.000	38.3	46.8	360	67.2	212.0	123.8
2.010	74.98	84.13	0.218	1.798	38.3	46.8	360	64.1	211.2	113.9
1.605	74.96	86.59	0.217	1.389	38.3	46.8	360	66.3	211.6	120.9

Table 6.4: Experimental data for water-ethylene glycol at different operating conditions with the experimental heat transfer coefficients.

Ethylene Glycol						**Evaporator**			**Hot Oil**		
Feed kg/hr	x_{in} %	Vapor kg/hr	y %	x_{out} %	Liquid kg/hr	Pressure torr	T_{evap} °C	Speed rpm	U_{ov} W/m^2-K	h_o W/m^2-K	h_p W/m^2-K
1.125	72.78	0.209	1.99	88.70	0.916	32.0	45.1	360	56.9	212.6	92.7
1.495	73.62	0.211	1.57	85.37	1.284	35.1	43.5	361	57.6	212.1	94.5
1.871	73.89	0.217	1.87	83.34	1.654	35.0	44.3	359	58.2	218.7	95.1
1.121	73.98	0.202	2.30	89.66	0.920	32.0	44.4	360	55.7	214.6	89.3
1.118	74.16	0.207	2.12	90.47	0.911	32.0	43.9	540	57.8	214.9	94.6
1.498	73.73	0.359	4.15	95.71	1.139	31.8	48.8	538	68.4	245.3	118.2

Figure 6.7 shows the experimental heat transfer coefficient for the process side (h_p) for water-sucrose, water-glycerol, and water-ethylene glycol systems as a function of the liquid feed rate. As the flowrate is increased, the HTC decreases for both water-sucrose and glycerol-sucrose. The water-ethylene glycol system presents an almost constant HTC for all flowrates (only 6 data points were taken for this system).

When plotting the process side HTC as a function of the film Reynolds number, as depicted in Figure 6.8, a similar behavior is observed as for the flowrate. One difference is that for the water-sucrose and water-glycerol systems, two different functions of the h_p can be observed. This is due to the evaporation temperature of the wiped film evaporator. For these two systems, two different evaporation temperatures were run, while for the water-ethylene glycol system only one evaporation temperature was analyzed.

Figure 6.9 shows the experimental heat transfer coefficient for the process side (h_p) for the three experimental systems as a function of the rotational Reynolds number. The same functionality as shown in Figure 6.8 (film Reynolds number) was observed.

Figure 6.10 shows the experimental heat transfer coefficient for the process side (h_p) for water-sucrose, water-glycerol, and water-ethylene glycol systems as a function of the Prandtl number.

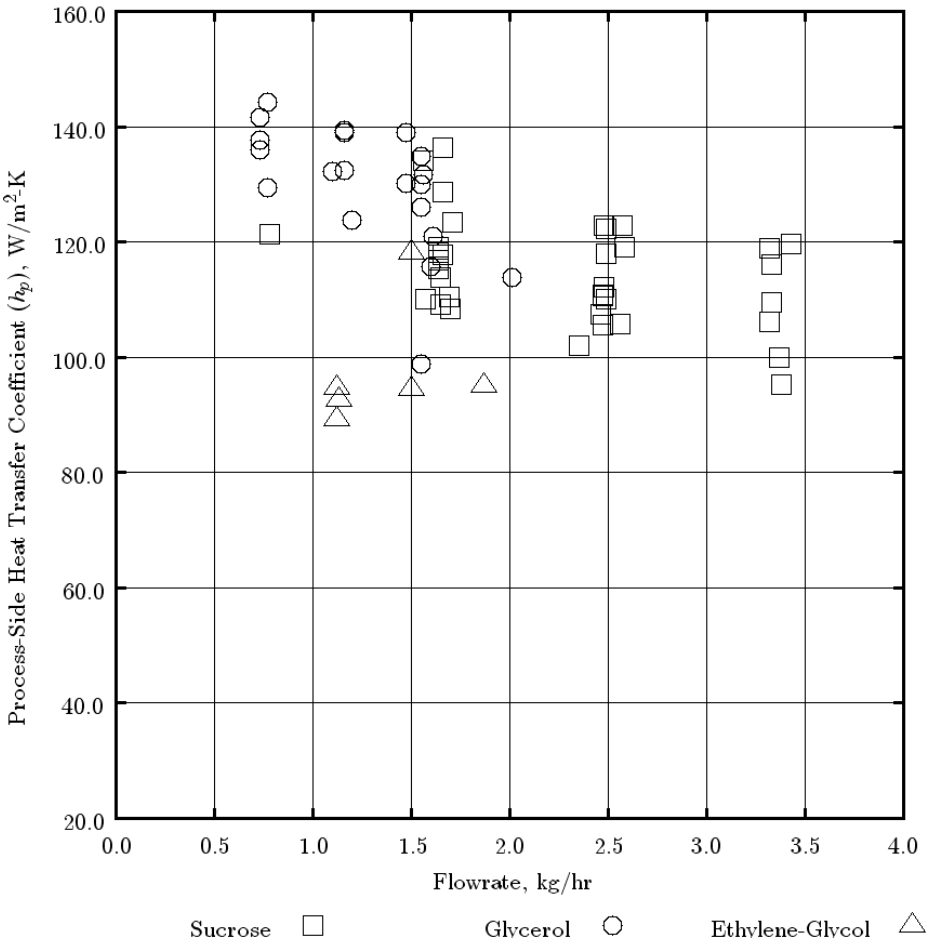

Figure 6.7: Experimental heat transfer coefficient for the process side as a function of the liquid feed flow rate.

6.2.2 Predicted Mass Transfer Coefficient

The proposed model predicts the mass transfer coefficient assuming the heat and mass transfer analogy. This means that the heat enhancement factor is the same as for mass transfer. The heat enhancement factor is predicted

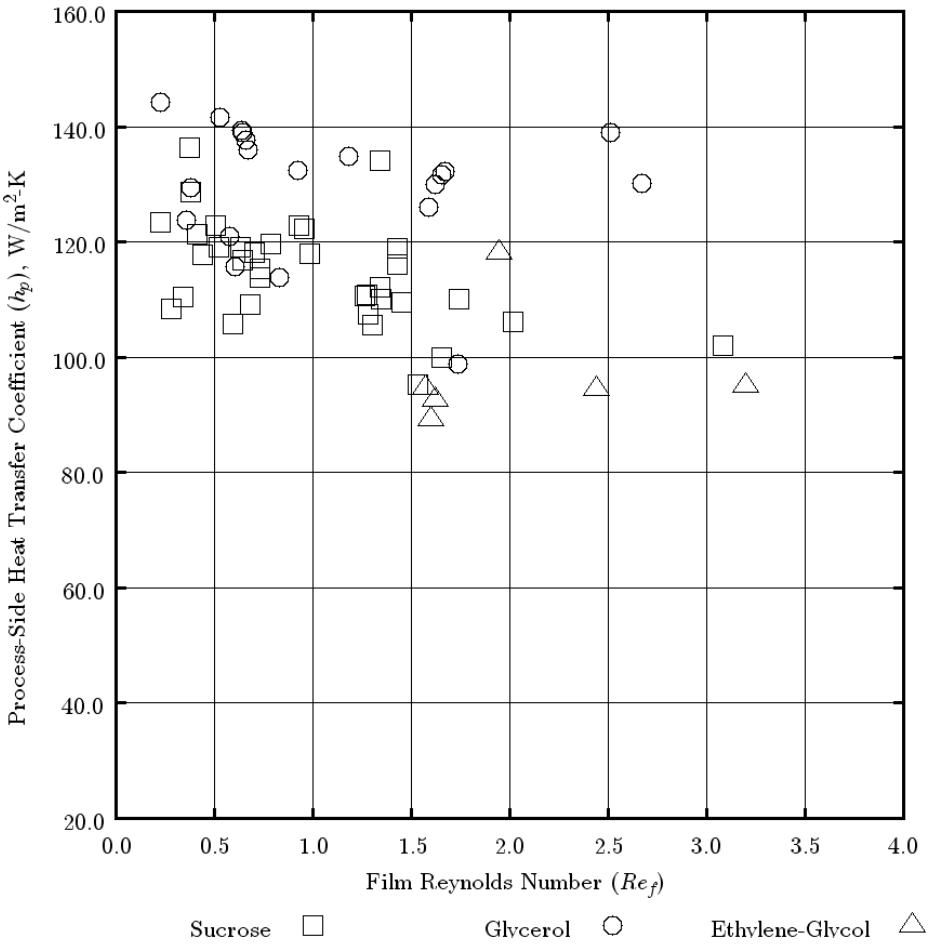

Figure 6.8: Experimental heat transfer coefficient for the process side as a function of the film Reynolds number.

with the following equation:

$$\beta_h = \frac{h_p^{WFE}}{h_p^{FFE}} \tag{4.6}$$

And the mass transfer coefficient for a falling film (k_L^{FFE}) with the

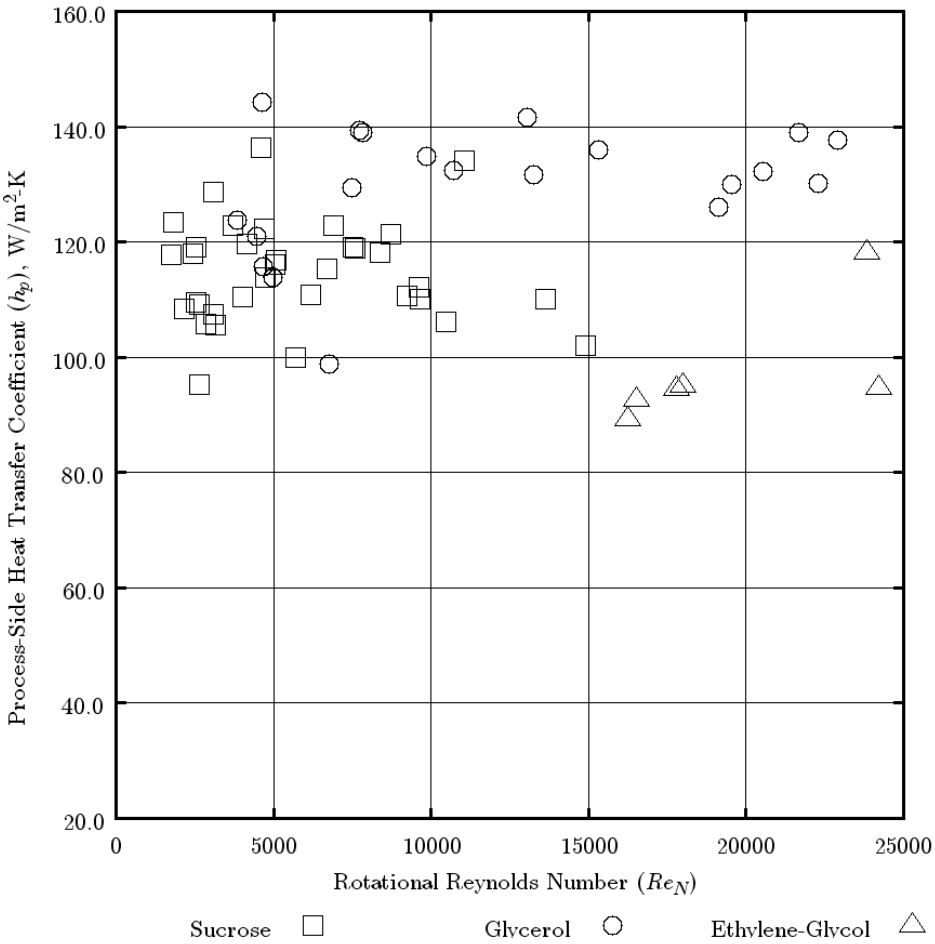

Figure 6.9: Experimental heat transfer coefficient for the process side as a function of the rotational Reynolds number.

correlation from Nielsen et al. [71]:

$$k_L^{FFE} = \left(a \cdot Re_f^b \cdot Sc_L^{1/2}\right)\left(\frac{D\rho_L^{2/3} g^{1/3}}{\mu_L^{2/3}}\right) \tag{3.36}$$

Then the mass transfer coefficient for wiped film evaporator (k_L^{WFE}) is

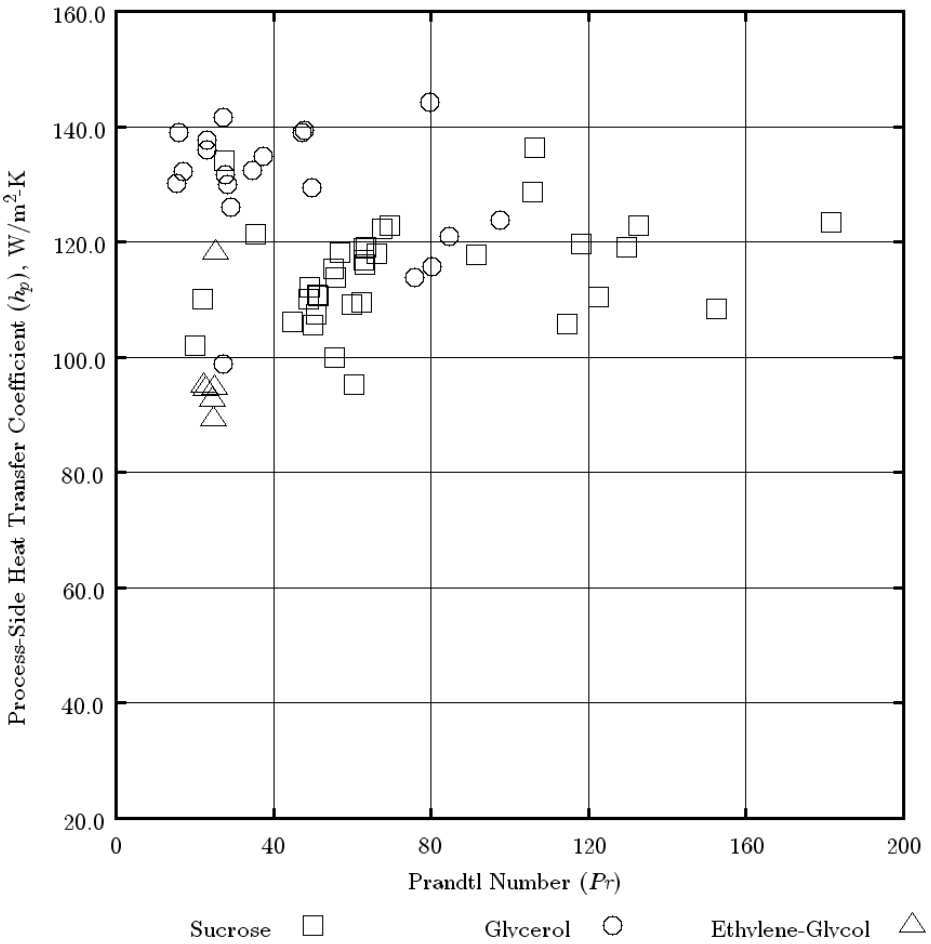

Figure 6.10: Experimental heat transfer coefficient for the process side as a function of the Prandtl number.

predicted with the equation:

$$k_L^{WFE} = \beta_h \cdot k_L^{FFE} \tag{4.29}$$

Because there are four possible combinations for the correlation of the heat enhancement factor, there will be four different correlated mass transfer

coefficients. Tables 6.5, 6.6, and 6.7 show the correlated values for k_L^{WFE} for water-sucrose, water-glycerol, and water-ethylene glycol, respectively.

Figures 6.11, 6.13, and 6.15 depict the correlated mass transfer coefficient when using the combination of models, Bott and Romero for the HTC of the wiped film evaporator and Ahmed and Kaparthi for the HTC of the falling film evaporator.

Figure 6.11 is for the water-sucrose system. It shows that the average mass transfer coefficient increases with the rotational speed and when the feed rate is increased. This is because at higher speeds, the rotational Reynolds number raises, increasing the heat transfer coefficient for the wiped film evaporator. This affects the value of the heat enhancement factor, which at the end increases the mass transfer coefficient. Figure 6.13 depicts a similar behavior for the water-glycerol system. The average mass transfer coefficient for this system is higher than for water-sucrose. This is because the viscosity of the system is lower, thus favoring mass transfer. Figure 6.15 displays the same pattern for water-ethylene glycol as the previous two systems: the average mass transfer coefficient is lower at low rotational speed and low flowrates. The value of the coefficient is higher than the other two systems too, because this system has the lowest viscosity of the three studied solutions.

Figures 6.12, 6.14, and 6.16 show the correlated mass transfer coefficient as a function of the dimensionless Sherwood number for the liquid. This number is obtained using the models of Bott and Romero [11] for the HTC for the WFE, Ahmed and Kaparthi [3] for the HTC for the FFE, and Yih and

Chen [98] for the mass transfer coefficient for the FFE, as follows:

$$Sh_L^{WFE} = \beta_h \times Sh_L^{FFE} \tag{6.11}$$

$$\beta_h = \frac{0.018 Re_f^{0.46} Re_N^{0.6} Pr^{0.87} \left(\frac{D}{L}\right)^{0.48} N_b^{0.24}}{6.92 \times 10^{-3} Re_L^{0.345} Pr_L^{0.4}} \tag{6.12}$$

$$Sh_L^{FFE} = 1.099 \times 10^{-2} Re_f^{0.3955} Sc_L^{1/2} \tag{6.13}$$

substituting the correlations for the Sherwood number for WFE:

$$Sh_L^{WFE} = 0.02859 Re_f^{0.5105} Re_N^{0.6} Pr_L^{0.47} (D/L)^{0.48} N_b^{0.24} Sc_L^{0.5} \tag{6.14}$$

Figure 6.12 for the water-sucrose syetem is not predicted with a single curve because. From Figure 6.11, it can be seen that the correlated mass transfer coefficients change for a fixed rotational speed. This is because data points with different compositions are included in the analysis, and this change the physical properties.

Figures 6.14 for the water-glycerol system and 6.16 for the water-ethylene glycol system, show a better fit with a single curve, although for Figure 6.14 there is a deviation at low Sherwood numbers. This is also because the data points represent different compositions for water-glycerol. The nice curve representing water-ethylene glycol is because only one inlet concentration was analyzed for this system.

Table 6.5: Correlated average mass transfer coefficient for the water-sucrose system. $k_L^{WFE} \times 10^5$, m/s

Feed	Re_f	Re_N	Pr	k_L^{WFE}, Equations 5.6-5.10, 5.11-5.17				k_L^{WFE}, GCM			
kg/hr				BS-AK	BS-N	BR-AK	BR-N	BS-AK	BS-N	BR-AK	BR-N
1.645	0.67	2400.1	74.8	0.65	1.56	1.09	2.67	3.24	5.99	9.08	16.79
1.659	0.41	1471.9	144.0	0.52	1.31	0.79	2.03	3.10	5.84	8.62	16.18
2.464	1.25	2892.7	56.7	0.87	1.97	1.41	3.18	4.02	7.16	10.30	18.37
2.472	1.30	2987.7	54.6	0.89	1.99	1.44	3.24	4.09	7.27	10.41	18.51
3.330	1.41	2393.3	68.4	0.93	2.08	1.35	3.03	4.63	8.12	10.92	19.13
3.382	1.54	2560.8	63.4	0.99	2.20	1.45	3.22	4.89	8.44	11.58	19.96
2.494	0.95	2191.5	77.8	0.77	1.79	1.16	2.74	3.92	7.07	9.91	17.86
1.648	0.74	4372.5	66.9	0.91	2.16	1.44	3.45	4.32	8.00	11.19	20.72
0.780	0.52	8118.7	58.8	0.75	1.89	1.52	3.91	3.16	6.26	9.51	18.77
1.564	1.35	10040.1	32.5	1.23	2.75	2.21	4.97	4.47	8.47	11.31	21.38
1.640	0.65	4687.1	76.4	0.96	2.33	1.45	3.52	4.86	9.03	12.17	22.59
1.664	0.37	2646.7	164.0	0.75	1.91	1.00	2.57	4.67	8.82	11.56	21.80
1.703	0.29	2034.5	207.3	0.72	1.88	0.90	2.36	5.01	9.27	12.42	22.97
1.705	0.24	1720.9	271.3	0.65	1.74	0.79	2.11	4.67	8.82	11.65	21.92
2.350	3.24	14932.4	20.1	1.90	3.93	3.37	6.98	6.07	10.78	14.01	24.88
2.470	1.25	5794.6	56.4	1.32	3.00	1.89	4.26	6.11	10.90	13.90	24.82
2.488	0.92	4282.9	79.7	1.15	2.68	1.57	3.62	5.91	10.68	13.30	24.04
2.557	0.58	2679.9	131.3	1.01	2.46	1.22	2.99	6.33	11.24	14.23	25.26
2.578	0.52	2365.0	152.0	0.94	2.31	1.11	2.72	6.10	10.97	13.58	24.42
3.327	1.39	4726.2	69.3	1.40	3.15	1.80	4.06	6.96	12.22	14.64	25.71
3.365	1.66	5540.3	58.2	1.54	3.39	2.04	4.48	7.34	12.68	15.50	26.79
1.568	1.82	13144.7	23.6	1.43	3.13	2.72	5.93	4.94	9.07	12.40	22.79

Continued on next page

Table 6.5 – continued from previous page

Feed kg/hr	Re_f	Re_N	Pr	k_L^{WFE}, Equations 5.6-5.10, 5.11-5.17				k_L^{WFE}, GCM			
				BS-AK	BS-N	BR-AK	BR-N	BS-AK	BS-N	BR-AK	BR-N
1.640	0.71	5981.6	69.3	1.09	2.62	1.64	3.94	5.33	9.90	13.00	24.13
1.636	0.63	6840.8	79.8	1.21	2.94	1.70	4.14	6.15	11.44	14.41	26.83
2.571	0.50	3433.0	159.3	1.20	2.94	1.29	3.23	7.73	13.93	16.11	29.02
1.638	0.70	7576.3	70.8	1.26	3.03	1.84	4.35	6.19	11.50	14.46	26.89
1.662	0.36	3971.9	159.7	0.95	2.45	1.19	3.08	5.92	11.23	13.73	25.95
1.692	0.35	3692.9	164.0	0.98	2.52	1.19	3.09	6.31	11.70	14.67	27.20
2.468	1.24	8650.7	56.8	1.68	3.82	2.25	5.12	7.77	13.88	16.52	29.53
2.483	0.91	6395.3	79.4	1.46	3.39	1.83	4.25	7.51	13.60	15.79	28.60
2.483	1.32	9096.7	53.7	1.72	3.90	2.32	5.27	7.88	14.03	16.69	29.74
2.486	1.32	9064.8	54.0	1.72	3.90	2.32	5.26	7.89	14.05	16.70	29.76
3.321	2.01	10112.3	47.1	2.11	4.54	2.72	5.86	9.17	15.91	18.21	31.59
3.325	1.37	7027.9	70.0	1.78	4.01	2.13	4.82	8.83	15.53	17.36	30.53
3.430	0.78	3942.1	129.9	1.46	3.46	1.54	3.65	9.07	15.88	17.69	30.97

Table 6.6: Correlated average mass transfer coefficient for the water-glycerol system. $k_L^{WFE} \times 10^5$, m/s.

Feed kg/hr	Re_f	Re_N	Pr	k_L^{WFE}, DIPPR				k_L^{WFE}, GCM			
				BS-AK	BS-N	BR-AK	BR-N	BS-AK	BS-N	BR-AK	BR-N
1.5552	2.74	7776.3	22.0	3.06	6.34	5.94	12.30	3.09	6.68	5.05	10.90
0.774	0.69	4669.9	42.4	1.97	4.61	4.04	9.65	2.11	5.09	3.49	8.84
1.203	0.79	6291.1	58.7	3.55	8.28	5.31	12.39	3.60	9.15	3.92	9.93
2.010	1.49	6957.5	52.5	4.72	10.43	6.45	14.28	4.89	11.50	5.13	12.04
1.605	1.05	6301.6	58.6	4.11	9.36	5.78	13.20	4.27	10.39	4.54	11.04
1.598	1.13	6742.5	54.4	4.27	9.66	6.09	13.81	4.40	10.66	4.77	11.53
1.161	1.24	10844.3	34.7	3.87	8.63	6.68	14.95	4.06	9.42	5.80	13.49
1.158	0.79	7243.8	59.3	3.48	8.16	5.55	13.22	3.71	8.99	4.91	12.21
1.545	1.53	9834.3	37.1	4.11	9.01	6.56	14.40	4.23	9.68	5.64	13.06
1.156	0.80	7352.0	57.9	3.34	7.82	5.35	12.70	3.56	8.59	4.81	11.66
0.770	0.48	6609.3	75.7	2.57	6.20	4.39	10.69	2.66	6.83	3.56	9.32
0.775	0.63	8567.1	52.6	2.90	6.83	5.20	12.42	3.05	7.59	4.31	11.11
1.556	2.08	13018.7	27.2	4.32	9.23	7.28	15.54	4.52	9.99	6.38	14.20
0.733	1.41	20149.4	17.7	2.90	6.28	6.55	14.23	2.93	6.55	5.79	13.13
0.731	0.76	12116.1	40.6	2.64	6.20	5.39	13.13	2.79	6.66	4.98	12.47
1.467	2.77	19452.9	17.1	4.17	8.69	8.06	16.89	4.33	9.11	7.66	16.17
1.100	2.26	21538.6	15.6	3.87	8.21	8.15	17.35	4.04	8.67	7.66	16.63
1.467	3.86	24915.9	12.8	4.48	9.01	9.04	18.18	4.57	9.35	8.42	17.24
1.549	2.26	13704.9	25.4	4.42	9.37	7.50	15.88	4.54	10.01	6.42	14.18
1.554	2.55	22486.9	22.9	5.79	12.14	9.30	19.49	5.86	12.82	7.86	17.20
0.731	1.06	24733.4	24.7	3.68	8.34	7.46	17.37	3.91	9.01	7.01	16.77

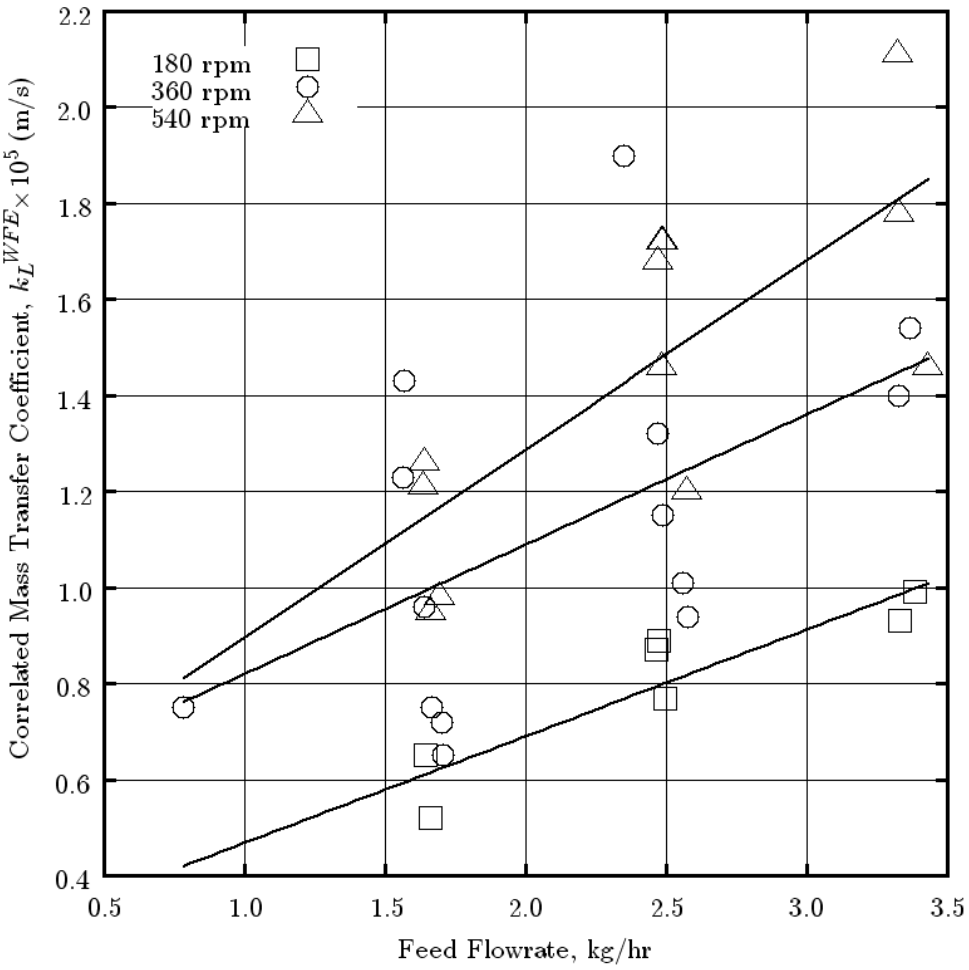

Figure 6.11: Correlated average mass transfer coefficient for the water-sucrose system as a function of feed flowrate at different rotational speeds.

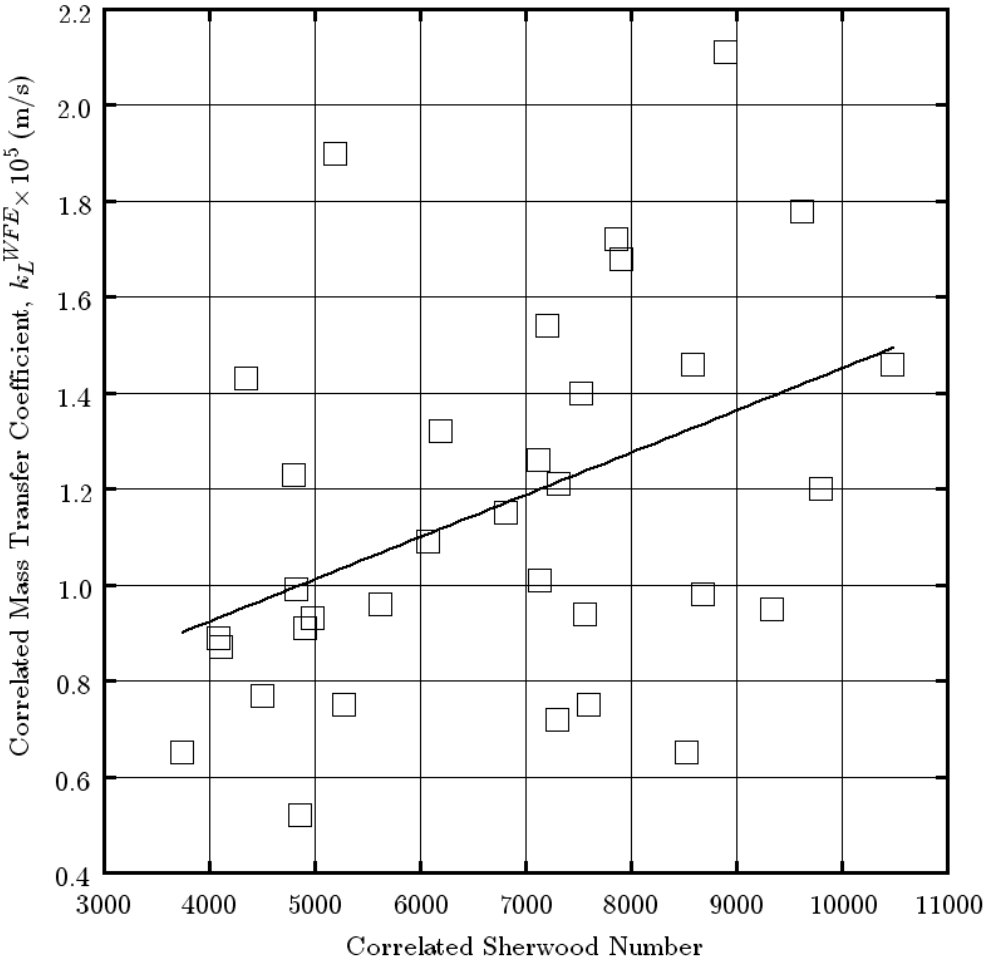

Figure 6.12: Correlated average mass transfer coefficient for the water-sucrose system as a function of the dimensionless Sherwood number ($Sh_L^{WFE} = 0.02859 Re_f^{0.5105} Re_N^{0.6} Pr_L^{0.47} (D/L)^{0.48} N_b^{0.24} Sc_L^{0.5}$).

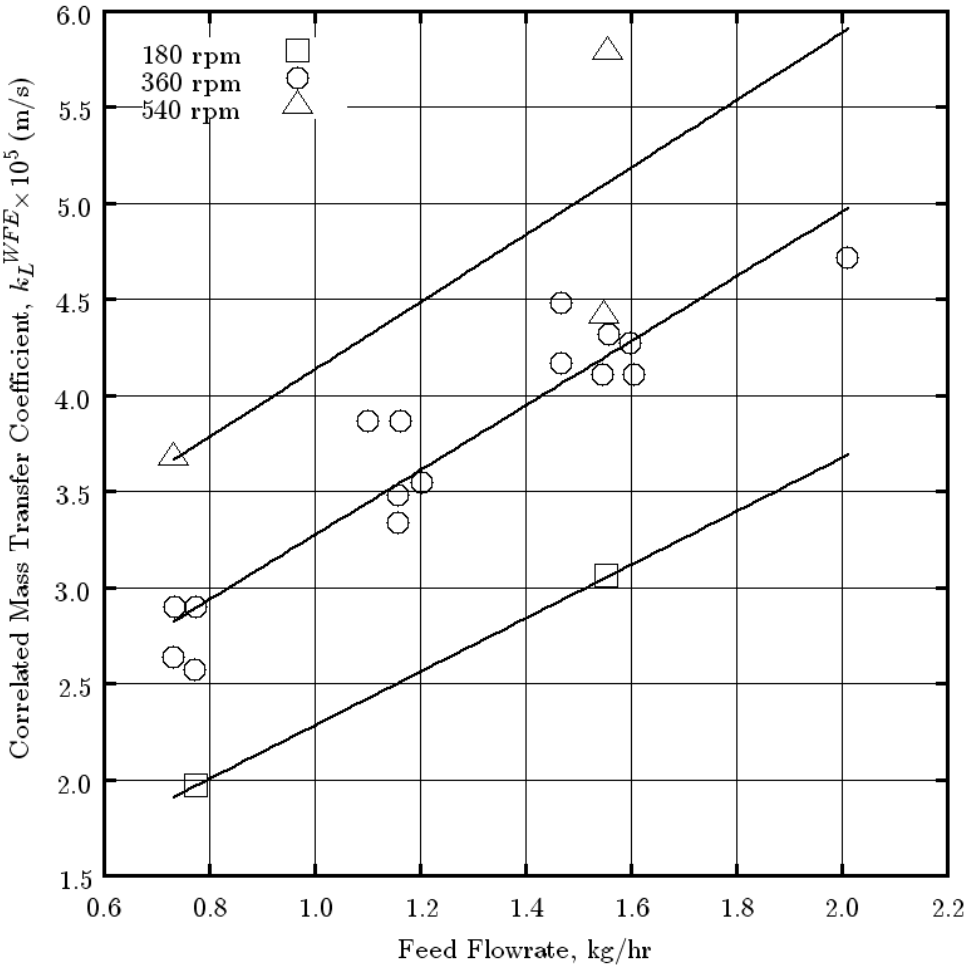

Figure 6.13: Correlated average mass transfer coefficient for the water-glycerol system as a function of feed flowrate at different rotational speeds.

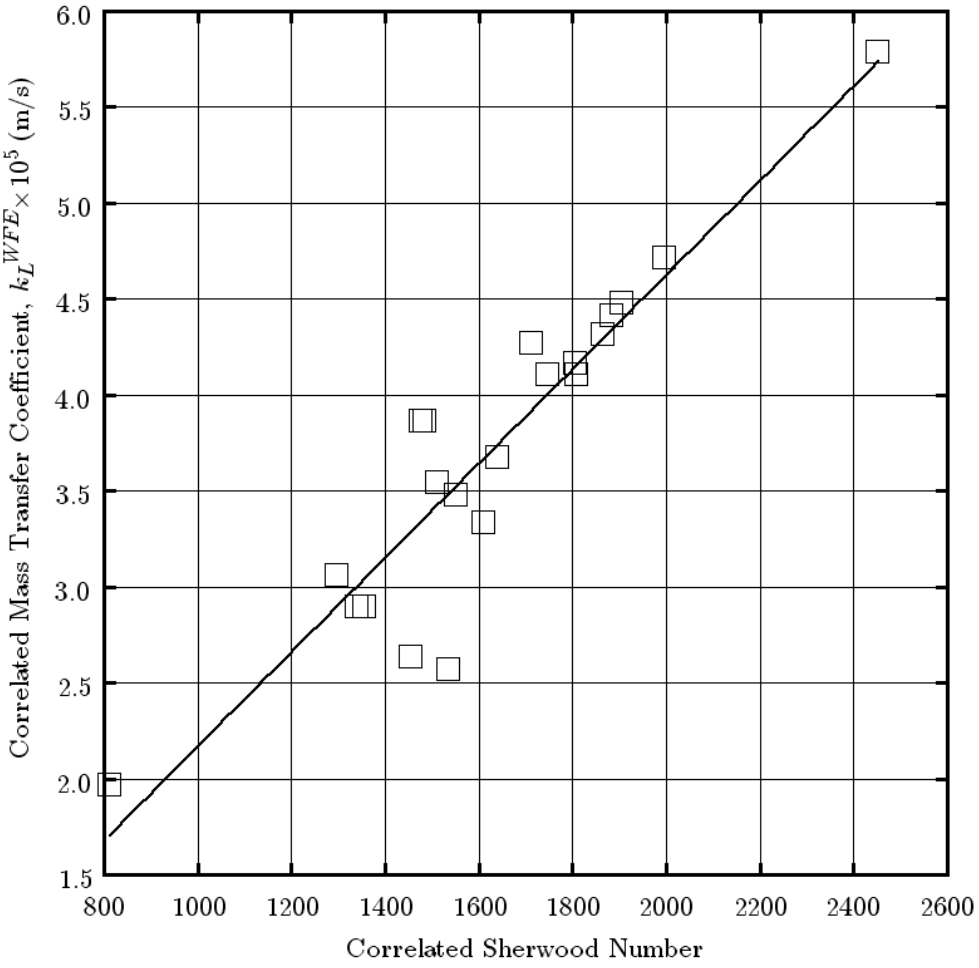

Figure 6.14: Correlated average mass transfer coefficient for the water-glycerol system as a function of the dimensionless Sherwood number ($Sh_L^{WFE} = 0.02859 Re_f^{0.5105} Re_N^{0.6} Pr_L^{0.47} (D/L)^{0.48} N_b^{0.24} Sc_L^{0.5}$).

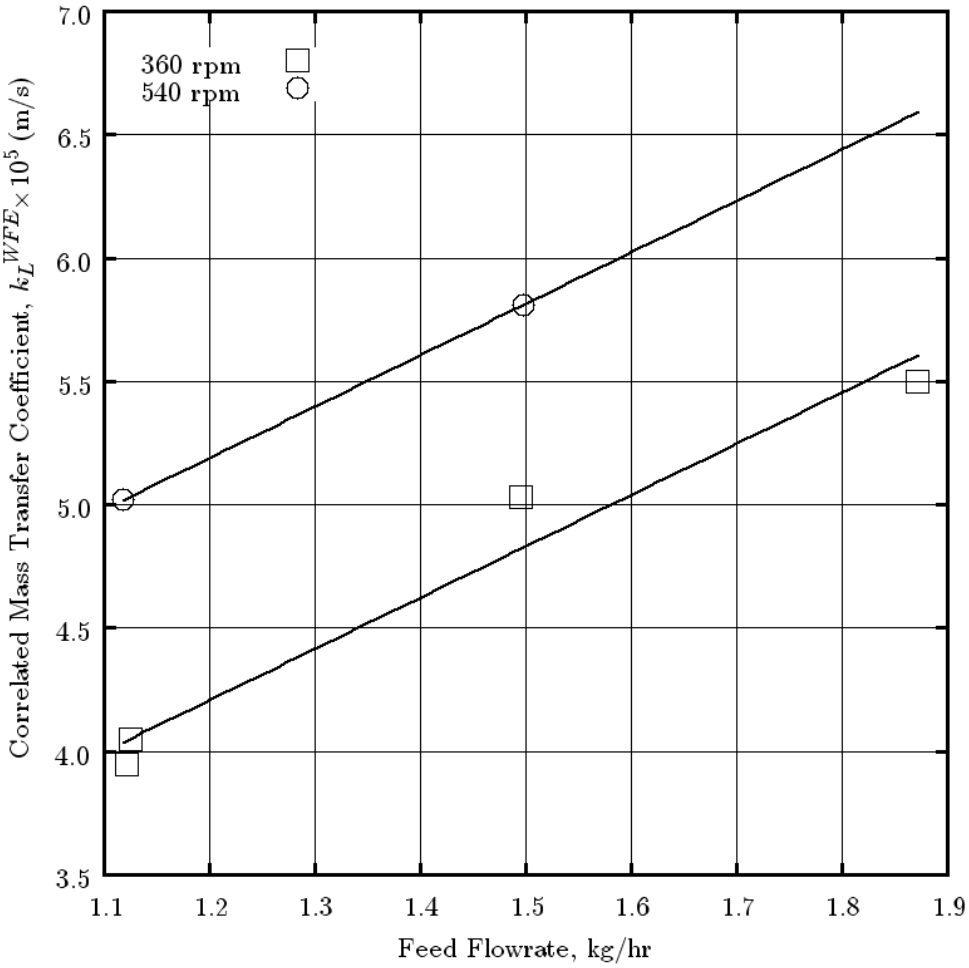

Figure 6.15: Correlated average mass transfer coefficient for the water-ethylene glycol system as a function of feed flowrate at different rotational speeds.

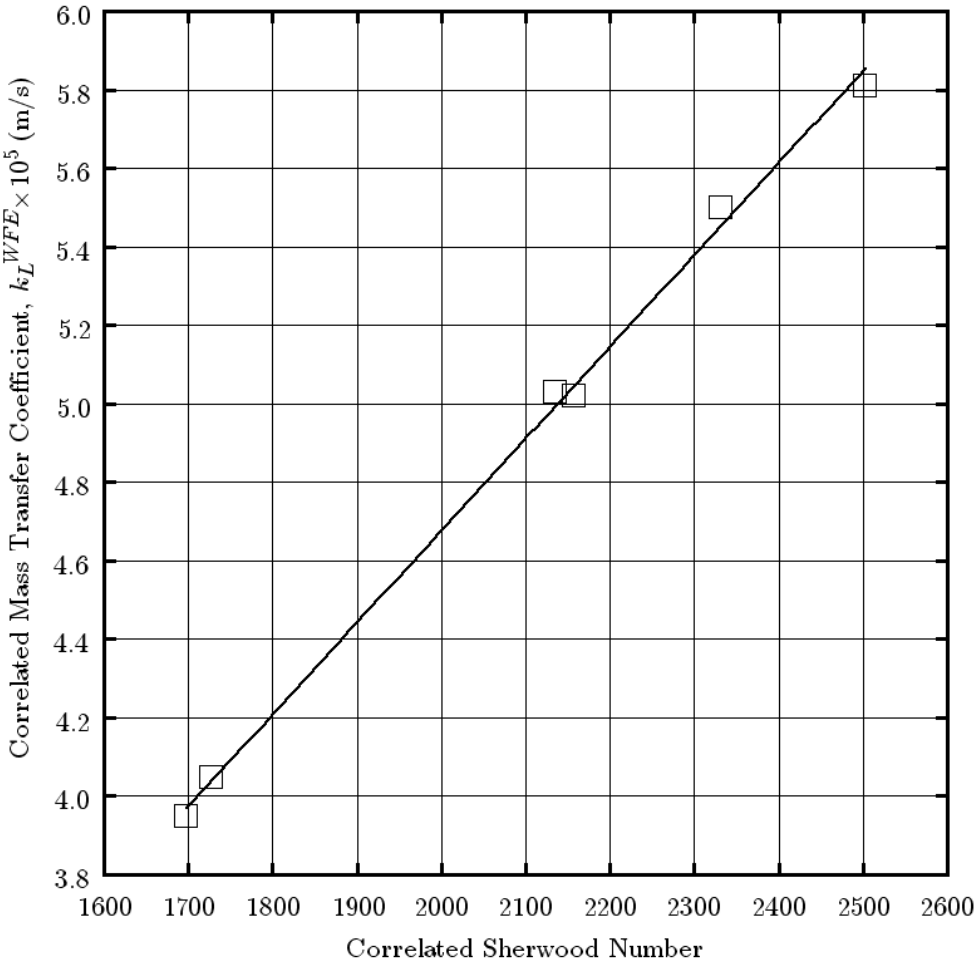

Figure 6.16: Correlated average mass transfer coefficient for the water-ethylene glycol system as a function of the dimensionless Sherwood number ($Sh_L^{WFE} = 0.02859 Re_f^{0.5105} Re_N^{0.6} Pr_L^{0.47} (D/L)^{0.48} N_b^{0.24} Sc_L^{0.5}$).

Table 6.7: Correlated average mass transfer coefficient for the water-ethylene glycol system. $k_L^{WFE} \times 10^5$, m/s

Feed kg/hr	Re_f	Re_N	Pr	k_L^{WFE}, DIPPR				k_L^{WFE}, GCM			
				BS-AK	BS-N	BR-AK	BR-N	BS-AK	BS-N	BR-AK	BR-N
1.125	1.80	15051.6	26.4	4.05	8.71	6.93	14.93	4.10	9.01	6.42	14.37
1.495	3.30	18661.52	20.64	5.03	10.29	8.39	17.18	4.93	10.38	7.52	15.91
1.871	3.71	17478.44	22.23	5.50	11.16	8.67	17.58	5.53	11.43	8.06	16.72
1.121	1.61	13822.35	29.18	3.95	8.59	6.67	14.52	4.08	9.01	6.36	14.11
1.118	1.59	20664.01	29.28	5.02	10.96	7.91	17.29	5.19	11.50	7.56	16.86
1.498	2.12	20670.08	29.31	5.81	12.34	8.63	18.33	5.97	12.91	7.99	17.40

6.3 WFE-SRP Model Applied to Experimental Data

The WFE-SRP computer program was used to analyze the experimental data. As the program has the option of using DIPPR equations to calculate the physical properties and group contribution methods (GCM) to predict the physical properties, a comparison was carried out for the three experimental systems.

WFE-SRP has two models for the prediction of the process side heat transfer coefficient for a wiped film evaporator [11, 14] and two for the falling film evaporator [3, 73], thus giving four different combinations for the heat enhancement factor (β_h), and predicting four different exiting concentrations of water. The following sections present the results when the computer program is applied to the experimental data for each system.

6.3.1 Water-Sucrose

The WFE-SRP program was used with Equations 5.6-5.10 for the prediction of physical properties, and the modified UNIQUAC equations from Peres and Macedo [75] for the prediction of the activity coefficients (Equations 5.11-5.17), as well as the group contribution methods for physical properties and activity coefficient. Figure 6.17 shows the prediction of the concentration of water when using Bott and Romero [11] for the HTC of the wiped film evaporator and Ahmed and Kaparthi [3] for the falling film evaporator, while Figure 6.18 presents the relative error using the same equations. The average error for the combination of the equations was 0.21%, and for the

GCM was 1.36%.

The experiments using water-sucrose were run at different inlet concentrations of sucrose, varying from 35 to 55 wt percent. They were not run at higher concentrations due to the solubility limit of sucrose in water at 20 °C. Outlet concentrations varied from 40 to 66 wt percent of sucrose.

From Figure 6.17 it can be seen that the computer program predicts the exiting concentration of water with good accuracy when using Equations 5.6-5.10 for physical properties and 5.11-5.17 for the activity coefficient. The GCM option is less accurate. This is mainly due to the estimation of viscosity and liquid enthalpies that are very different from the actual values. When the evaporation rate is low (i.e., concentration of water > 0.95) the prediction is more accurate than when the evaporation rate is high.

Using the combination of equations with the Bott and Sheikh [14] correlation for the wiped film evaporator, gives a similar result as shown in Figure 6.19. The average error was 0.10% and 1.38%. Figure 6.20 depicts the relative error for this combination.

From these plots, it can be seen than when using the Equations 5.6-5.10 for the prediction of physical properties, and the modified UNIQUAC equations from Peres and Macedo [75] for the prediction of the activity coefficients (Equations 5.11-5.17) in the WFE-SRP program, the prediction of exiting composition of water is very accurate. This confirms that the proposed model predicts the behavior of the water-sucrose system.

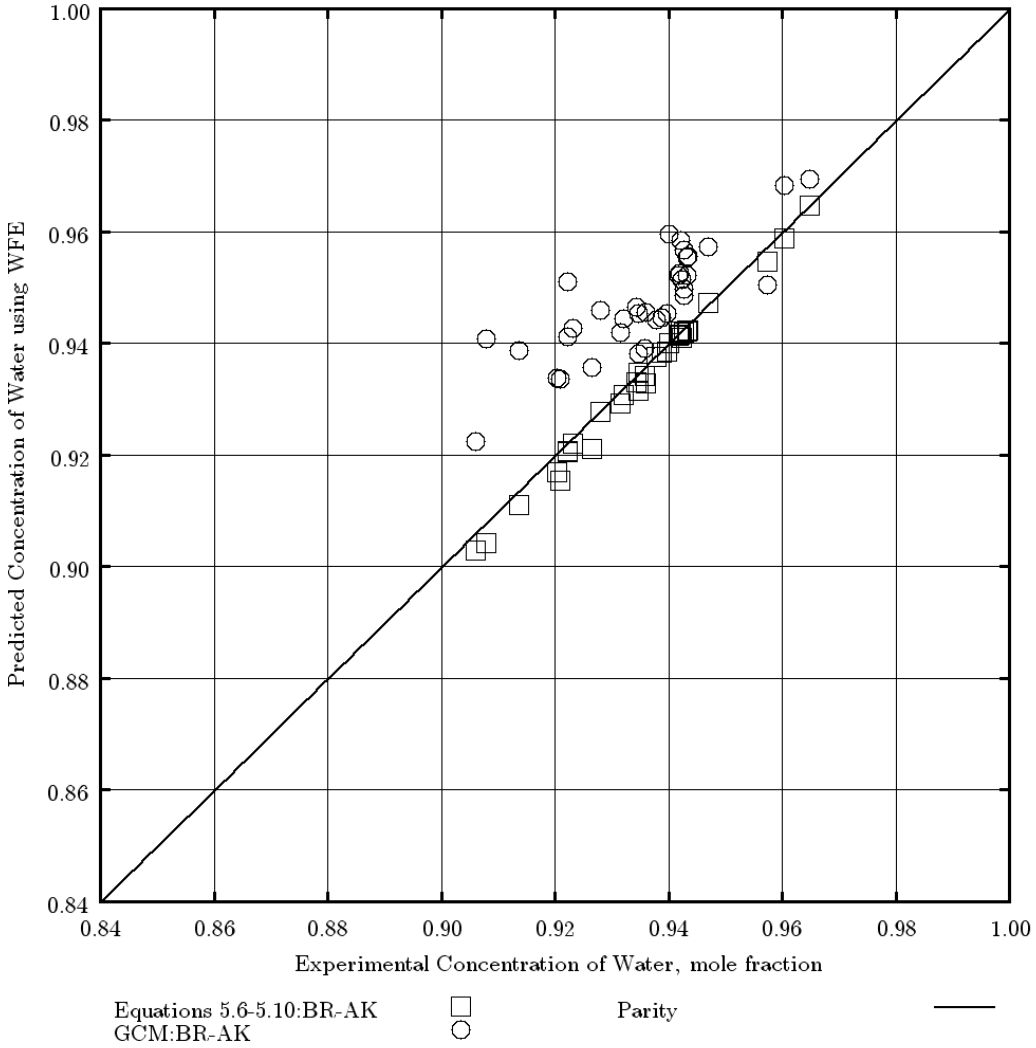

Figure 6.17: Predicted versus experimental exiting concentration of water using WFE-SRP for the water-sucrose system when using Equations 5.6-5.17 and GCM for physical properties and Bott and Romero-Ahmed and Kaparthi for HTC.

6.3.2 Water-Glycerol

The WFE-SRP program was used with the DIPPR equations, as well as the group contribution methods, for the prediction of physical properties.

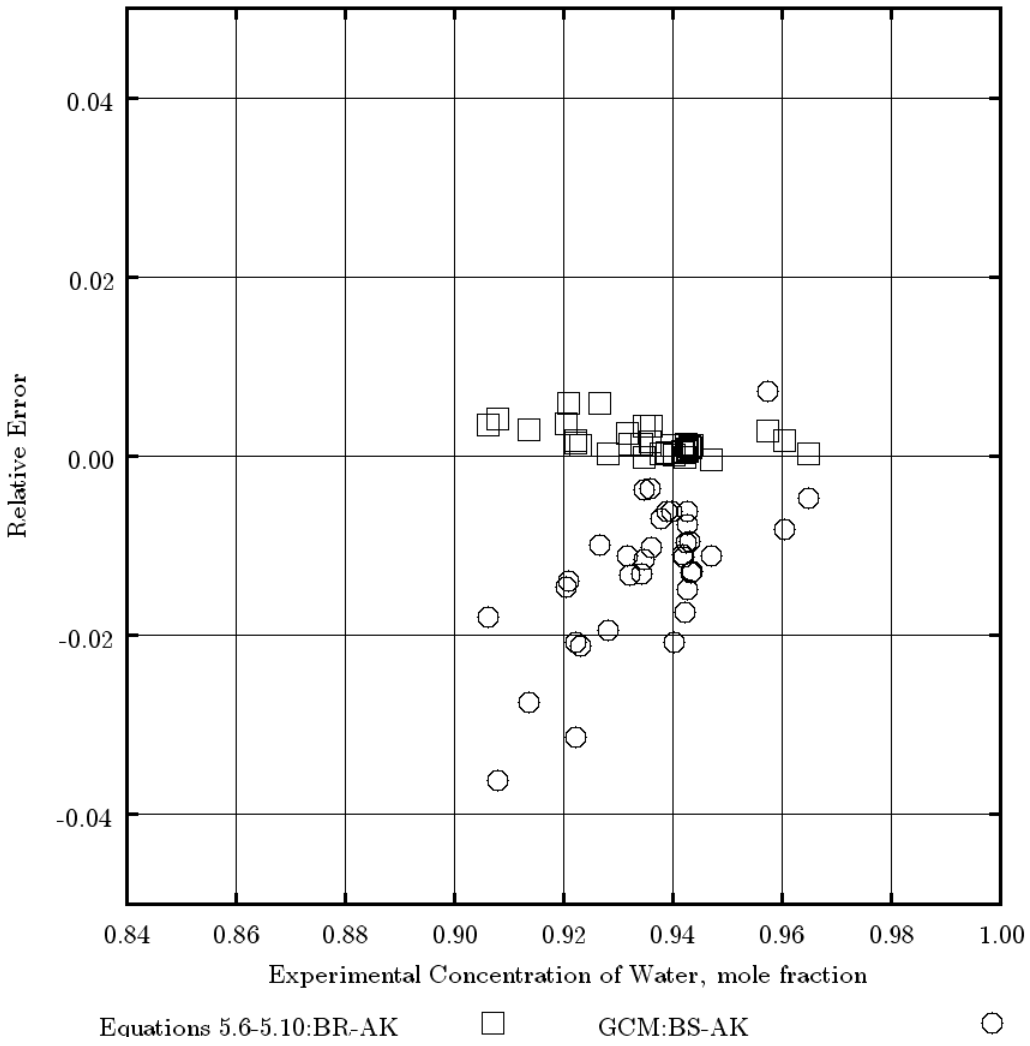

Figure 6.18: Relative error of the experimental exiting concentration of water using WFE-SRP for the water-sucrose system when using Equations 5.6-5.17 and GCM for physical properties and Bott and Romero-Ahmed and Kaparthi for HTC.

Figure 6.21 shows the prediction of the concentration of water when using Bott and Romero [11] for the HTC of the wiped film evaporator and Ahmed

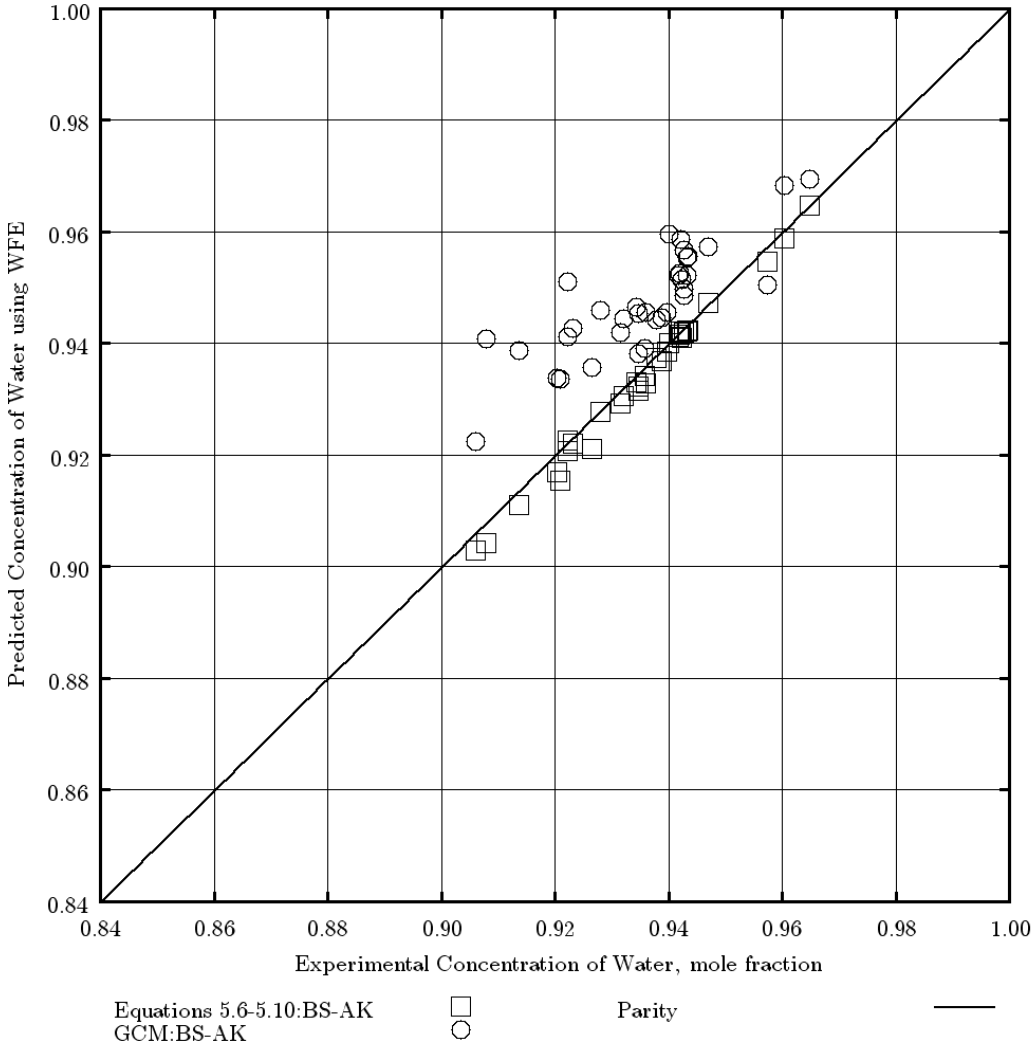

Figure 6.19: Predicted versus experimental exiting concentration of water using WFE-SRP for the water-sucrose system when using Equations 5.6-5.17 and GCM for physical properties and Bott and Sheikh-Ahmed and Kaparthi for HTC.

and Kaparthi [3] for the falling film evaporator, while Figure 6.22 presents the relative error using the same equations. The average error for the combination

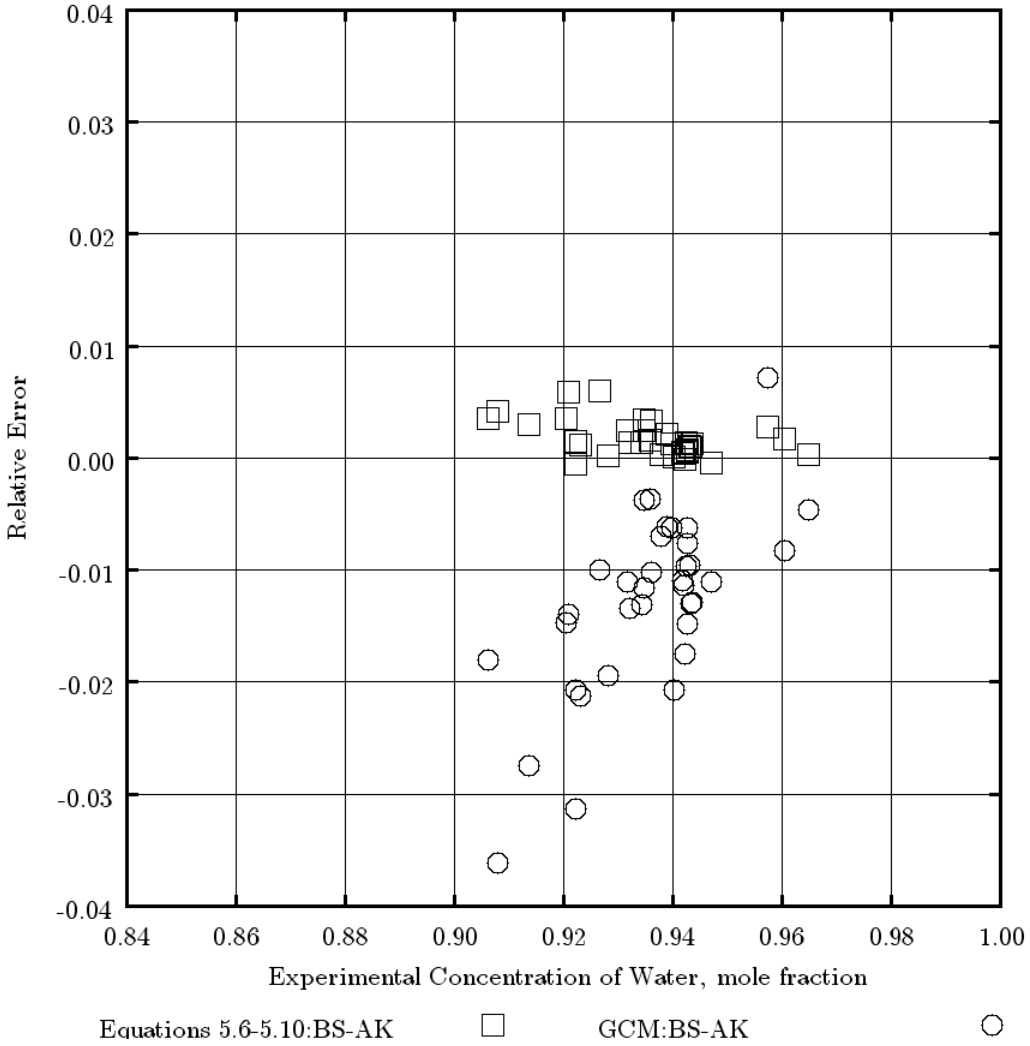

Figure 6.20: Relative error of the experimental exiting concentration of water using WFE-SRP for the water-sucrose system when using Equations 5.6-5.17 and GCM for physical properties and Bott and Sheikh-Ahmed and Kaparthi for HTC.

of the equations was 10.92%, and for the GCM was 6.23%.

These experiments were also run at different inlet concentrations of

glycerol, varying from 38 to 75 wt percent. The outlet concentrations varied from 48 to 90 wt percent of glycerol.

From Figure 6.21 it can be seen that the computer program predicts the exiting concentration of water with excellent accuracy for all the range of exiting water composition. The GCM method works even better than the DIPPR prediction for this system.

Using the combination of equations with the Bott and Sheikh [14] correlation for wiped film evaporators, gives a similar result as shown in Figure 6.23. The average error was 9.59% and 2.74%. Figure 6.24 shows the relative error for this combination.

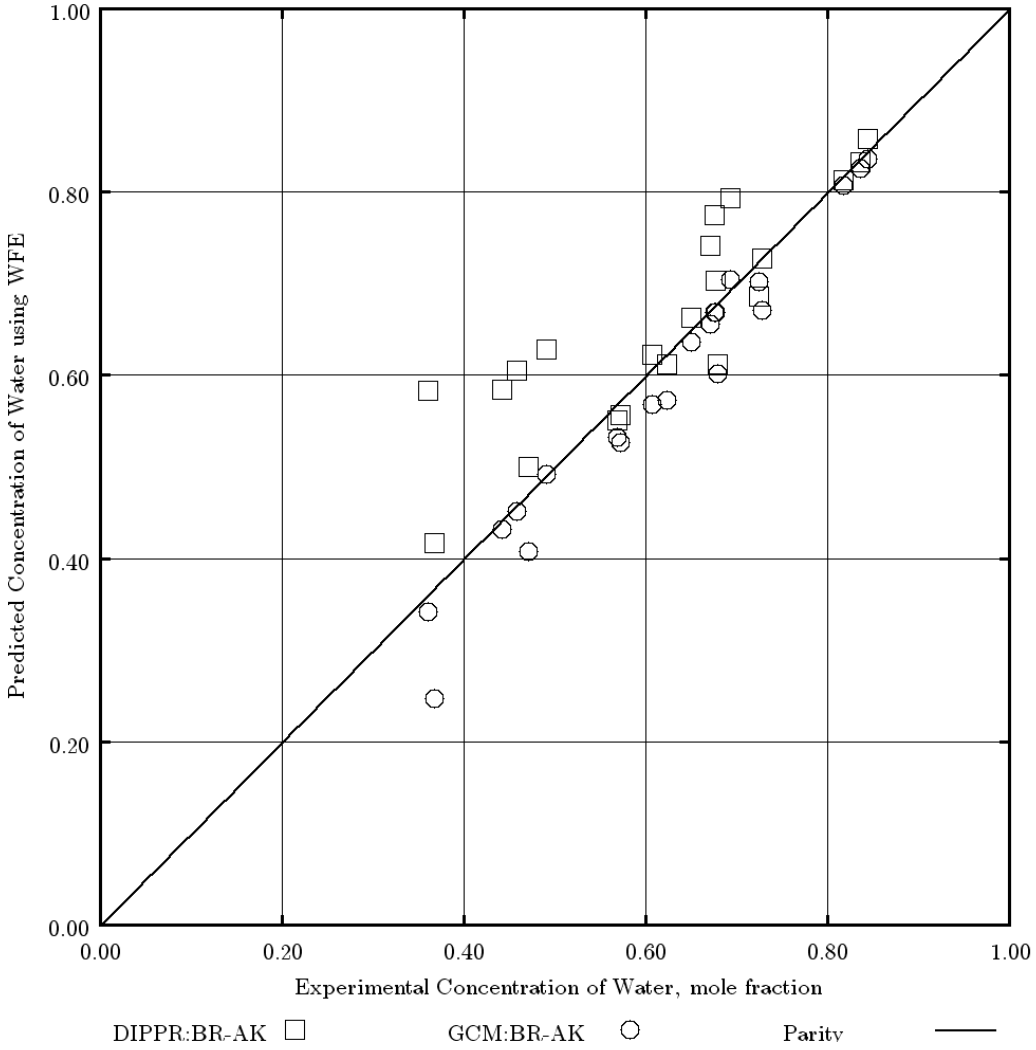

Figure 6.21: Predicted versus experimental exiting concentration of water using WFE-SRP for the water-glycerol system when using DIPPR and GCM for physical properties and Bott and Romero-Ahmed and Kaparthi for HTC.

6.3.3 Water-Ethylene Glycol

The WFE-SRP computer program was also used with the DIPPR equations, as well as the group contribution methods for the prediction of physical

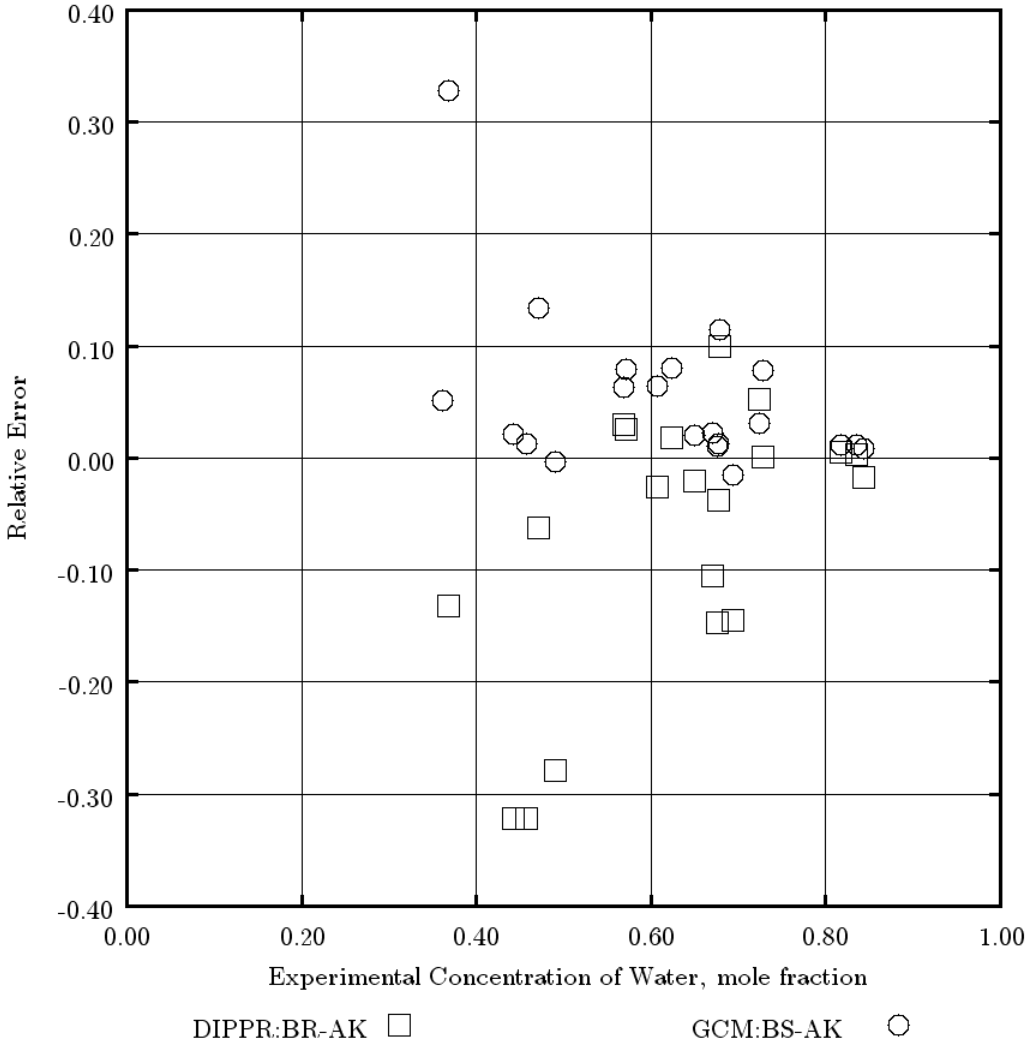

Figure 6.22: Relative error of the experimental exiting concentration of water using WFE-SRP for the water-glycerol system when using DIPPR and GCM for physical properties and Bott and Romero-Ahmed and Kaparthi for HTC.

properties for the six experimental data points. Figure 6.25 shows the prediction of the concentration of water when using Bott and Romero [11] for the

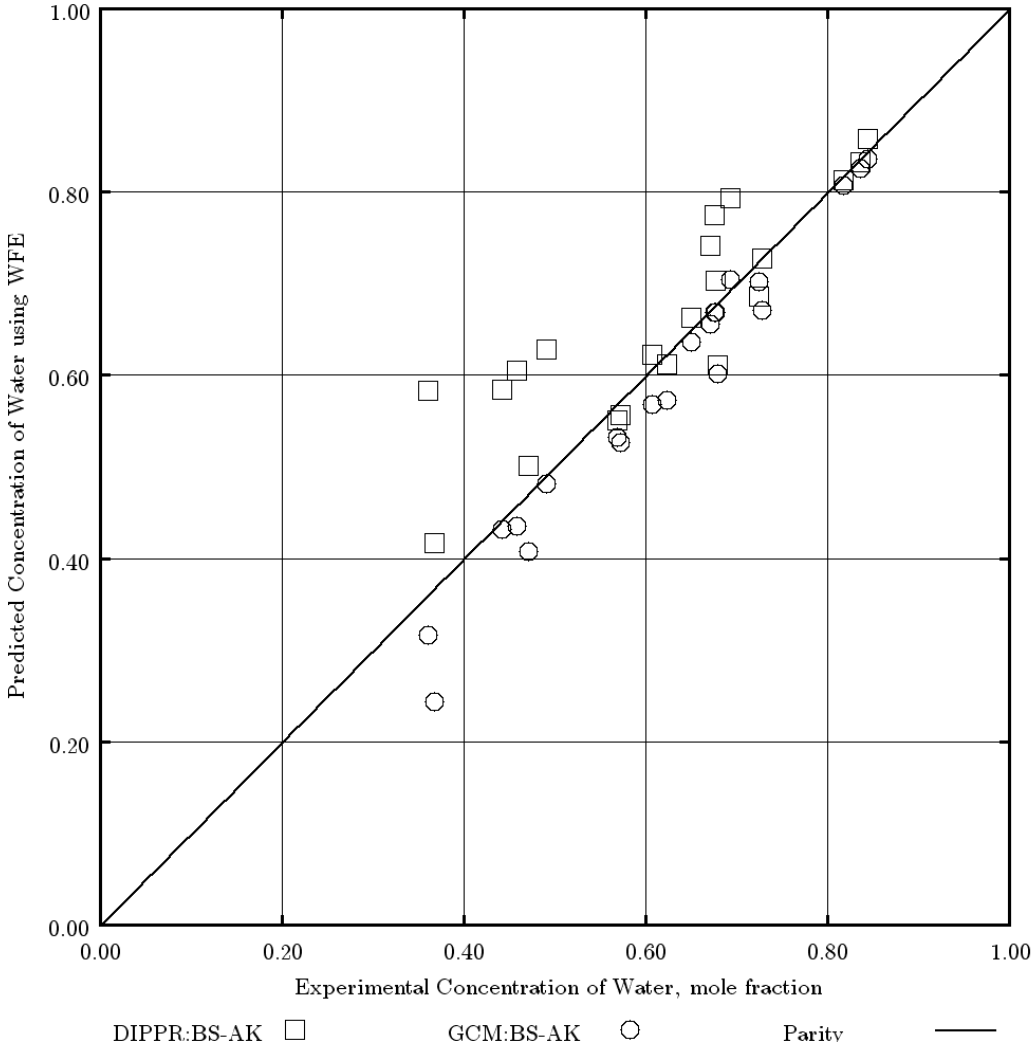

Figure 6.23: Predicted versus experimental exiting concentration of water using WFE-SRP for the water-glycerol system when using DIPPR and GCM for physical properties and Bott and Sheikh-Ahmed and Kaparthi for HTC.

HTC of the wiped film evaporator and Ahmed and Kaparthi [3] for the falling film evaporator, while Figure 6.26 presents the relative error using the same

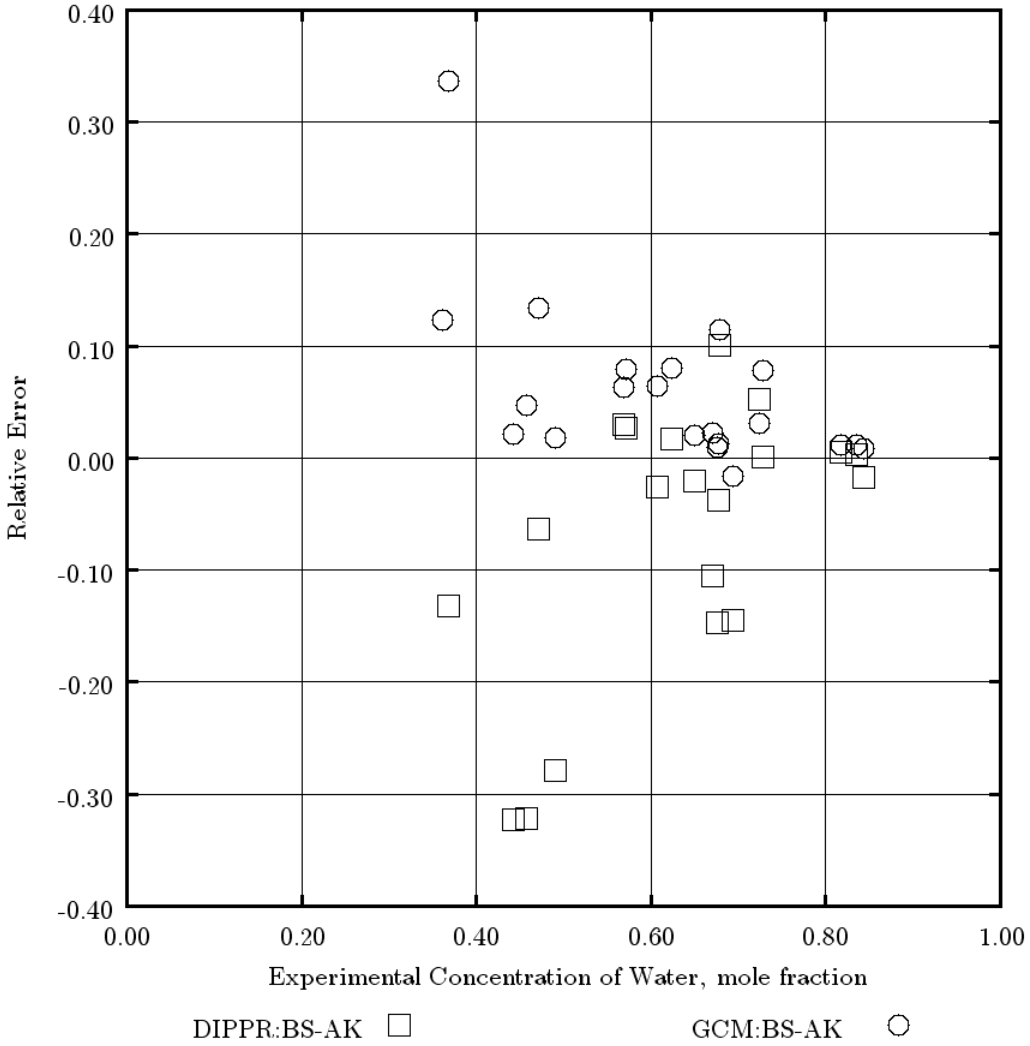

Figure 6.24: Relative error of the experimental exiting concentration of water using WFE-SRP for the water-glycerol system when using DIPPR and GCM for physical properties and Bott and Sheikh-Ahmed and Kaparthi for HTC.

equations. The average error for the combination of the equations was 38.12%, and for the GCM was 4.91%.

These experiments were run at only one inlet concentration of ethylene glycol, around 75 wt percent. The outlet concentrations varied from 83 to 95 wt percent of glycerol.

From Figure 6.25, it can be seen that the computer program predicts the exiting concentration of water with good accuracy for the range of exiting water composition. The GCM method works even better than the DIPPR prediction for this system.

Using the combination of equations with the Bott and Sheikh [14] correlation for a wiped film evaporator, gives a similar result as shown in Figure 6.27. The average error was 35.90% and 13.63%. Figure 6.28 shows the relative error for this combination.

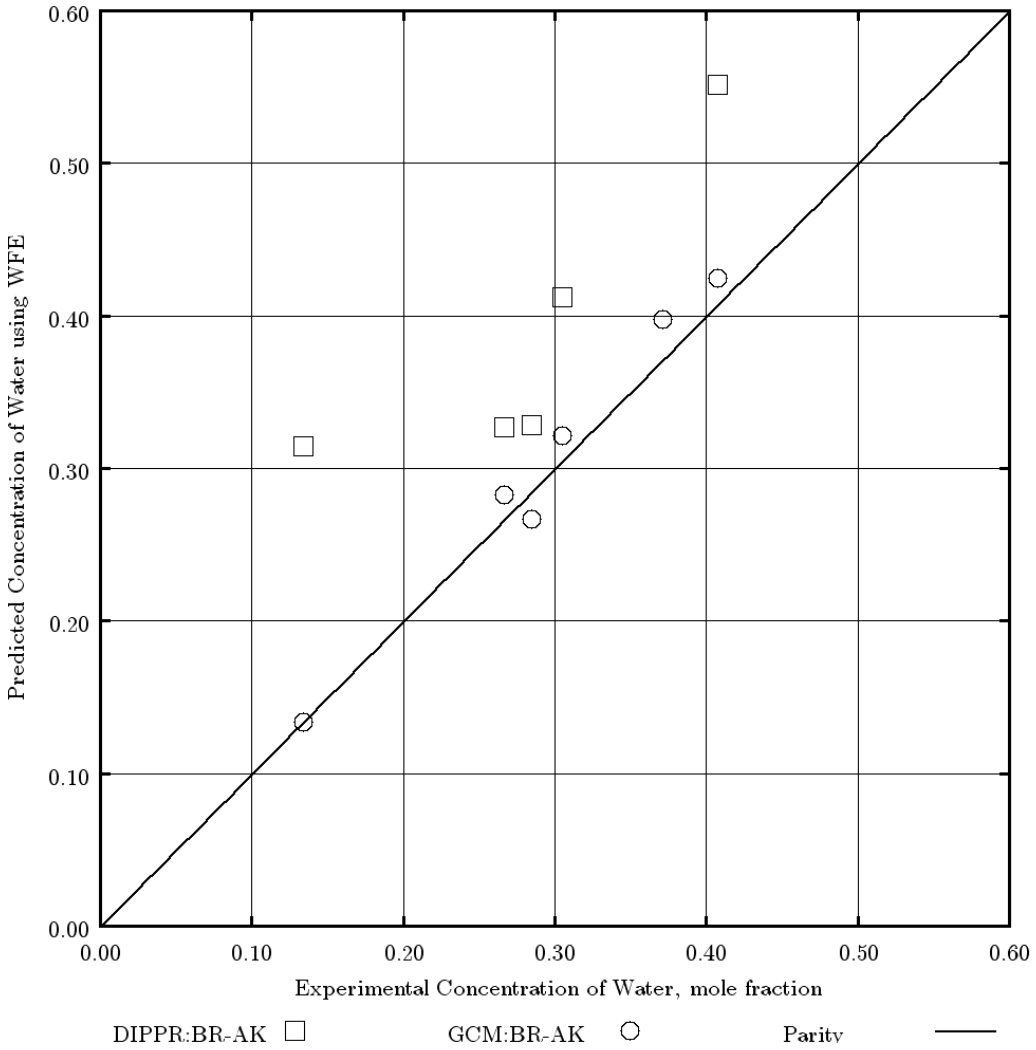

Figure 6.25: Predicted versus experimental exiting concentration of water using WFE-SRP for the water-ethylene glycol system when using DIPPR and GCM for physical properties and Bott and Romero-Ahmed and Kaparthi for HTC.

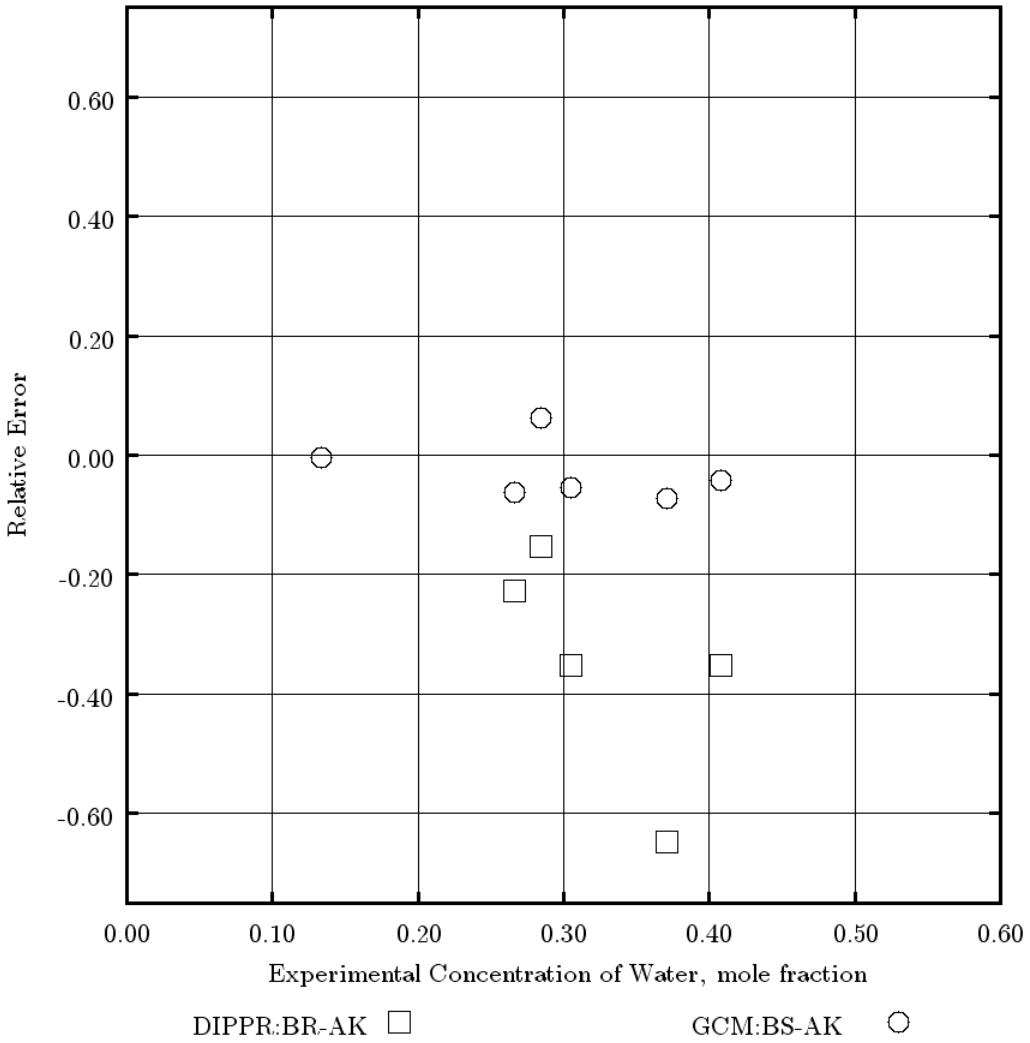

Figure 6.26: Relative error of the experimental exiting concentration of water using WFE-SRP for the water-ethylene glycol system when using DIPPR and GCM for physical properties and Bott and Romero-Ahmed and Kaparthi for HTC.

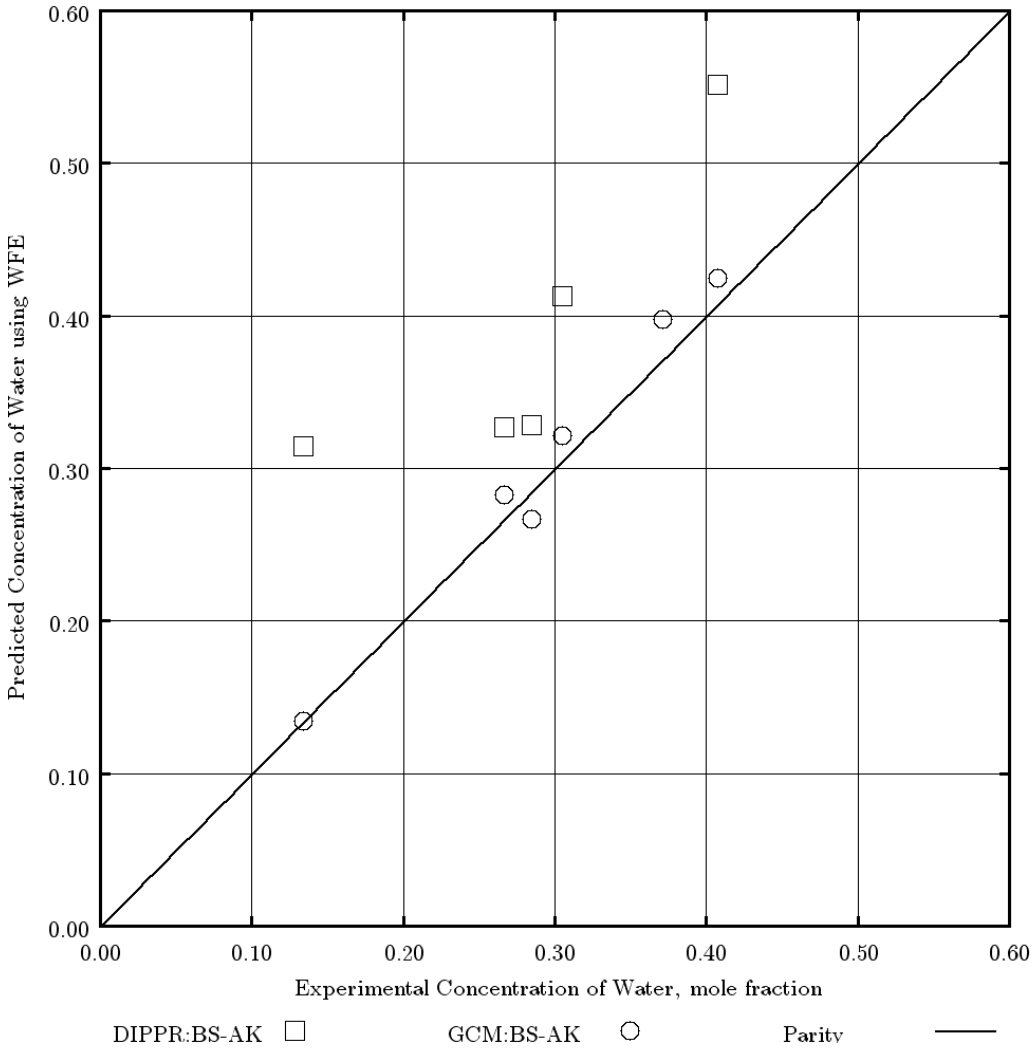

Figure 6.27: Predicted versus experimental exiting concentration of water using WFE-SRP for the water-ethylene glycerol system when using DIPPR and GCM for physical properties and Bott and Sheikh-Ahmed and Kaparthi for HTC.

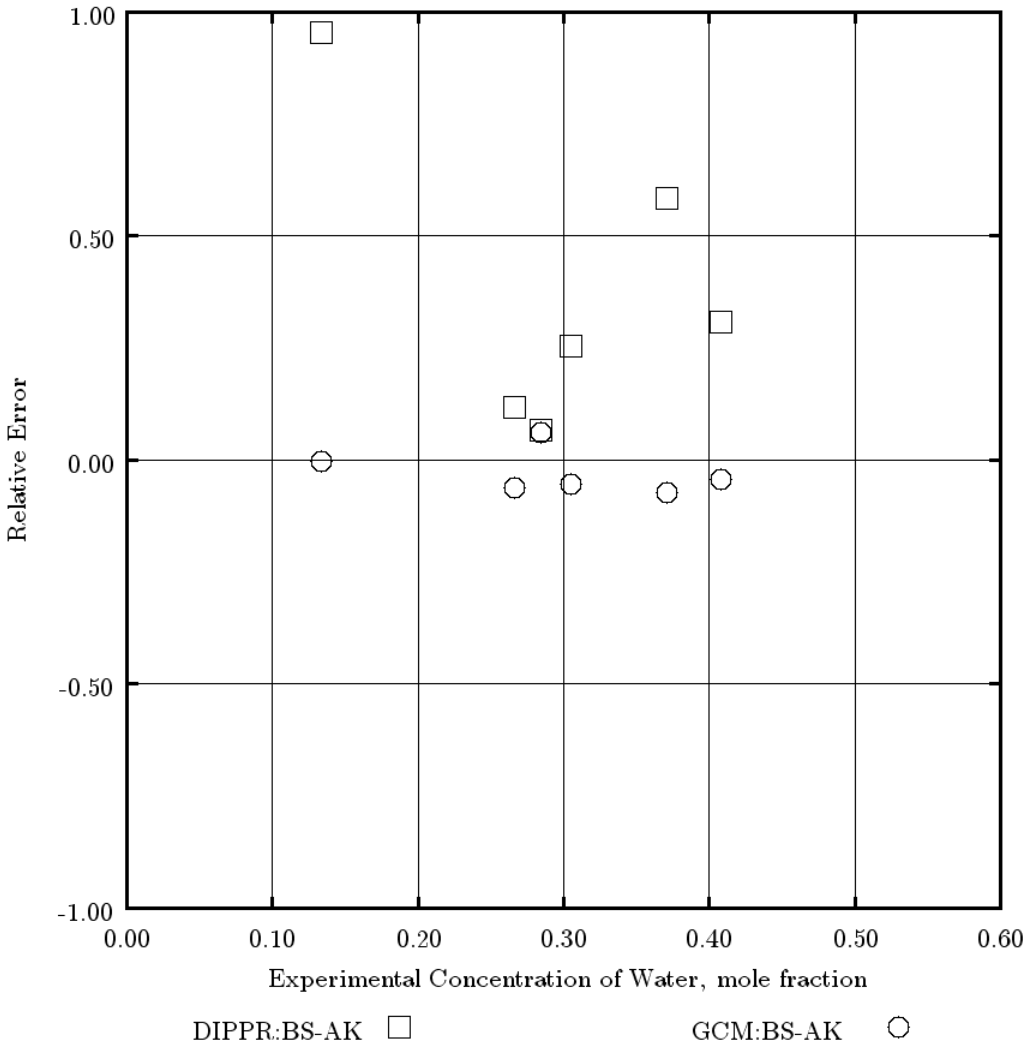

Figure 6.28: Relative error of the experimental exiting concentration of water using WFE-SRP for the water-ethylene glycol system when using DIPPR and GCM for physical properties and Bott and Sheikh-Ahmed and Kaparthi for HTC.

Chapter 7

Conclusions and Future Work

7.1 Wiped Film Evaporator as an Isothermal Flash

The results reveal that a wiped film evaporator (WFE) can be treated as an isothermal flash in a process simulator only when some particular conditions are met:

- **Temperature profile is small, around 1 °C**: this can be due to a high relative volatility of the compound to be evaporated with respect to the other compound, like the water-sucrose system.
- **The concentration of the volatile component is small**: this will cause the evaporation rate to be small, like the water-glycerol and water-ethylene glycol systems when the evaporation rate was small.

Figures 6.1, 6.3, and 6.5 show the good agreement of the experimental exiting concentration of water for the three systems when the wiped film evaporator is treated as an isothermal flash.

When any of the mentioned conditions is met, the WFE can be treated as an isothermal flash in a process simulator. It should be pointed out that when using the simulator, the results will only be about the required heat duty and product distribution of vapor and liquid. The effect of the number

of blades or the rotational speed on the heat duty and product distribution could not be evaluated.

7.2 Proposed Model: Simultaneous Heat and Mass Transfer

The proposed rigorous model for considering the simultaneous heat and mass transfer in the wiped film evaporator, from the results presented in Chapter 6, seems to work, especially when the physical properties are predicted with good accuracy, like the special equations for the water-sucrose system. The agreement of the proposed model with the experimental data is shown in Figures 6.17 and 6.19 for water-sucrose, 6.21 and 6.23 for water-glycerol, and 6.25 and 6.27 for water-ethylene glycol.

The model takes into account several characteristics of the wiped film evaporator: length and diameter, number of blades, and rotational speed. Some features of a WFE are not considered directly by the proposed model, such as the blade geometry, blade spacing, and blade clearance. These characteristics are sometimes included in the correlation for the prediction of the heat transfer coefficient, and are therefore indirectly considered by the proposed model.

7.2.1 Heat Enhancement Factor and Mass Transfer Coefficient

Using the heat enhancement factor (β_h) to predict the mass transfer coefficient appears to be a reasonable approach. The model predicts β_h values

for the experimental points for the three system from 2 up to 10. This means that the WFE has a better heat and mass transfer of twice up to 10 times better than a falling film evaporator (FFE).

The value of β_h, which depends on the heat transfer coefficient for a WFE and FFE, can be adjusted for each particular system. There are several correlations for the calculation of the heat transfer coefficient for WFE and FFE, and a suitable combination for a system can be selected.

7.2.1.1 Falling Film Evaporator

The falling film evaporator was selected as a base case for the heat enhancement factor because it is a well-studied and well-characterized equipment. Also, the FFE should represent a WFE without agitation. This continuity was not considered with the proposed model. From the equation for β_h, using the correlations of Bott and Romero [11] for WFE and Ahmed and Kaparthi [3] for FFE, the equation for β_h is:

$$\beta_h = \frac{0.018 Re_f^{0.46} Re_N^{0.6} Pr_L^{0.87} (D/L)^{0.48} N_b^{0.24}}{6.92 \times 10^{-3} Re_f^{0.345} Pr_L^{0.4}}$$

$$\beta_h = 2.6012 Re_f^{0.115} Re_N^{0.6} Pr_L^{0.47} (D/L)^{0.48} N_b^{0.24} \tag{7.1}$$

From this equation, the limit $N \to 0$ or $N_b \to 0$ (i.e., the case when the WFE approaches the conditions of a FFE) should go to unity, but it can be seen from the previous equation that the limit goes to zero. The continuity of the model was not considered (i.e., $h_p^{WFE} \neq h_p^{FFE}$ when $N \to 0$ or $N_b \to 0$). The mass transfer coefficient for the WFE using the proposed model for this

case would predict a value of zero, when the reasonable value should be the same as for a FFE (i.e., $k_L^{WFE} = k_L FFE$).

7.3 WFE-SRP Computer Program

The WFE-SRP Excel computer program is a useful tool for analyzing the performance of existing wiped film evaporators, as it was shown to be useful for analyzing experimental data for water-sucrose, water-glycerol, and water-ethylene glycol.

The program should be used only as another tool when designing a new WFE. Laboratory scale and pilot plant experiments still need to be carried out in order to validate any results from the computer program.

When analyzing an existing WFE in operation, one of the mixture component is usually well-characterized, while the other is not. WFE-SRP has the option of predicting the activity coefficient using the UNIFAC method [33], and group contribution methods (GCM) for the estimation of physical properties. As the results presented in Chapter 6, the prediction of physical properties affect the accuracy of the model. The GCM should be used when no other methods for the calculation of physical properties are available.

7.4 Future Work

The proposed future work for this project are:

- Acquire pilot-plant and commercial-scale data for further validation of

the model and computer program (WFE-SRP).

- Expand the current model to include multicomponent systems.
- Consider the continuity of the heat enhancement factor equation for the case when the wiped film evaporator approaches the conditions of a falling film evaporator (i.e., $N \rightarrow 0$ or $N_b \rightarrow 0$.)
- Modify WFE-SRP to allow the combination of estimation/prediction of activity coefficient and physical properties.
- Evaluate the effect of other characteristics of the wiped film evaporator (i.e., blade clearance) on its performance.

Appendices

Appendix A

WFE-SRP Computer Program

An Excel program (WFE-SRP) was developed to analyze the performance of existing wiped film evaporators, or help in the design of a new one. Figure A.1 shows the flow diagram for the calculation procedure in this program. All the necessary inputs are provided in the Excel worksheets while the calculations are performed in Visual Basic. Results are presented in Excel.

WFE-SRP has a color coded input and output: **Black** is used for input, **Blue** for output, **Green** for normal messages, and **Red** for error messages.

The top three boxes in Figure A.1 show the required input to run the program. These are:

- **Geometrical parameters**: diameter (D), length (L), thickness of the wall (δ_{wall}), thermal conductivity of the wall (k_{wall}), and number of blades (N_b).
- **Operational parameters**: feed rate (F), temperature (T), pressure (P), and composition (x).
- **Components**: select light and heavy components from the database. If the desired component is not in the database, it can be added by pressing

the button **'Add Component'** (Figure A.2).

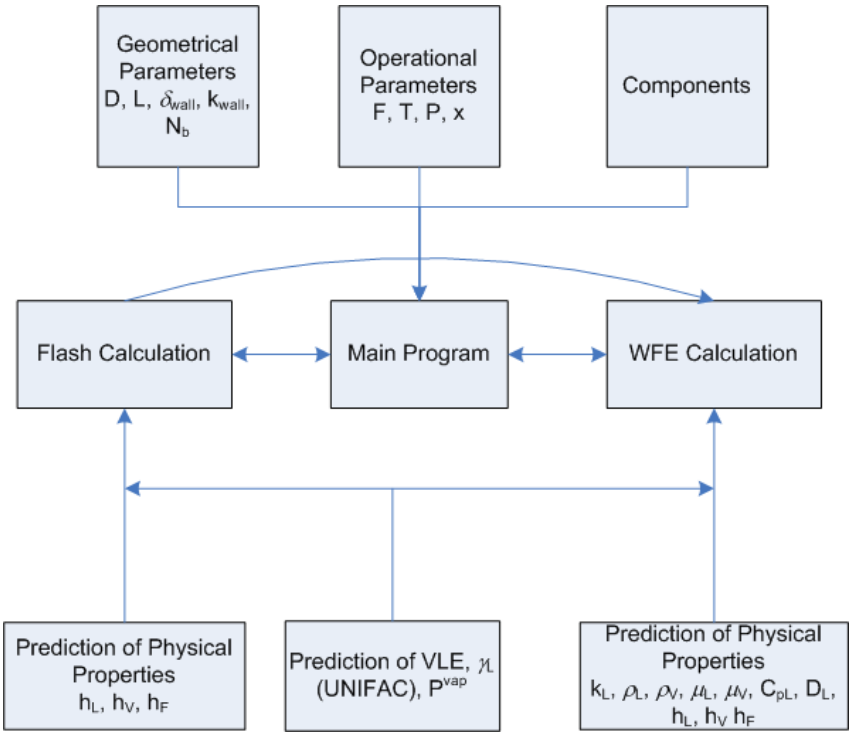

Figure A.1: Flowchart for the WFE-SRP Excel program.

A.1 Types of Calculation

After all the inputs are provided, the type of calculation is selected from the **Input** worksheet (see Figure A.2). The two types of calculations are **Flash** and **WFE**.

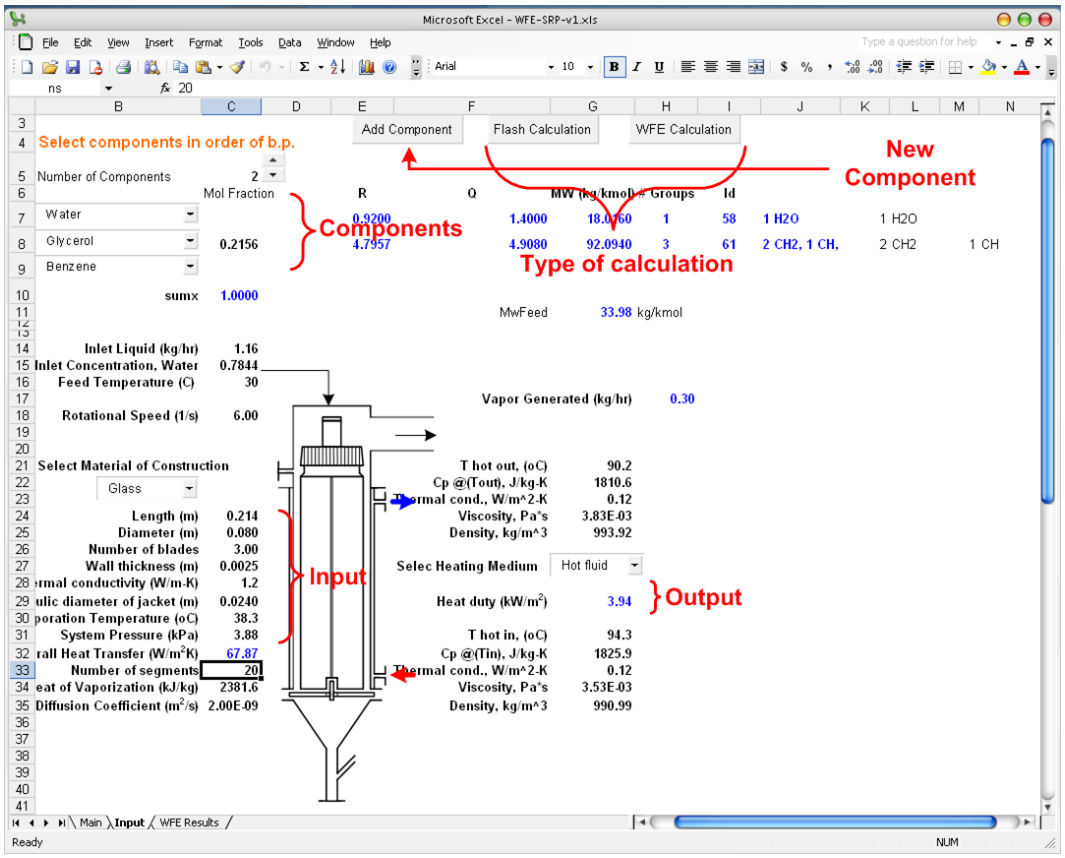

Figure A.2: WFE-SRP. Main input screen. All the necessary information is provided in this worksheet.

A.1.1 Flash Calculation

The two-phase flash equation for a fixed pressure and temperature is solved. The results are presented in the same **Main** worksheet. Figure A.3 shows an example of the results for a flash calculation. In order to solve the energy balance, liquid and vapor enthalpies are predicted. Liquid activity coefficients are predicted using the UNIFAC method [33].

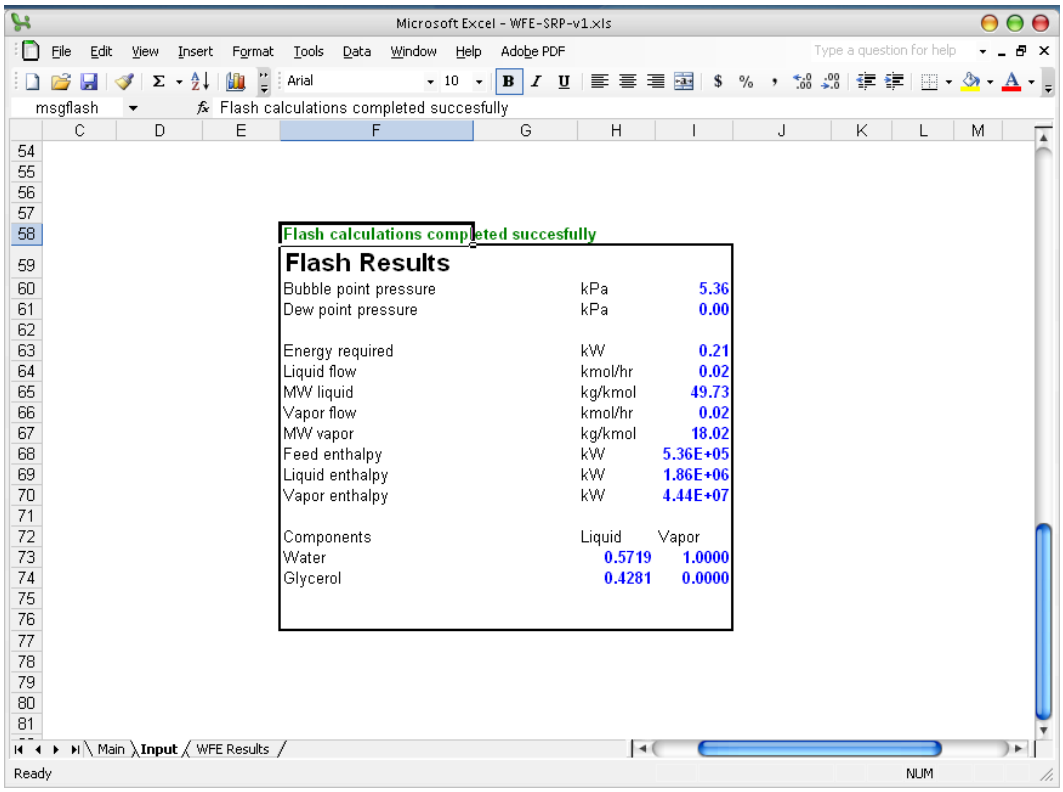

Figure A.3: WFE-SRP output result for a flash calculation.

A.1.2 WFE Calculation

The mechanistic equations for the vertical wiped film evaporator are solved (explained in Chapter 4). The results are presented in the **WFE Results** worksheet. Figure A.4 shows an example of the results for a rigorous WFE calculation. The physical properties are calculated using the DIPPR equations [22] or with group contribution methods.

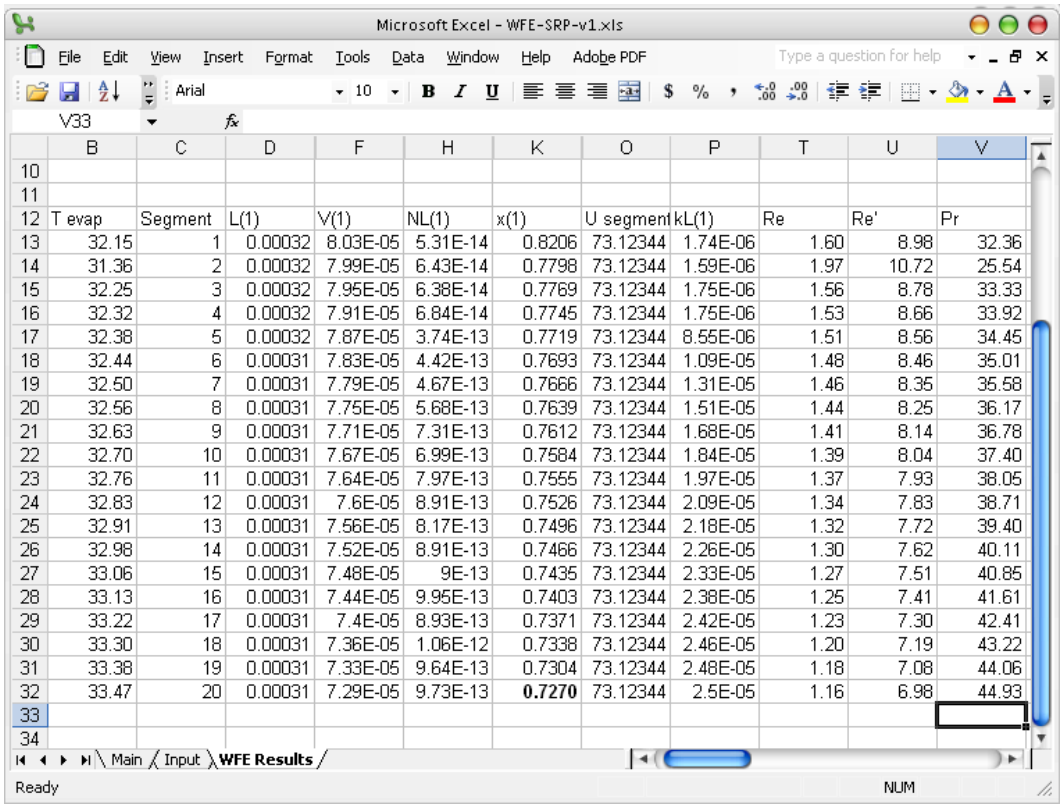

	B	C	D	F	H	K	O	P	T	U	V
10											
11											
12	T evap	Segment	L(1)	V(1)	NL(1)	x(1)	U segment	kL(1)	Re	Re'	Pr
13	32.15	1	0.00032	8.03E-05	5.31E-14	0.8206	73.12344	1.74E-06	1.60	8.98	32.36
14	31.36	2	0.00032	7.99E-05	6.43E-14	0.7798	73.12344	1.59E-06	1.97	10.72	25.54
15	32.25	3	0.00032	7.95E-05	6.38E-14	0.7769	73.12344	1.75E-06	1.56	8.78	33.33
16	32.32	4	0.00032	7.91E-05	6.84E-14	0.7745	73.12344	1.75E-06	1.53	8.66	33.92
17	32.38	5	0.00032	7.87E-05	3.74E-13	0.7719	73.12344	8.55E-06	1.51	8.56	34.45
18	32.44	6	0.00031	7.83E-05	4.42E-13	0.7693	73.12344	1.09E-05	1.48	8.46	35.01
19	32.50	7	0.00031	7.79E-05	4.67E-13	0.7666	73.12344	1.31E-05	1.46	8.35	35.58
20	32.56	8	0.00031	7.75E-05	5.68E-13	0.7639	73.12344	1.51E-05	1.44	8.25	36.17
21	32.63	9	0.00031	7.71E-05	7.31E-13	0.7612	73.12344	1.68E-05	1.41	8.14	36.78
22	32.70	10	0.00031	7.67E-05	6.99E-13	0.7584	73.12344	1.84E-05	1.39	8.04	37.40
23	32.76	11	0.00031	7.64E-05	7.97E-13	0.7555	73.12344	1.97E-05	1.37	7.93	38.05
24	32.83	12	0.00031	7.6E-05	8.91E-13	0.7526	73.12344	2.09E-05	1.34	7.83	38.71
25	32.91	13	0.00031	7.56E-05	8.17E-13	0.7496	73.12344	2.18E-05	1.32	7.72	39.40
26	32.98	14	0.00031	7.52E-05	8.91E-13	0.7466	73.12344	2.26E-05	1.30	7.62	40.11
27	33.06	15	0.00031	7.48E-05	9E-13	0.7435	73.12344	2.33E-05	1.27	7.51	40.85
28	33.13	16	0.00031	7.44E-05	9.95E-13	0.7403	73.12344	2.38E-05	1.25	7.41	41.61
29	33.22	17	0.00031	7.4E-05	8.93E-13	0.7371	73.12344	2.42E-05	1.23	7.30	42.41
30	33.30	18	0.00031	7.36E-05	1.06E-12	0.7338	73.12344	2.46E-05	1.20	7.19	43.22
31	33.38	19	0.00031	7.33E-05	9.64E-13	0.7304	73.12344	2.48E-05	1.18	7.08	44.06
32	33.47	20	0.00031	7.29E-05	9.73E-13	**0.7270**	73.12344	2.5E-05	1.16	6.98	44.93
33											
34											

Figure A.4: WFE-SRP output result for a wiped film evaporator calculation. Results are shown for all segments.

A.2 Adding Components

When the component of interest is not available in the built-in database, it should be added. Pressing the **Add Component** in the **Input** worksheet (Figure A.2) will open a new window. Figure A.5 presents a sample screen when adding a new component. WFE-SRP has the ability to predict vapor-liquid equilibria using UNIFAC [33], and physical properties using the constants from the DIPPR equations [22] (Figure A.6) or group contribution

methods.

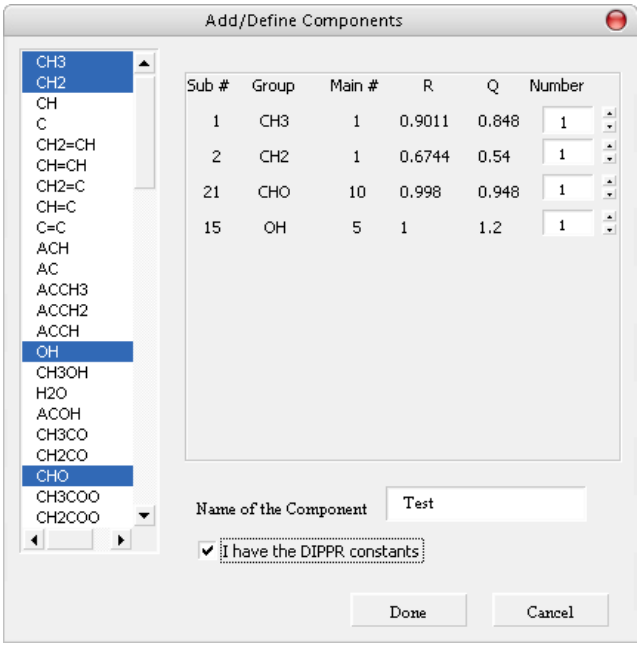

Figure A.5: Defining a new component based on UNIFAC groups.

If DIPPR constant [22] are available for the new component, there is an option in the program to use them to predict all physical properties. At the bottom of Figure A.5 is the option to let the program know that constants are available, and they should be provided in the form shown in Figure A.6.

When these constants are not available, group contributions methods are used to predict the properties and the groups for each property need to be defined. The available methods are: Ihmels and Gmehling [37] for liquid density (ρ_L), Hsu et al. [36] for liquid viscosity (μ_L), Sastri and Rao [82] for thermal conductivity (λ_L), Li et al. [55] for vapor pressure (P^{vap}), Růžička and

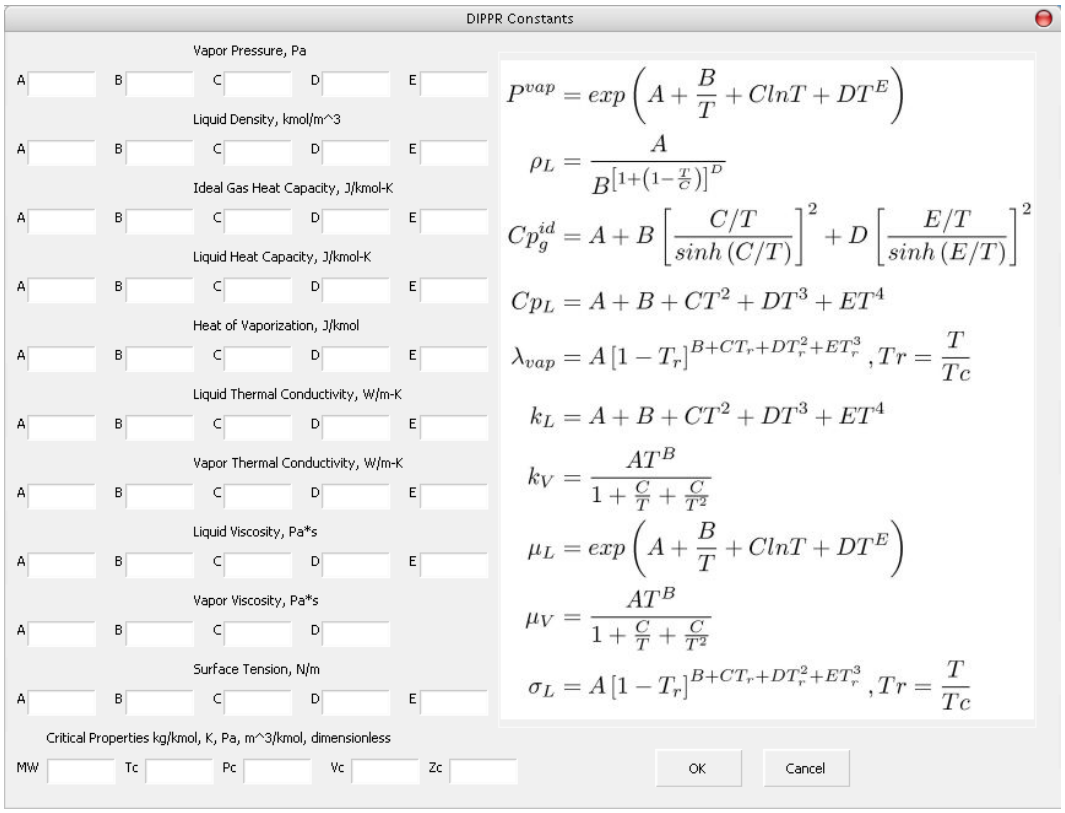

Figure A.6: Adding a new component with known DIPPR constants.

Domalski [77, 78] for liquid heat capacity (C_{pL}), and Joback and Reid [38] for the critical properties (P_c, T_c, V_c, etc).

A.2.1 Liquid Density

The model of Ihmels and Gmehling [37] is used to predict the liquid density of pure components. Figure A.7 presents the available groups for this

method. The equation to predict the density is:

$$\rho = \frac{MW}{\sum n_i \Delta v_i} \tag{A.1}$$

$$\Delta v_i = A_i + B_i T + C_i T^2 \tag{A.2}$$

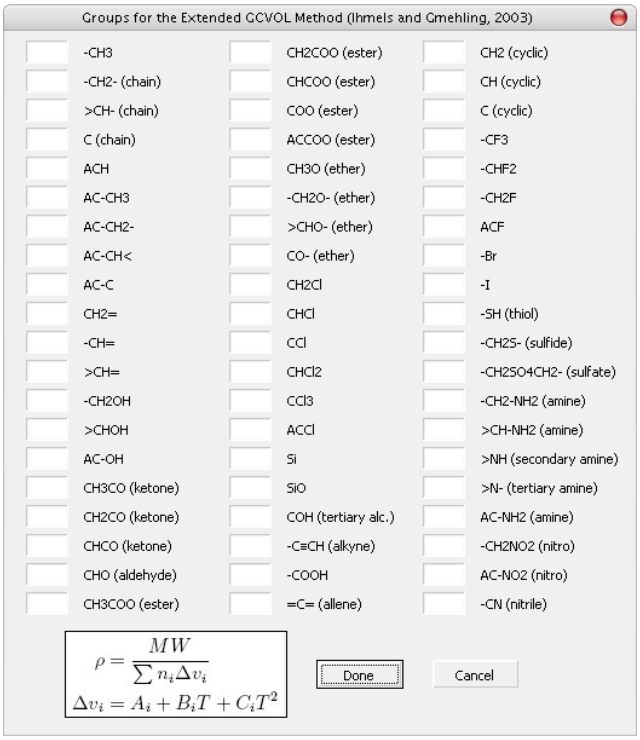

Figure A.7: Groups for the prediction of liquid density.

where MW is the molecular weight, n_i is the number of i groups, A_i, B_i, C_i are temperature-dependent contributions for group i, and T is the temperature.

A.2.2 Liquid Viscosity

The model of Hsu et al. [36] is used to predict the liquid viscosity of pure components. Figure A.8 shows the available groups for this method. The equation to estimate the viscosity is:

$$\ln \mu_L = \sum_i N_i \left\{ a_i + b_i T + \frac{c_i}{T^2} + d_i \ln P_c \right\} \tag{A.3}$$

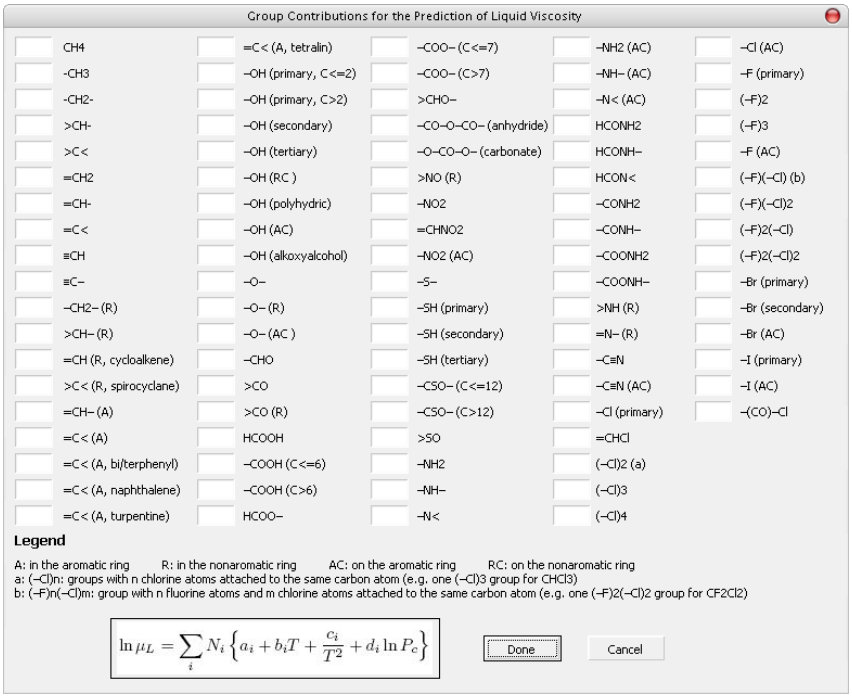

Figure A.8: Groups for the prediction of liquid viscosity.

where N_i is the number of i groups, a_i, b_i, c_i are temperature-dependent contributions, d_i is a pressure-dependent contribution, P_c is the estimated critical pressure using the Joback and Reid [38] method, and T is the temperature.

A.2.3 Liquid Thermal Conductivity

The model of Sastri and Rao [82] is used to predict the liquid thermal conductivity of pure components. Figure A.9 presents the available groups for this method. The equation to calculate the thermal conductivity is:

$$\lambda_L = \lambda_{L,B} \cdot a^m \tag{A.4}$$

$$\lambda_{L,B} = \sum \Delta\lambda_{L,B} + \sum \Delta\lambda_{L,corr} \tag{A.5}$$

$$m = 1 - \left(\frac{1 - T_r}{1 - T_{Br}}\right)^n \tag{A.6}$$

For alcohols and phenols: $a = 0.856$, $n = 1.23$. For other liquids: $a = 0.160$, $n = 0.20$. $\Delta\lambda_{L,B}$ is the contribution for a particular group, $\Delta\lambda_{L,corr}$ is the contribution due to correction, $T_r = \dfrac{T}{T_C}$ is the reduced temperature, $T_{Br} = \dfrac{T_B}{T_C}$ is the reduced boiling point.

A.2.4 Vapor Pressure

The model of Li et al. [55] is used to predict the vapor pressure. Figure A.10 shows the available groups for this method. The equation to estimate the vapor pressure is:

$$\ln P_r^* = A - \frac{B}{T_r^*} + C ln T_r^* + D T_r^{*6} \tag{A.7}$$

where $P_r^* = \dfrac{P}{P_c^*}$ is the pseudo-reduced pressure, $T_r^* = \dfrac{T}{T_c^*}$ is the pseudo-reduced temperature, $T_{br}^* = \dfrac{Tb}{T_c^*}$ is the pseudo-reduced boiling point, P_c^* is the predicted critical pressure, T_c^* is the predicted critical temperature. $A = -35Q$, $B =$

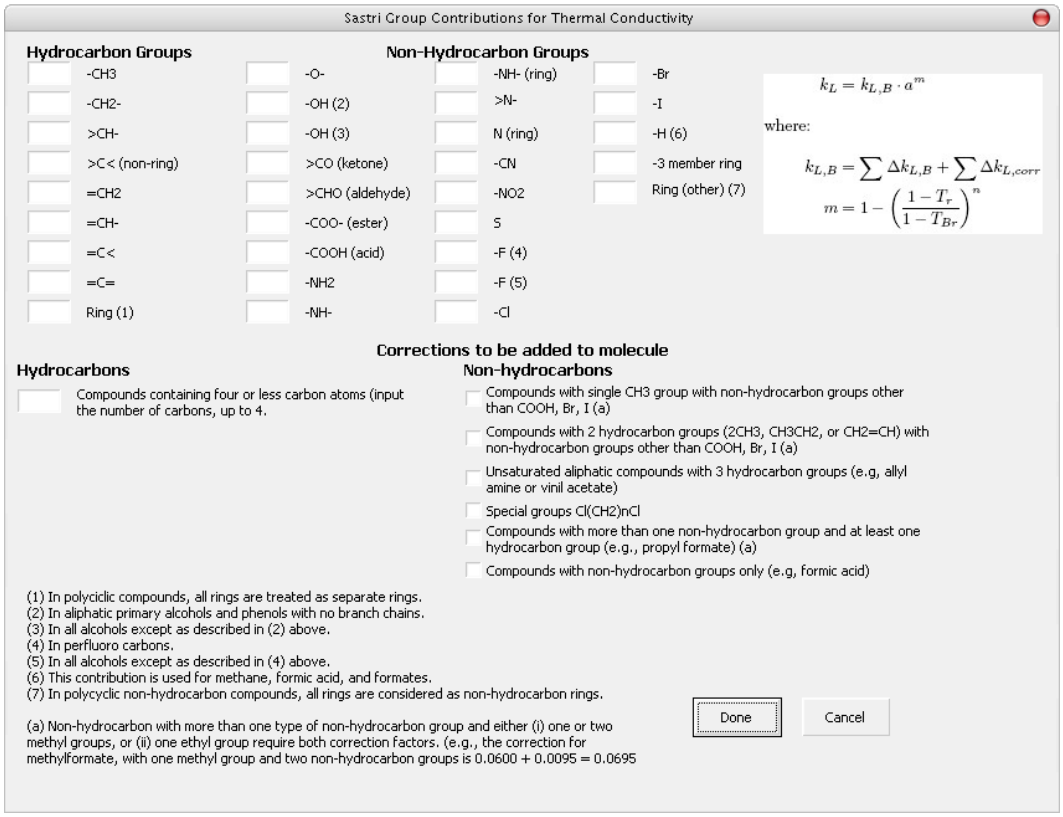

Figure A.9: Groups for the prediction of liquid thermal conductivity.

$-36Q$, $C = 42Q\alpha_c$, $D = -Q$, $Q = K\,(a - \alpha_c)$, $\alpha_c = \dfrac{aK\psi_b + ln\,(P_c^*/101.325)}{K\psi_b - lnT_{br}^*}$, $K = B_1 + C_1 H$, $H = \dfrac{T_{br}^* \ln\,(P_c^*/101.325)}{1 - T_{br}^*}$, and $\psi_b = -35 + \dfrac{36}{T_{br}^*} + 42lnT_{br}^* - T_{br}^{*6}$ are intermediate variables necessary to calculate the vapor pressure.

A.2.5 Liquid Heat Capacity

The method of Růžička and Domalski [77, 78] is used to predict the heat capacity of the liquid. Figure A.11 shows the available groups for this

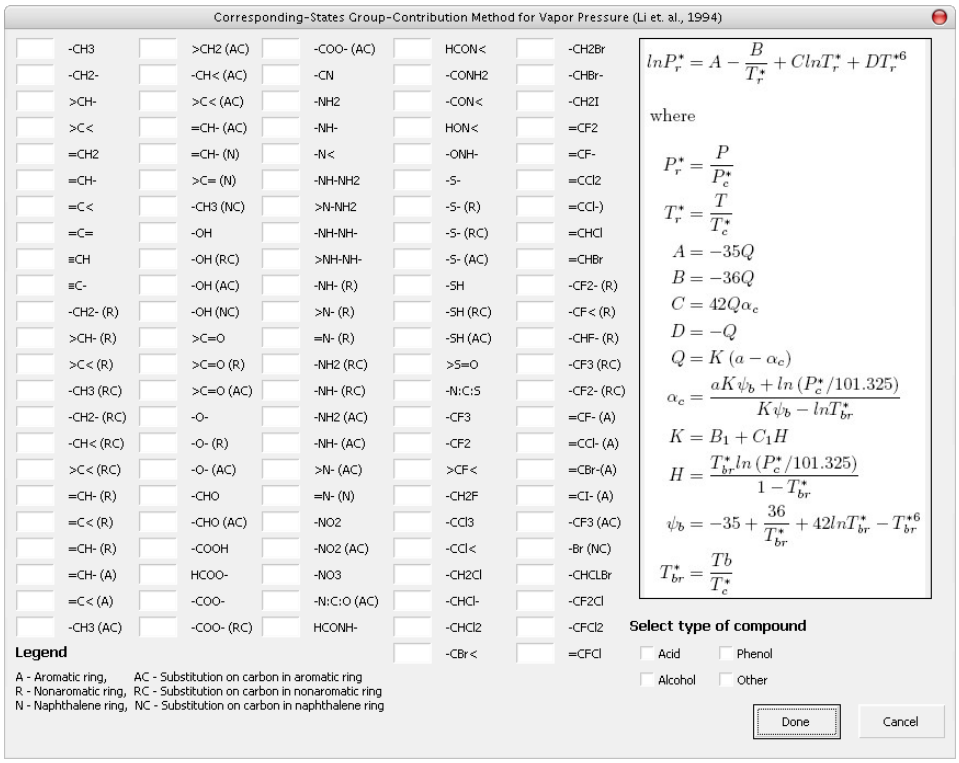

Figure A.10: Groups for the prediction of vapor pressure.

method. The equations to estimate heat capacity are:

$$\frac{C_p}{R} = \sum_{i=1}^{k} n_i \Delta c_i \tag{A.8}$$

$$\Delta c_i = a_i + b_i \frac{T}{100} + d_i \left(\frac{T}{100}\right)^2 \tag{A.9}$$

where $R = 8.31451$ J/K-mol, n_i is the number of groups of type i, Δc_i is the contribution to heat capacity for group i, k is the total number of different groups, T is the temperature, and a_i, b_i, c_i are the adjusted parameters to calculate Δc_i.

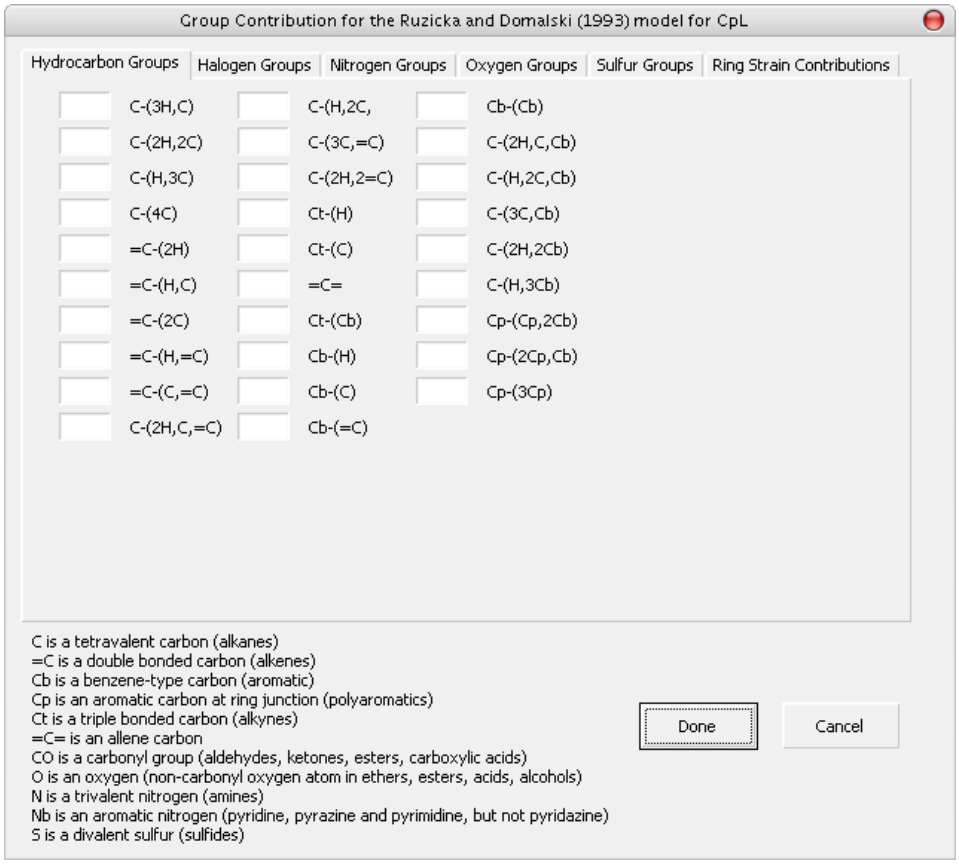

Figure A.11: Groups for the prediction of heat capacity for liquid.

A.2.6 Critical Constants

The method of Joback and Reid [38] is used to estimate critical properties and boiling temperature. Figure A.12 shows the available groups for this method. The equations to calculate the properties are:

$$T_b = 198.2 + \sum_i n_i \Delta T_i \tag{A.10}$$

$$T_c = \frac{T_b}{0.584 + 0.965 \sum_i n_i \Delta T_i - \left(\sum_i n_i \Delta T_i\right)^2} \tag{A.11}$$

$$P_c = \frac{1}{(0.113 + 0.0032 n_{atoms} - \sum_i n_i \Delta P_{c,i})^2} \tag{A.12}$$

$$V_c = \sum_i n_i \Delta V_{c,i} \tag{A.13}$$

A.3 Example: Adding Glycerol

An example of adding a new component to the database is presented. Glycerol (formula $C_3H_8O_3$, boiling temperature of 563 K) already exists in the database, but it will be used to show how to add a new component and also to compare the results of the WFE-SRP program when using DIPPR constants [22] (Glycerol in the database) and the estimation using group contribution methods.

The molecular structure of glycerol is shown in Figure A.13. It contains three alcohol groups ($-$OH), two methyl groups ($-CH_2$), and one methyl group (>CH$-$). The described procedure in the previous section for adding a component will be followed. When choosing a name for this component, it should be different than the names already in the database (i. e., it will be named Glycerol GCM).

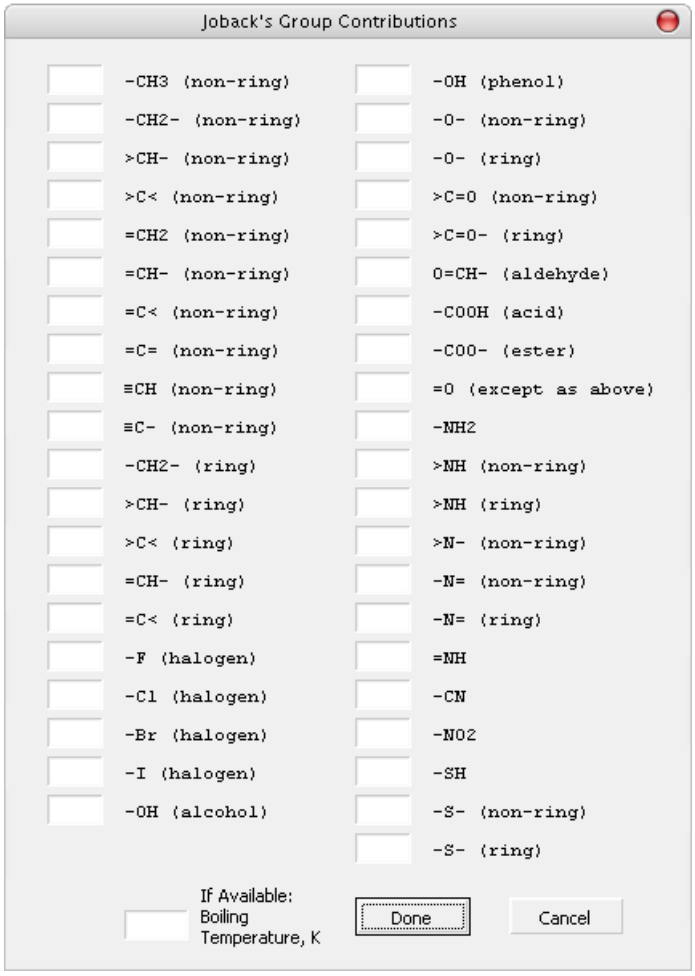

Figure A.12: Groups for the prediction of critical properties.

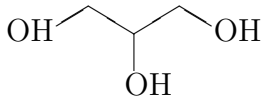

Figure A.13: Structure of the glycerol molecule.

Figures A.14 to A.23 show a series of screens that appear when adding this component to the database. In Figure A.14, the options to **'Add/Edit Components'** and **'Exit'** exist. The first option is for adding or viewing existing components, and the second option is to return to the **'Input'** worksheet. When the first option is selected, Figure A.14 appears.

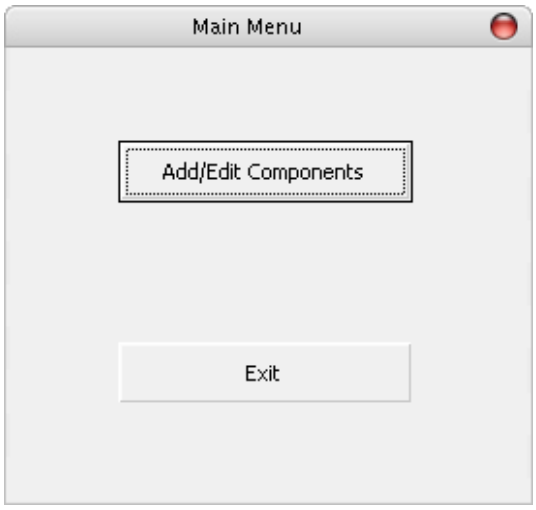

Figure A.14: First screen that shows when adding a new component in WFE-SRP.

This screen presents three options: **'View existing components'**, **'Add components'**, and **'Return'**. The first option is to show the existing components in the database, as well as the components that have been added. The second option is for adding a new component, and the last option is to return to the previous screen (Figure A.14).

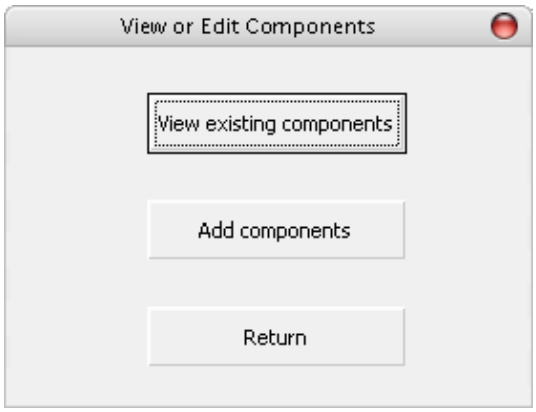

Figure A.15: Screen that appears after selecting 'Add/Edit Components' in Figure A.14.

In this screen, the groups for the UNIFAC model [33] are selected. After selecting the first group (i.e., CH_2), the right part of the screen shows the R and Q parameters for the selected group, as well as the option to select the number of groups in the molecule. If the new component has more than one group, all of them should be selected on the left part of the screen. After defining all the groups, a name should be given to the new component at the bottom of the screen. The program does not allow to continue to the next screen if no name is provided.

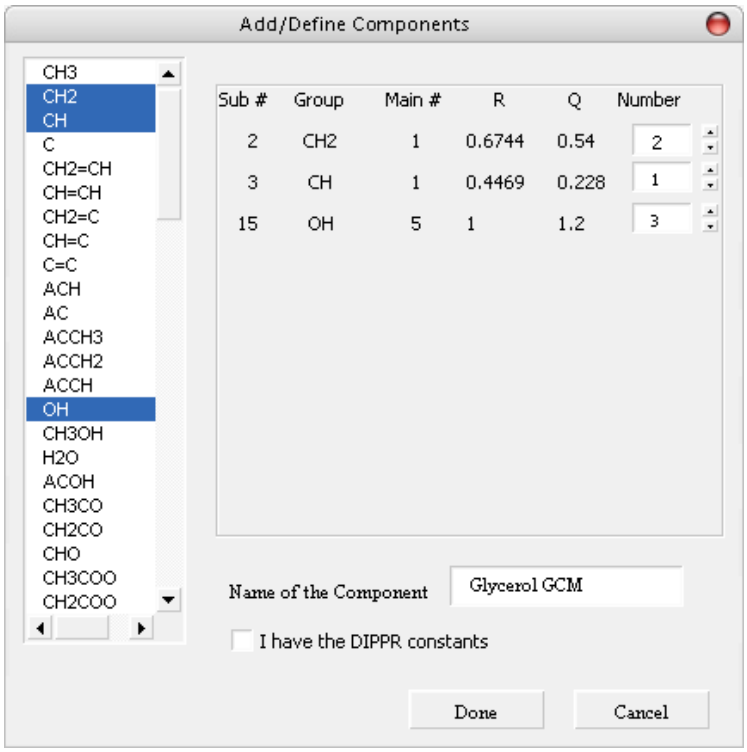

Figure A.16: Defining groups for the UNIFAC model [33] and naming the new component.

This screen shows the available groups for the estimation of critical properties using the Joback and Reid [38] method. If the experimental boiling temperature is available, it should be provided here (the accuracy of the estimation increases when this parameter is provided).

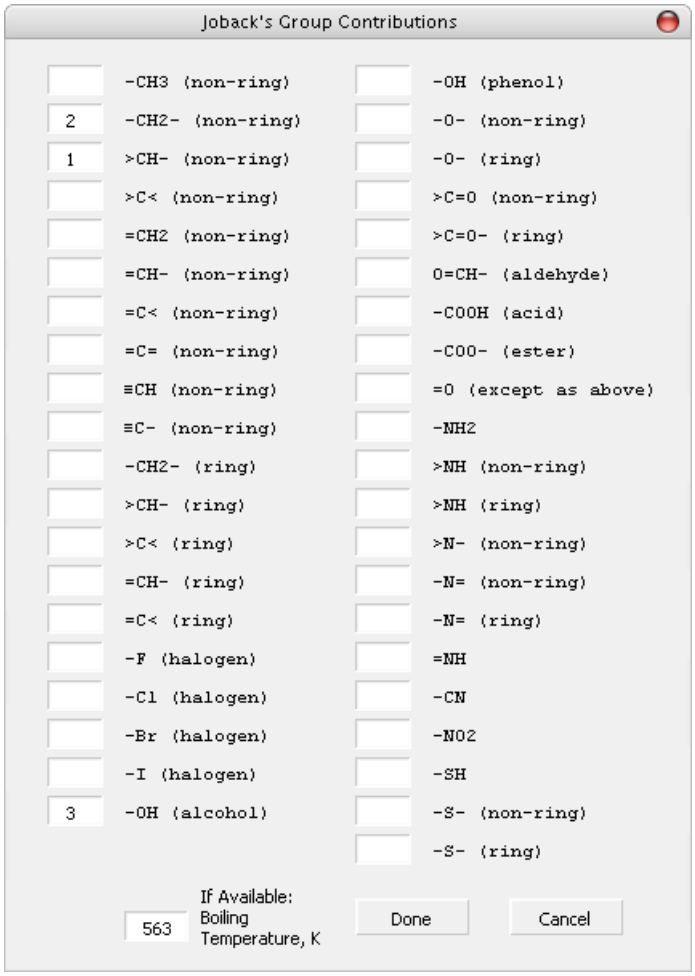

Figure A.17: Defining groups for the prediction of the critical properties using the Joback and Reid [38] method.

This screen shows the available groups for the prediction of the vapor pressure using the Li et al. [55] method. Besides selecting the groups for the component, the type of molecule also needs to be selected at the bottom.

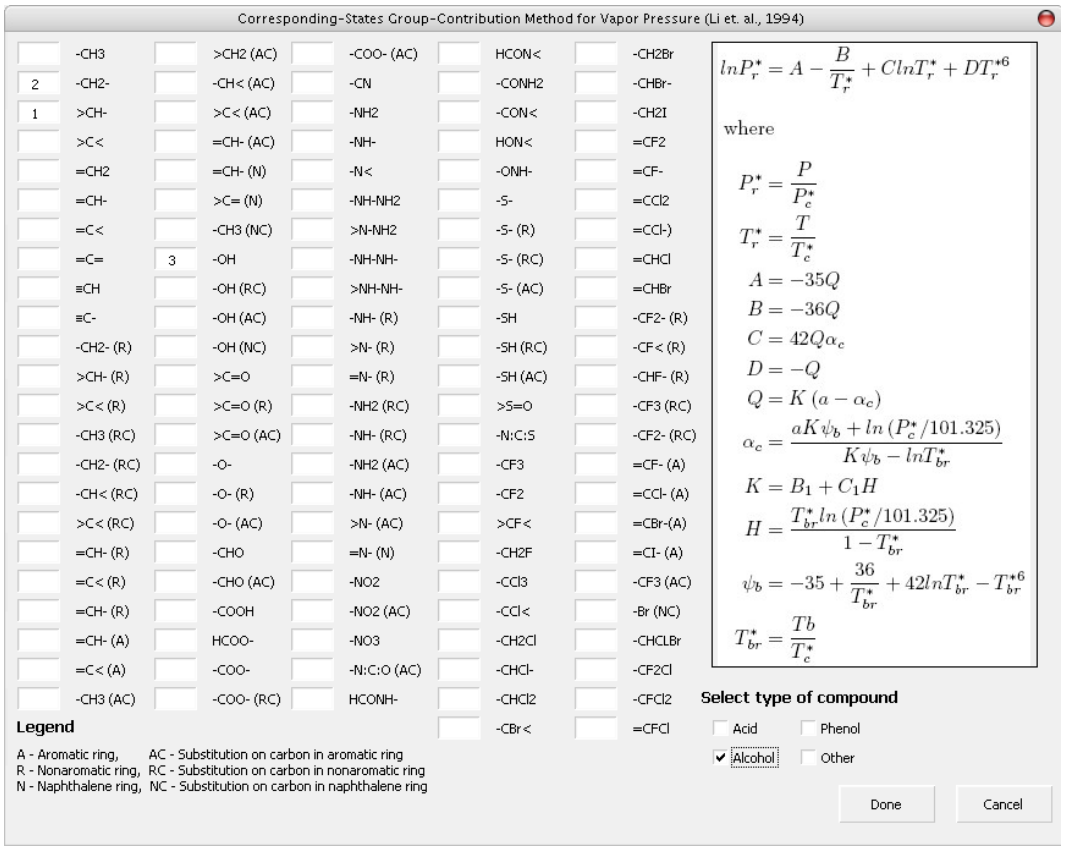

Figure A.18: Defining groups for the estimation of the vapor pressure using the Li et al. [55] method.

This screen shows the available groups for the estimation of the liquid thermal conductivity using the Sastri and Rao [82] method. The options after selecting all the groups for the new component are important for the estimation of the thermal conductivity. Check all that apply to the new molecule.

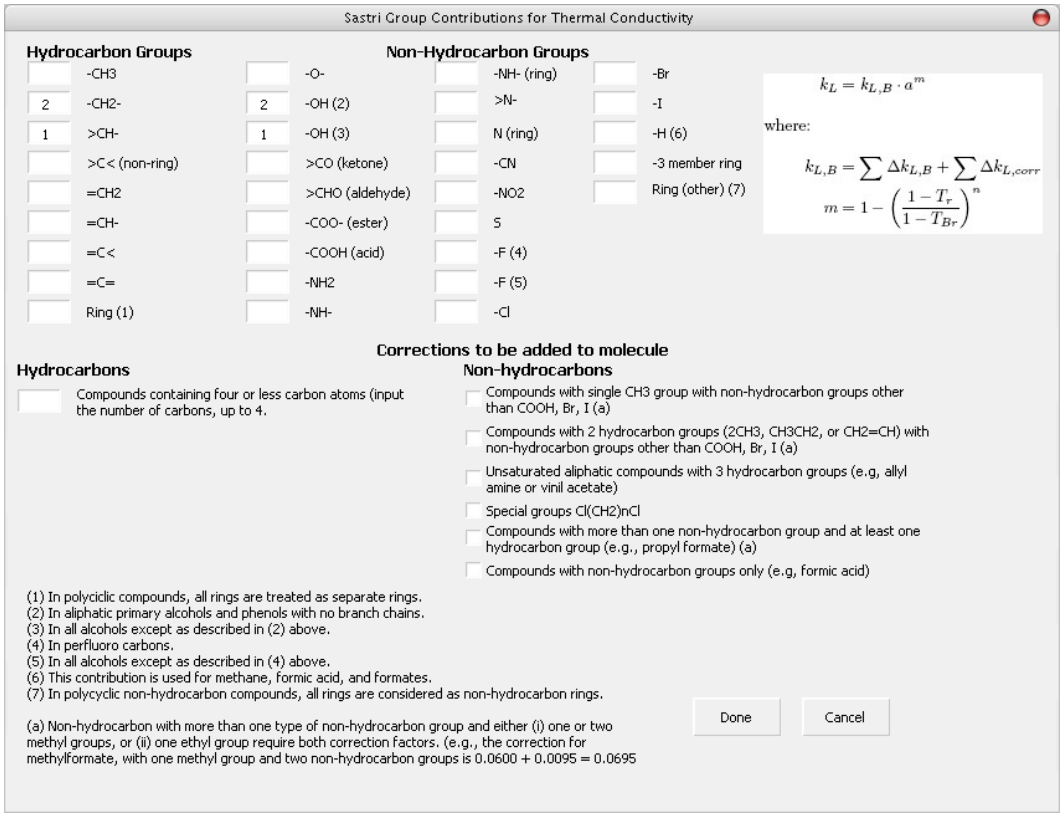

Figure A.19: Defining groups for the prediction of the liquid thermal conductivity using the Sastri and Rao [82] method.

This screen shows the available groups for the prediction of the liquid density using the Ihmels and Gmehling [37] method. It should be noticed that the groups from one property no another are not similar.

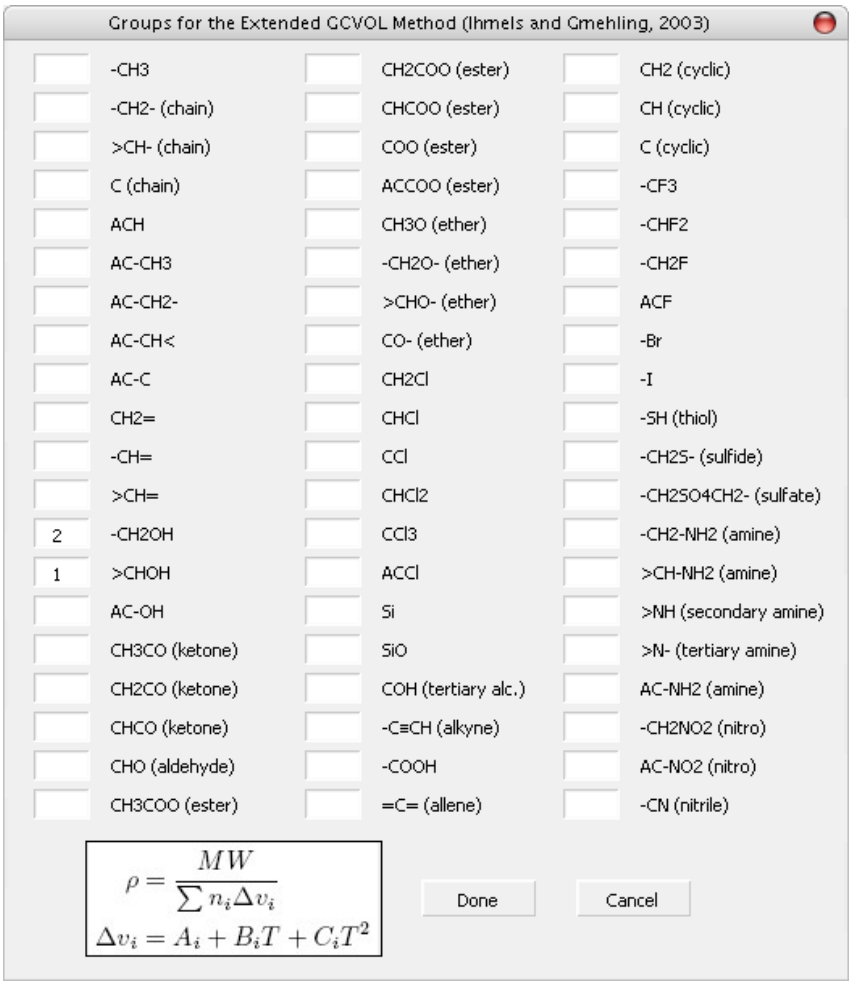

Figure A.20: Defining groups for the estimation of the liquid density using the Ihmels and Gmehling [37] method.

This screen shows the available groups for the estimation of the liquid viscosity using the Hsu et al. [36] method. The legends in each method are also different.

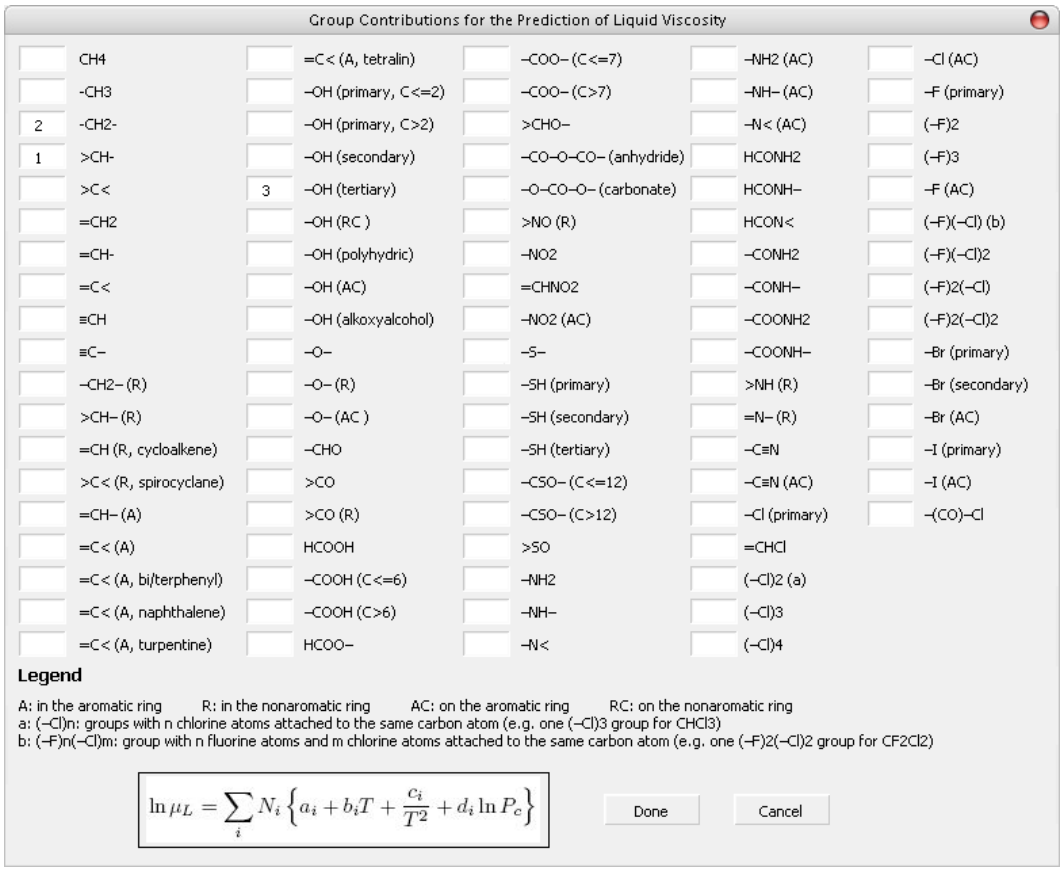

Figure A.21: Defining groups for the prediction of the liquid viscosity using the Hsu et al. [36] method.

This screen shows the available oxygen groups for the prediction of the liquid heat capacity using the Růžička and Domalski [77] method. It has three $-$OH groups attached to Carbon, two $-CH_2$ groups attached to Carbon on one end and Oxygen on the other, and one $-$CH group attached to two Carbon molecules and one Oxygen.

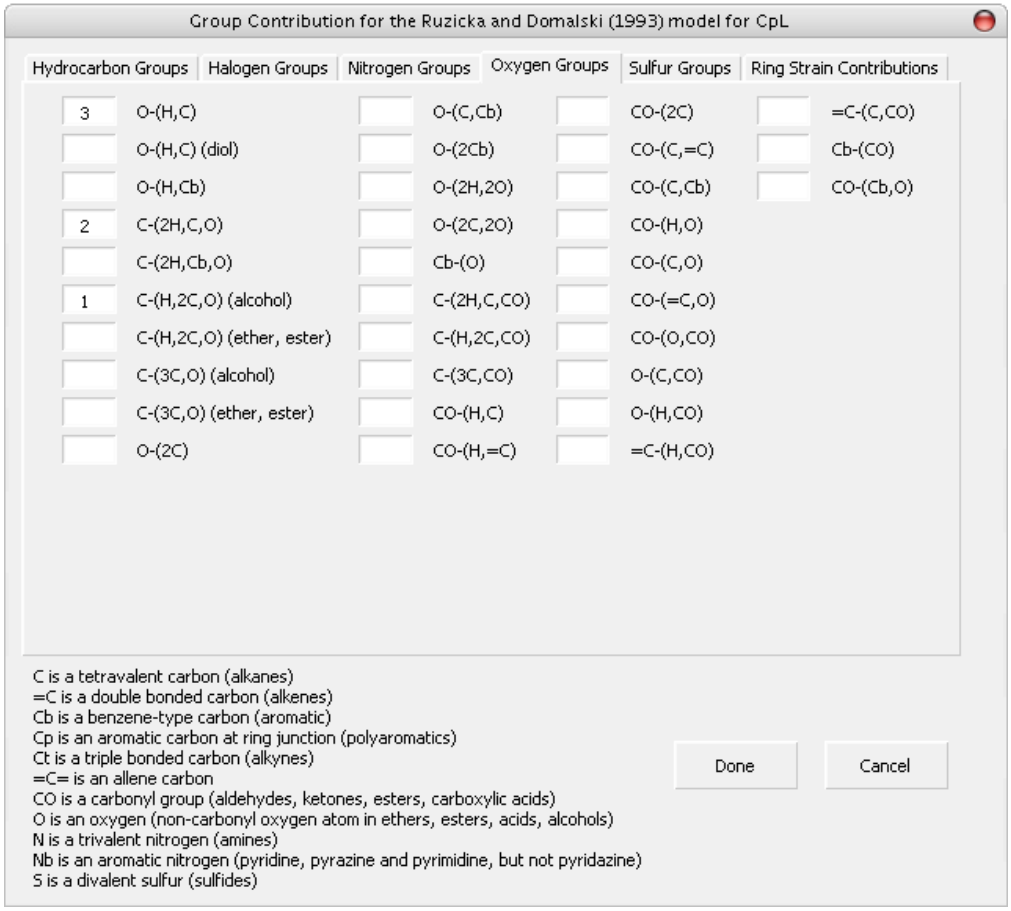

Figure A.22: Defining groups for the estimation of the liquid heat capacity for the new component using the Růžička and Domalski [77, 78] method.

This screen shows the available groups for the estimation of the enthalpy of vaporization using the Li et al. [54] method. If the experimental heat of vaporization at the boiling point is available, it should be provided at the bottom of the screen.

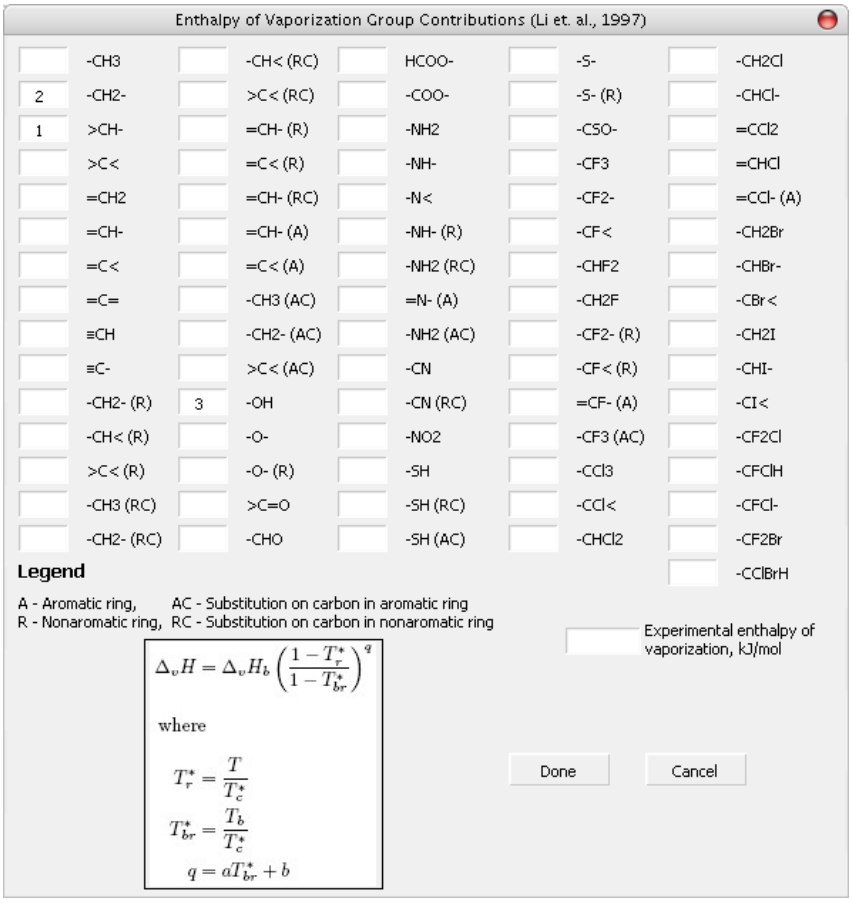

Figure A.23: Defining groups for the prediction of the enthalpy of vaporization for the new component using the Li et al. [54] method.

After finishing with the previous screen, the new component will be available in the database. The newly added component will be at the bottom of the database.

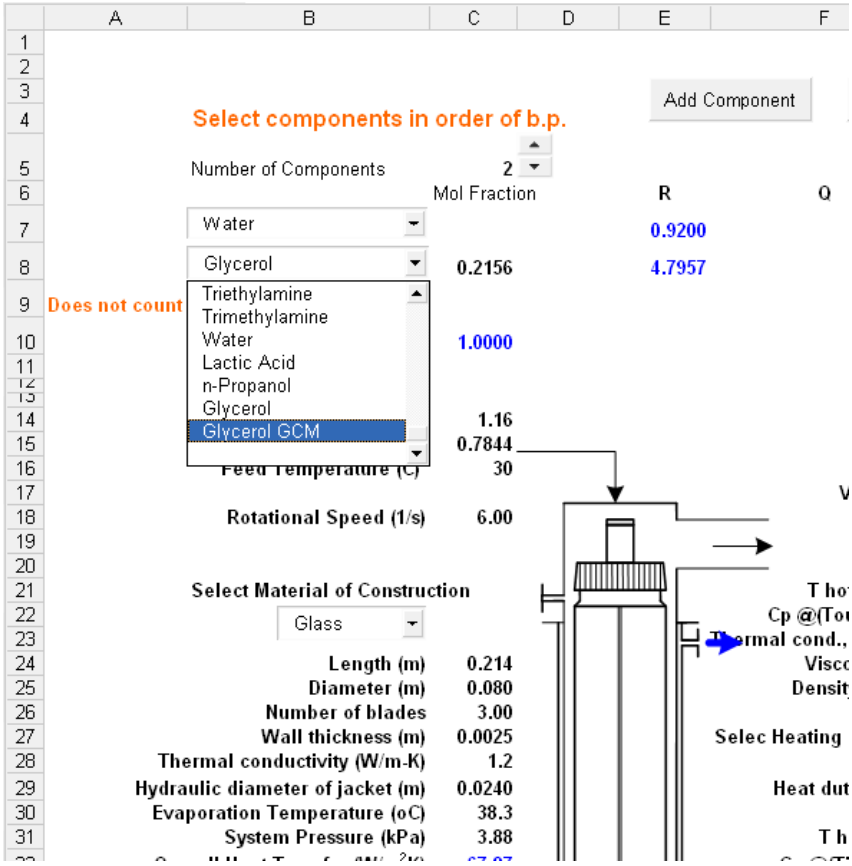

Figure A.24: Selecting the new component Glycerol GCM from the available components.

Appendix B

Marlotherm® SH Heat Transfer Fluid

The following description of the hot oil is taken from the product information of Sasol North America [81] available on `http://www.marlotherm.com/pdf/MARLOTHERM_SH_GB.pdf`.

B.1 Product Information

Marlotherm® SH is a high-performance synthetic, organic heat-transfer medium for use in the liquid phase in closed, forced circulation heat-transfer systems.

Marlotherm® SH can be used over the whole working range without being kept under pressure. The boiling range of the product at atmospheric pressure is above the use limit. The heat-transfer medium is advantageously used in the temperature range from 250 to 340 °C. The upper use limit corresponds to a heater outlet temperature of 350 °C. The film temperature should not exceed the limit of 380 °C either significantly or for a prolonged period.

Marlotherm® SH is most suitable for indirect heating of reactors, polymerization vessels and distillation columns, of processing machines and driers, and also heat exchangers in process plants and systems for heat recovery.

Marlotherm® SH is also suitable for use in heating and cooling systems. The technical characteristics of a Marlotherm® SH charge can also be matched to the specific requirements of a system and optimized by mixing with Marlotherm® LH.

The heat-transfer systems should be designed and operated in accordance with the recommendations of DIN 4754 “heat-transfer installation working with organic heat-transfer fluids”.

Marlotherm® SH is thermally stable up to an operating temperature of 300 °C. The Marlotherm® SH charge can be used for several years without significant changes. At higher temperatures, low-boiling and high-boiling decomposition products are formed. Their degree of formation rises with increasing operating temperatures. The decomposition products remain completely dissolved in the Marlotherm® SH charge. A build-up of low boilers should, however, be avoided, since they can impair the operation of the heat-transfer system, particularly in the upper range from 340 to 350 °C. For this reason, the low ends should be removed; their removal may be discontinuous, but at temperatures above 340 °C should be continuous via the expansion vessel. To assist this measure, the temperature of the expansion vessel should be raised to about 150 °C. lf used according to the recommended operation parameters, Marlotherm® SH forms no deposits on the walls and does not lead to accumulation of solids in the heat-transfer circuit. Marlotherm® SH plants can be operated reliably and without high maintenance costs.

B.2 Typical Physical and Chemical Properties

Table B.1 presents the physical and chemical properties of MARLOTHERM® SH and Table B.2 shows other properties like density, heat capacity, thermal conductivity, and kinematic viscosity. Figures B.1 to B.4 presents the plots for these properties.

Table B.1: Physical and chemical properties of Marlotherm® SH.

Property	**Value**	**Unit**	**Test Method**
Appearance at 20 °C	liquid, clear	-	visual
Chlorine	< 10	ppm	DIN 51408
Acid number	< 0.02	mg KOH/g	DIN EN ISO 3682
Density at 20 °C	1.04 1.05	g/ml	DIN 51757
Viscosity at 20 °C	42 - 52	mm^2/s	DIN 51562
Boiling range at 1013 mbar	approx. 385-395	°C	ASTM D1078
Pour point	< -34	°C	DIN ISO 3016
Flash point	approx. 200	°C	EN 22719
Ignition temperature	approx. 450	°C	DIN 51 794

Table B.2: Physical properties for Marlotherm® SH.

Temperature		**Density**		**Heat Capacity**		**Thermal Conductivity**		**Kinematic Viscosity**
°C	°F	kg/m^3	lb/ft^3	kJ/kg-K	BTU/lb-F	W/m-K	BTU/ft-hr-F	mm^2/s
0	32	1058	66.0	1.48	0.354	0.133	0.077	321.0
20	68	1044	65.2	1.55	0.370	0.131	0.076	47.0
40	104	1030	64.3	1.62	0.387	0.128	0.074	16.5
60	140	1016	63.4	1.70	0.406	0.125	0.072	8.10
80	176	1001	62.5	1.77	0.423	0.123	0.071	4.70
100	212	987	61.6	1.85	0.442	0.120	0.069	3.10
120	248	973	60.7	1.92	0.459	0.117	0.068	2.30
140	284	958	59.8	1.99	0.475	0.115	0.066	1.80
160	320	944	58.9	2.07	0.494	0.112	0.065	1.40
180	356	930	58.1	2.15	0.514	0.110	0.064	1.20
200	392	915	57.1	2.22	0.530	0.107	0.062	0.92
220	428	901	56.2	2.29	0.547	0.104	0.060	0.77
240	464	887	55.4	2.37	0.566	0.102	0.059	0.65
260	500	873	54.5	2.44	0.583	0.099	0.057	0.57
280	536	858	53.6	2.52	0.602	0.096	0.055	0.50
300	572	844	52.7	2.59	0.619	0.094	0.054	0.45
320	608	830	51.8	2.67	0.638	0.091	0.053	0.40
340	644	815	50.9	2.74	0.654	0.088	0.051	0.36
360	680	801	50.0	2.82	0.674	0.086	0.050	0.32

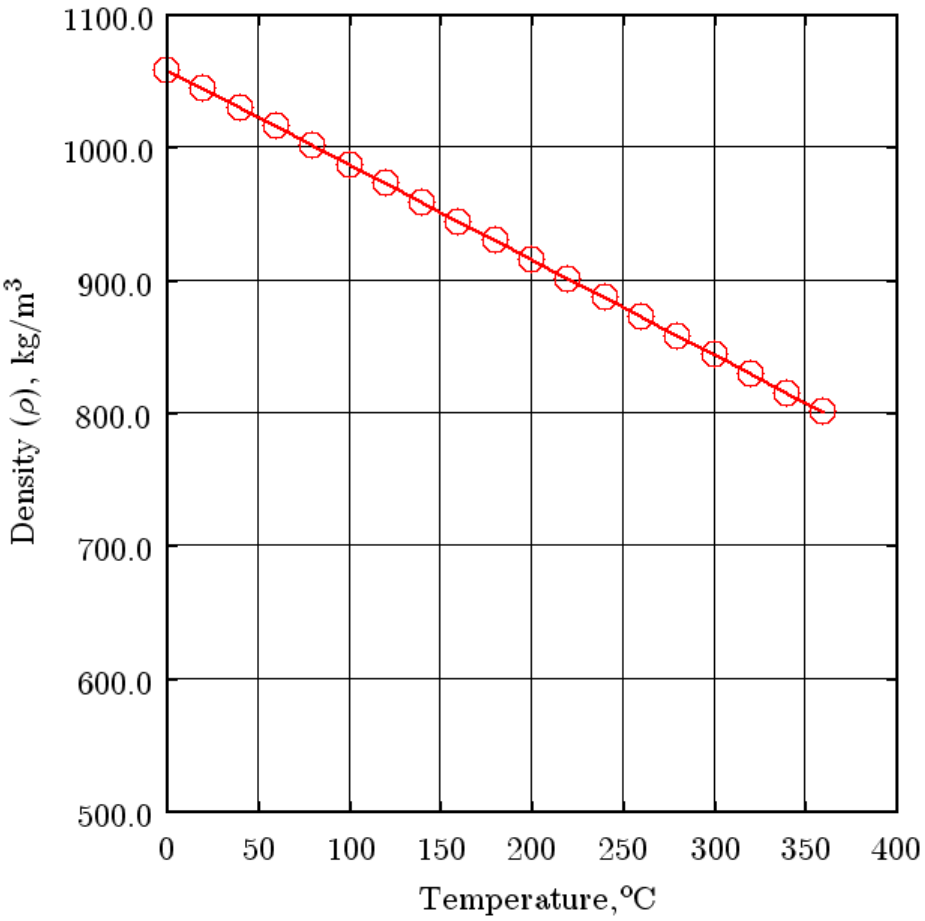

Figure B.1: Variation of density ($\rho = 1058.4 - 0.7184T$) with temperature for Marlotherm® SH.

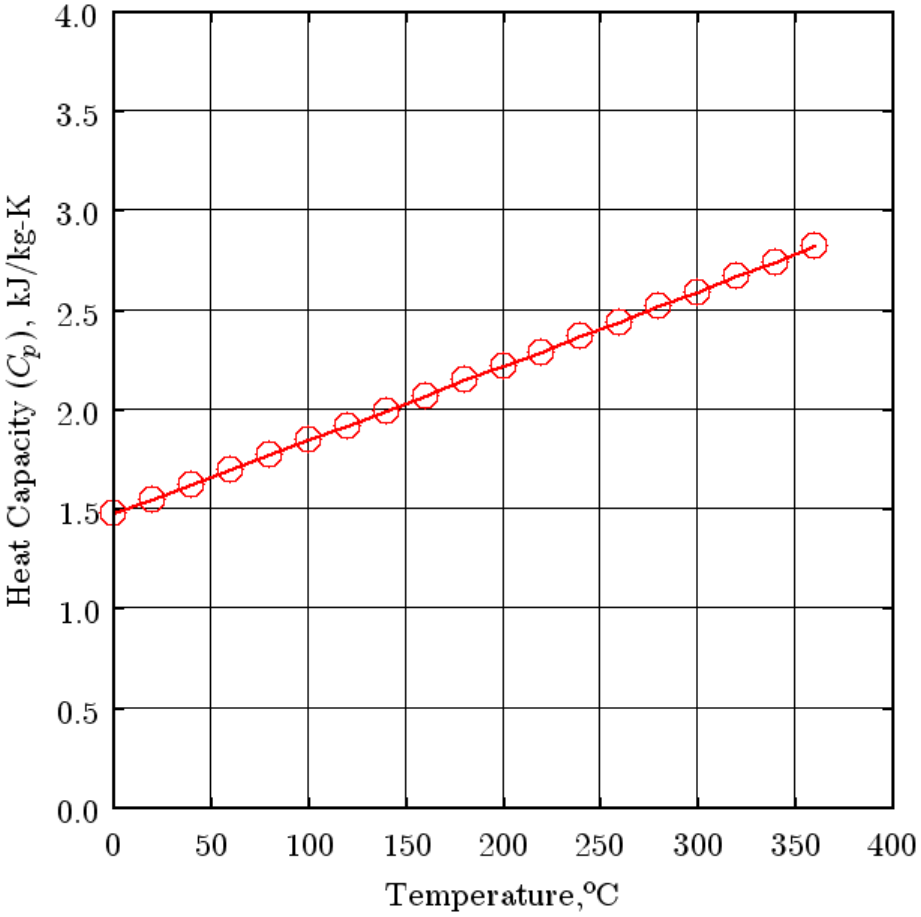

Figure B.2: Variation of heat capacity ($C_p = 1.4745 + 0.003726T$) with temperature for Marlotherm® SH.

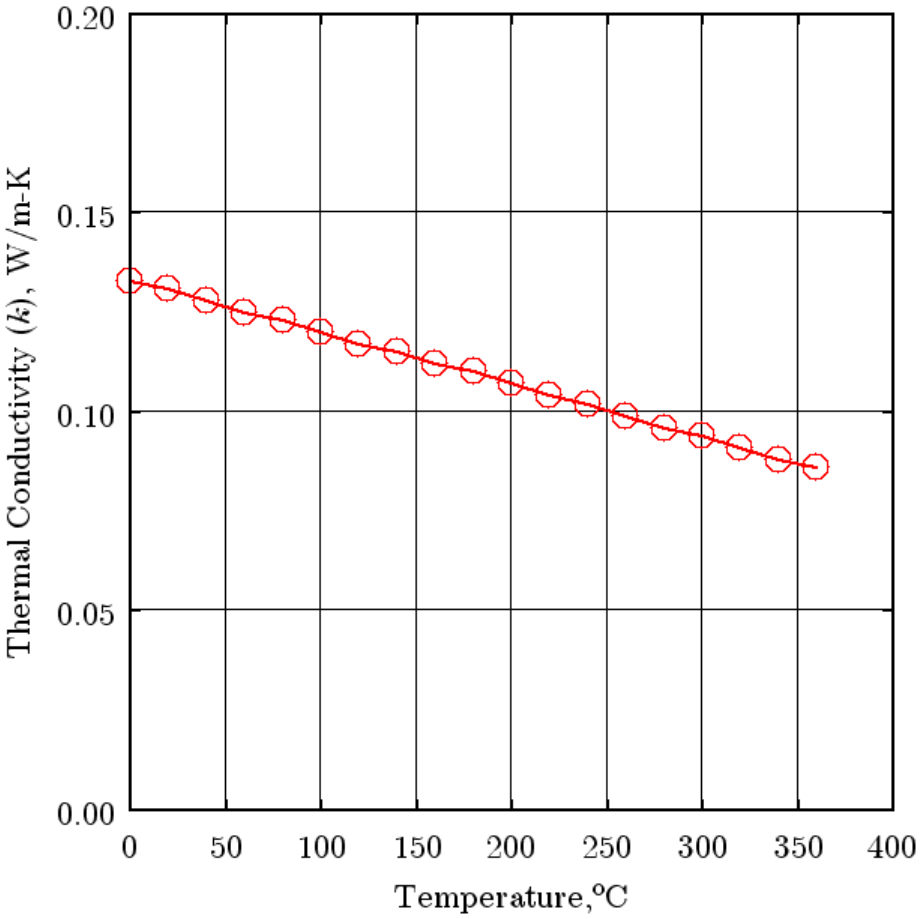

Figure B.3: Variation of thermal conductivity ($k = 0.1333 - 0.00013T$) with temperature for Marlotherm® SH.

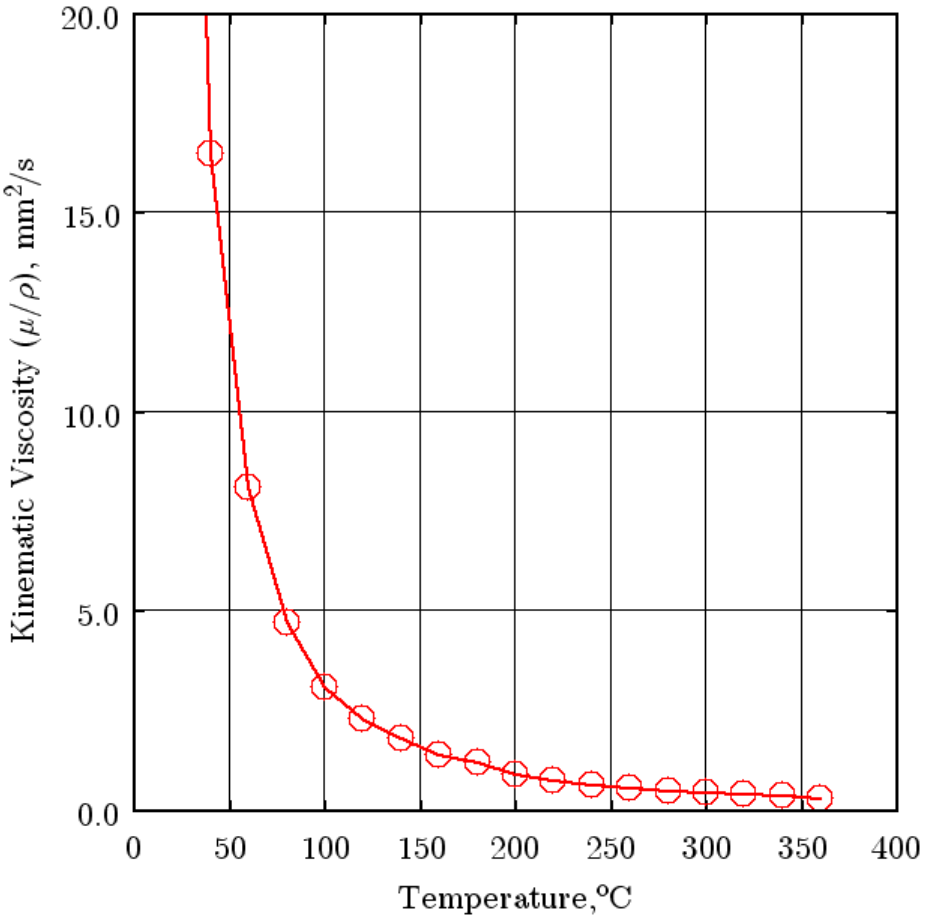

Figure B.4: Variation of kinematic viscosity $\left(\frac{\mu}{\rho} = 12294T^{-1.792}\right)$ with temperature for Marlotherm® SH.

Bibliography

[1] H. Abichandani and S. C. Sarma, Heat Transfer and Power Requirements in Horizontal Thin Film Scraped Surface Heat Exchangers. *Chem. Eng. Sci.*, 43(4):871–881, 1988. doi:10.1016/0009-2509(88)80083-6.

[2] H. Abichandani, S. C. Sarma, and D. R. Heldman, Hydrodynamics and Heat Transfer in Thin Film Scraped Surface Heat Exchangers – A Review. *J. Food Process Eng.*, 9(2):143–172, 1987.

[3] S. Y. Ahmed and R. Kaparthi, Heat Transfer Studies of Falling Film Heat Exchangers. 1(1):3717–381, 1963.

[4] N. M. Al-Najeem, K. Y. Ezuddin, and M. A. Darwish, Heat Transfer Analysis of Preheated Falling Films in Vertical Tube Evaporators. *Desalination*, 115(1):43–55, 1998. doi:10.1016/S0011-9164(98)00025-3.

[5] A. A. Alhusseini, K. Tuzla, and J. C. Chen, Falling Film Evaporation of Single Component Liquids. *Int. J. Heat Mass Transfer*, 41(12):1623–1632, 1998. doi:10.1016/S0017-9310(97)00308-6.

[6] D. B. Arlidge, Wiped Film Evaporators as Pilot Plants. *Chem. Eng. Prog.*, 79(8):35–40, August 1983.

[7] S. Azzory and T. R. Bott, Local Heat Transfer Coefficients in a Model

"Falling Film" Scraped Surface Exchanger. *Can. J. Chem. Eng.*, 48:373–377, 1970.

[8] R. Billet, *Distillation Engineering*. Chapter 9. Partial Distillation. B. Continuous Distillation in Falling Film Evaporators and Thin Film Evaporators, pp. 365–380. New York: Chemical Publishing Co., 1979.

[9] R. B. Bird, W. E. Stewart, and E. N. Lightfoot, *Transport Phenomena*. Chapter 13. Interphase Transport in Nonisothermal Systems, pp. 389–425. New York: Wiley, 1st edition, 1960.

[10] J. Bishop and D. Arlidge, Evaporators: Use in Re-refining. *Hydrocarb. Process.*, 58(7):131–136, July 1979.

[11] T. R. Bott and J. J. B. Romero, Heat Transfer Across a Scrapped Surface. *Can. J. Chem. Eng.*, 41:213–219, 1963.

[12] T. R. Bott and J. J. B. Romero, The Characteristic Dimension in Scrapped Surface Heat Transfer. *Can. J. Chem. Eng.*, 44:226–230, 1966.

[13] T. R. Bott and M. R. Sheikh, Effects of Blade Design in Scrapped Surface Heat Transfer. *Brit. Chem. Eng.*, 9(4):229–231, 1964.

[14] T. R. Bott and M. R. Sheikh, Evaporation at a Scraped Surface. *Chem Eng. Prog. Symp. Ser.*, 62(64):97–103, 1966.

[15] M. J. Burrows and G. S. G. Beveridge, The Centrifugally Agitated Wiped Film Evaporator. *Chem. Eng. (London)*, pp. 229–232, April 1979.

[16] N. Chawankul, S. Chuaprasert, P. Douglas, and W. Luewisutthichat, Simulation of an Agitated Thin Film Evaporator for Concentrating Orange Juice using AspenPlus. *J. Food Eng.*, 47(4):247–253, 2001. doi: 10.1016/S0260-8774(00)00122-9.

[17] S. Chuaprasert, P. Douglas, and M. Nguyen, Data Reconciliation of an Agitated Thin Film Evaporator Using AspenPlus. *J. Food Eng.*, 39(3):261–267, 1999. doi:10.1016/S0260-8774(98)00149-6.

[18] K. R. Chun and R. A. Seban, Heat Transfer to Evaporating Liquid Films. *J. Heat Transfer*, 93(4):391–396, 1971.

[19] M. L. Corradini, Fundamentals of Multiphase Flow. Available on: `http://wins.engr.wisc.edu/teaching/mpfBook/node26.html`, 1997.

[20] J. Cvengros, Three-Stage Wiped-Film Molecular Evaporator: Design and Application. *Chem. Eng. Technol.*, 18(1):49–58, 1995.

[21] J. Cvengros, V. Badin, and S. Pollak, Residence Time Distribution in a Wiped Liquid Film. *Chem. Eng. J.*, 59(3):259–263, 1995. doi:10.1016/0923-0467(94)02960-1.

[22] Design Institute for Physical Properties (DIPPR), Project 801: Evaluated Process Design Data. New York : American Institute of Chemical Engineers, 2005.

[23] A. J. Eckles, Difficult to Process? Vacuum It! *Chem. Eng. (New York)*, 104(9):94–100, September 1997.

[24] R. Fischer, Agitated Thin-Film Evaporators. Part 3. Process Applications. *Chem. Eng. (New York)*, 72(19):186–190, September 13 1965.

[25] J. T. Frank and J. Lutcha, Thickness of the Film of Material Treated in a Film-Type Rotary Evaporator. *Intn. Chem. Engng.*, 20(1):65–76, 1980.

[26] H. L. Freese and G. B. Glover, Mechanically Agitated Thin-Film Evaporators. *Chem. Eng. Prog.*, 75(1):52–58, January 1979.

[27] E. R. Gilliland and T. K. Sherwood, Diffusion of Vapors into Air Streams. *Ind. Eng. Chem.*, 26(5):516–523, 1934. doi:10.1021/ie50293a010.

[28] W. B. Glover, Selecting Evaporators for Process Applications. *Chem. Eng. Prog.*, 100(12):26–33, December 2004.

[29] H. J. Godau, Flow Process in Thin-Film Evaporators. *Intn. Chem. Engng.*, 15(3):445–449, 1975.

[30] T. H. Gouw and R. E. Jentoft, Efficiency Meaurements on an All-Glass Wiped-Film Still. *Ind. Eng. Chem. Process Des. Develp.*, 6(1):62–67, 1967.

[31] G. Gruber and J. L. Rak, Model of a Wiped-Film Still. *Chem. Eng. Prog.*, 85(12):12–18, 1989.

[32] M. S. Hameed and M. S. Muhammed, Mass Transfer into Liquid Falling Film in Straight and Helically Coiled Tubes. *Int. J. Heat Mass Transfer*, 46(10):1715–1724, 2003. doi:10.1016/S0017-9310(02)00500-8.

[33] H. K. Hansen, P. Rasmussen, A. Fredenslund, M. Schiller, and J. Gmehling, Vapor-Liquid Equilibria by UNIFAC Group Contribution. 5. Revision and Extension. *Ind. Engr. Chem. Res.*, 30(10):2352–2355, 1991. doi:10.1021/ie00058a017.

[34] P. Harriot, Heat Transfer in Scraped-Surface Exchangers. *Chem Eng. Prog. Symp. Ser.*, 55(29):137–139, 1958.

[35] B. C. Hoke, Jr. and J. C. Chen, Mass Transfer in Evaporating Falling Liquid Film Mixtures. *AIChE J.*, 38(5):781–787, 1992.

[36] H. C. Hsu, Y. W. Sheu, and C. H. Tu, Viscosity Estimation at Low Temperatures ($T_r < 0.75$) for Organic Liquids from Group Contributions. *Chem. Eng. J.*, 88(1–3):27–35, 2002. doi:10.1016/S1385-8947(01)00249-2.

[37] E. C. Ihmels and J. Gmehling, Extension and Revision of the Group Contribution Method GCVOL for the Prediction of Pure Compound Liquid Densities. *Ind. Engr. Chem. Res.*, 42(2):408–412, 2003. doi:10.1021/ie020492j.

[38] K. G. Joback and R. C. Reid, Estimation of Pure-Component Properties From Group-Contributions. *Chem. Eng. Commun.*, 57:233–243, 1987.

[39] D. Q. Kern and H. J. Karakas, Mechanically Aided Heat Transfer. *Chem Eng. Prog. Symp. Ser.*, 55(29):141–148, 1959.

[40] R. W. King, Distillation on Heat Sensitive Materials. Part 1. *Brit. Chem. Eng.*, 12(4):568–572, April 1967.

[41] R. W. King, Distillation on Heat Sensitive Materials. Part 2. *Brit. Chem. Eng.*, 12(5):722–727, May 1967.

[42] E. Kirschbaum and K. Dieter, Heat Transfer and Partial Distillation in Thin-Film Evaporators. *Chem. Ing. Tech.*, 30:715–720, 1958.

[43] J. G. Knudsen, H. C. Hottel, A. F. Sarofim, P. C. Wankat, and K. S. Knaebel, Section 5. Heat and Mass Transfer. In: R. H. Perry and D. W. Green, editors, *Perry's Chemical Engineers' Handbook*, pp. 5–1–5–79, New York: McGraw-Hill, 7th edition, 1997.

[44] S. Komori, K. Takata, and Y. Murakami, Flow Structure and Mixing Mechanism in an Agitated Thin Film Evaporator. *J. Chem. Engng. Japan*, 21(6):639–644, 1988.

[45] S. Komori, K. Takata, and Y. Murakami, Flow and Mixing Characteristics in an ATFE with Vertically Aligned Blades. *J. Chem. Engng. Japan*, 22(4):346–351, 1989.

[46] S. Komori, K. Takata, R. Nagaosa, and Y. Murakami, The Effects of Multistage Inclined Blades on Flow and Mixing Characteristics in an ATFE. *J. Chem. Engng. Japan*, 23(5):550–555, 1990.

[47] J. Kool, Heat Transfer in Scraped Vessels and Pipes Handling Viscous Materials. *Trans. Inst. Chem. Eng.*, 36(1):253–258, 1958.

[48] R. Krupiczka, A. Rotkegel, and Z. Ziobrowski, Heat Transfer to Evaporating Liquid Films within a Vertical Tube. *Chem. Eng. Process.*, 41(1):23–28, 2002. doi:10.1016/S0255-2701(00)00158-6.

[49] R. Krupiczka, A. Rotkegel, and Z. Ziobrowski, The Influence of Mass Transport on the Heat-Transfer Coefficients during the Film Boiling of Multicomponent Mixtures. *Chem. Eng. Process.*, 43(8):949–954, 2004. doi:10.1016/S0255-2701(03)00139-9.

[50] K. Larson, A. Andrews, B. Snyder, and C. Wighman, Integration of Wiped-Film Evaporation and Crossflow Microfiltration for the Purification of a Silylenol Ether Reaction Mixture. *Ind. Engr. Chem. Res.*, 35(4):1322–1331, 1996. doi:10.1021/ie950529i.

[51] G. A. Latinen, Discussion of the paper 'Correlation of Scraped-Film Heat Transfer in a Votator'. *Chem. Eng. Sci.*, 9(4):263–266, 1959. doi:10.1016/0009-2509(59)85008-9.

[52] G. Lavis, Evaporators: How to Make the Right Choice. *Chem. Eng. (New York)*, 4(101):93–102, April 1994.

[53] S. Leuthner, A. H. Maun, S. Fiedler, and H. Auracher, Heat and Mass Transfer in Wavy Falling Films of Binary Mixtures. *Int. J. Therm. Sci.*, 38(11):937–943, 1999. doi:10.1016/S1290-0729(99)00101-5.

[54] P. Li, Y.-H. Liang, P.-S. Ma, and C. Zhu, Estimations of Enthalpies of Vaporization of Pure Compounds at Different Temperatures by a Corresponding-States Group-Contribution Method. *Fluid Phase Equilib.*, 137(1-2):63–74, 1997. doi:10.1016/S0378-3812(97)00094-0.

[55] P. Li, P.-S. Ma, S.-Z. Yi, Z.-G. Zhao, and L.-Z. Cong, A New Corresponding-States Group-Contribution Method (CSGC) for Estimating Vapor Pressures of Pure Compounds. *Fluid Phase Equilib.*, 101(Oct 31):101–119, 1994. doi:10.1016/0378-3812(94)02607-6.

[56] J. F. Maingonnat and G. Corrieu, Study of the Thermal Performance of a Scraped-Surface Heat Exchanger. Part I. Review of the Principal Models Describing Heat Transfer and Power Consumption. *Intn. Chem. Engng.*, 26(1):45–54, 1986.

[57] A. Martinez-Chitoy, *Modelacion, Control, y Diagnostico de Fallas para una Columna de Destilacion Molecular de Trayecto Corto*. Ph.D. dissertation, Universidad Autonoma de Nuevo Leon, Mexico, August 1996.

[58] M. Mathlouthi and J. Génotelle. In: M. Mathlouthi and P. Reiser, editors, *Sucrose: Properties and Applications*, Chapter 6. Rheological Properties of Sucrose Solutions and Suspensions, pp. 126–154, New York : Blackie Academic & Professional, 1995.

[59] W. H. McAdams, *Heat Transmission*. Chapter 13. Condensing Vapors, pp. 325–367. New York: McGraw-Hill, 3rd edition, 1954.

[60] W. H. McAdams, *Heat Transmission*. Chapter 9. Heating and Cooling Inside Tubes, pp. 202–251. New York: McGraw-Hill, 3rd edition, 1954.

[61] J. M. McKelvey and C. V. Sharps, Jr., Fluid Transport in Film Polymer Processors. *Polym. Engng Sci.*, 19(9):651–659, 1979.

[62] T. F. McKenna, Design Model of a Wiped Film Evaporator. Applications to the Devolatilisation of Polymer Melts. *Chem. Eng. Sci.*, 50(3):453–467, 1995. doi:10.1016/0009-2509(94)00257-R.

[63] P. E. Minton, *Handbook of Evaporation Technology*. Chapter 3. What an Evaporator Does, pp. 3–4. Park Ridge, N. J.: Noyes Publications, 1st edition, 1986.

[64] H. Miyashita and T. W. Hoffman, Local Heat Transfer Coefficients in Scrapped-Film Heat Exchanger. *J. Chem. Engng. Japan*, 11(6):444–450, 1978.

[65] H. Miyashita, M. Yoshida, T. Yamane, and T. Nishimura, Heat Transfer Correlation in High Prandtl (High Schmidt) Number Fluid in Votator Type Scrapped Surface Heat Exchanger. *J. Chem. Engng. Japan*, 30(3):545–549, 1997.

[66] T. Mizushina, *Advances in Heat Transfer*, volume 7. New York: Academic Press, 1971.

[67] B. Mutzenberg and A. Giger, Chemical Reaction in Thin Film Equipment. *Trans. Inst. Chem. Eng.*, 46:T187–T189, 1968.

[68] A. B. Mutzenburg, Agitated Thin-Film Evaporators. Part 1. Thin-Film Technology. *Chem. Eng. (New York)*, 72(19):175–178, September 13 1965.

[69] E. Nadjer, Thin Film Evaporation. *Ind. Eng. Chem.*, 56(2):26–30, 1964.

[70] K. Nakamura and T. Watanabe, Flow in Agitated Thin Film Evaporator. *Chem. Eng. Commun.*, 18:173–190, 1982.

[71] C. H. E. Nielsen, S. Kiil, H. W. Thomsen, and K. Dam-Johansen, Mass Transfer in Wetted-Wall Columns: Correlations at high Reynolds Numbers. *Chem. Eng. Sci.*, 53(3):495–503, 1998. doi:10.1016/S0009-2509(97)00320-5.

[72] Niro Inc., Evaporation Technology. Available on: `http://www.niroinc.com/html/evaporator/etech.html`, 2005.

[73] R. Numrich, Heat Transfer in Turbulent Films. *Chem. Eng. Technol.*, 18(3):171–177, 1995.

[74] N. Parker, Agitated Thin-Film Evaporators. Part 2. Equipment and Economics. *Chem. Eng. (New York)*, 72(19):179–185, September 13 1965.

[75] A. M. Peres and E. A. Macedo, Thermodynamic Properties of Sugars in Aqueous Solutions: Correlation and Prediction using a Modified UNIQUAC Model. *Fluid Phase Equilib.*, 23(1-2):71–95, 1996. doi:10.1016/S0378-3812(96)90013-8.

[76] J. A. Rocha-Uribe and J. Lopez-Toledo, Design and Analysis of Wiped Film Evaporators. Annual Report, Separations Research Program, The University of Texas at Austin, 1999.

[77] V. Růžička, Jr. and E. S. Domalski, Estimation of the Heat Capacities of Organic Liquids as a Function of Temperature Using Group Additivity. I. Hydrocarbon Compounds. *J. Phys. Chem. Ref. Data*, 22(3):597–618, 1993.

[78] V. Růžička, Jr. and E. S. Domalski, Estimation of the Heat Capacities of Organic Liquids as a Function of Temperature Using Group Additivity. II. Compounds of Carbon, Hydrogen, Halogens, Nitrogen, Oxygen, and Sulfur. *J. Phys. Chem. Ref. Data*, 22(3):619–657, 1993.

[79] W. M. Salvagnini and M. E. S. Taqueda, A Falling Film Evaporator with Film Promoters. *Ind. Engr. Chem. Res.*, 43(21):6832–6835, 2004. doi:10.1021/ie0307636S0888-5885(03)00763-2.

[80] G. Sangrame, D. Bhagavathi, H. Thakare, S. Ali, and H. Das, Performance Evaluation of a Thin Film Scraped Surface Evaporator for Concentration of Tomato Pulp. *J. Food Eng.*, 43(4):205–211, 2000. doi: 10.1016/S0260-8774(99)00150-8.

[81] Sasol, MARLOTHERM® SH Heat Transfer Fluid. Available on: `http://www.marlotherm.com/pdf/MARLOTHERM_SH_GB.pdf`, 2005.

[82] S. R. S. Sastri and K. K. Rao, A New TemperatureThermal Conductivity Relationship for Predicting Saturated Liquid Thermal Conductivity. *Chem. Eng. J.*, 74(3):161–169, 1999. doi:10.1016/S1385-8947(99)00046-7.

[83] R. V. Schurter, Evaporation: Think Thin Film. *Chem. Eng. (New York)*, 101(4):104–106, April 1994.

[84] J. D. Seader and E. J. Henley, *Separation Process Principles*. Chapter 4. Single Equilibrium Stages and Flash Calculations., pp. 3–4. New York: Wiley, 1st edition, 1998.

[85] T. K. Sherwood, R. L. Pigford, and C. R. Wilke, *Mass Transfer*. Chapter 7. Simultaneous Heat and Mass Transfer. New York: McGraw-Hill, 1975.

[86] R. L. Shilling, K. J. Bell, P. M. Bernhagen, T. M. Flynn, V. M. Goldschmidt, P. S. Hrnjak, F. C. Standiford, and K. D. Timmerhaus, Section 11. Heat-Transfer Equipment. In: R. H. Perry and D. W. Green, editors, *Perry's Chemical Engineers' Handbook*, pp. 11–1–11–118, New York: McGraw-Hill, 7th edition, 1997.

[87] A. H. P. Skelland, Correlation of Scraped-film heat transfer in the Votator. *Chem. Eng. Sci.*, 7(3):166–175, 1958. doi:10.1016/0009-2509(58)80023-8.

[88] A. Skoczylas, Heat Transfer Coefficient for a Hinged Blade Wiped Film Evaporator. *Brit. Chem. Eng.*, 15(2):221–222, 1970.

[89] P. L. Spedding and M. T. Jones, Heat and Mass Transfer in Wetted-Wall Columns: I. *Chem. Eng. J.*, 37(3):165–176, 1988. doi:10.1016/0300-9467(88)80015-7.

[90] F. C. Standiford, *Kirk-Othmer Encyclopedia of Chemical Technology*, volume 9. Elastomers, Synthetic-Expert Systems. pp. 472–493. New York: John Wiley & Sons, Inc., 4th edition, 2005, doi:10.1002/0471238961.0522011619200114.a01.

[91] K. Stankiewicz and M. A. Rao, Heat Transfer in Thin Film Wiped-Surface Evaporation of Model Liquid Foods. *J. Food Process Eng.*, 10:113–131, 1988.

[92] J. R. Thome, Falling Film Evaporation: State-of-the-art Review of Recent Work. *J. of Enhanced Heat Transfer*, 6(2-4):263–277, 1999.

[93] A. M. Trommelen, W. J. Beek, and H. C. van de Westelaken, A Mechanism for Heat Transfer in a Votator-Type Scraped-Surface Heat Exchanger. *Chem. Eng. Sci.*, 26(12):1987–2001, 1971. doi:10.1016/0009-2509(71)80037-4.

[94] Y. L. Tsay and T. F. Lin, Evaporation of a Heated Falling Liquid Film into a Laminar Gas Stream. *Experimental Thermal and Fluid Science*, 11(1):61–71, 1995. doi:10.1016/0894-1777(94)00112-L.

[95] J. Tyzack, Applications for ATFEs – Drying and Concentration. *Chem. Eng. (London)*, pp. 33–38, November 15 1990.

[96] J. Tyzack, Applications for ATFEs – Distillation. *Chem. Eng. (London)*, pp. 20–23, February 14 1991.

[97] W. Unterberg and D. Edwards, Effect of a Dissolved Solid on Wiped-Film Evaporation. *Ind. Eng. Chem. Process Des. Develp.*, 6(3):268–276, 1967.

[98] S.-M. Yih and K.-Y. Chen, Gas Adsorption into Wavy and Turbulent Falling Liquid Films in a Wetted-Wall Column. *Chem. Eng. Commun.*, 17:123–136, 1982.

[99] M. L. Yüksel and E. U. Schlünder, Heat and Mass Transfer in Non-isothermal Absorption of Gases in Falling Films. Part I: Experimental Determination of Heat and Mass Transfer Coefficients. *Chem. Eng. Process.*, 22(4):193–202, 1987. doi:10.1016/0255-2701(87)85002-X.

[100] M. L. Yüksel and E. U. Schlünder, Heat and Mass Transfer in Non-isothermal Absorption of Gases in Falling Films. Part II: Theoretical Description and Numerical Calculation of Turbulent Falling Film Heat and Mass Transfer. *Chem. Eng. Process.*, 22(4):203–213, 1987. doi:10.1016/0255-2701(87)85003-1.

Vita

Jacinto Lopez-Toledo the son of Juan Lopez-Chevez and Juanita Toledo-Cristobal, was born in Union Hidalgo Oaxaca Mexico on December 31st, 1973. In 1991 he entered the Instituto Tecnologico de Oaxaca in Oaxaca, Mexico. He received the degree of Bachelor in Science in Chemical Engineering in July 1995. In August 1995, he entered the Instituto Tecnologico de Celaya, where he obtained the degree of Master in Science in Chemical Engineering in September 1997. On December 26th 1997 he married Nancy Ruiz-Castillo. In August 1998 he was invited to the Separations Research Program at The University of Texas at Austin. In August 2000 he entered the Graduate School of The University of Texas at Austin.

Permanent address: Av. 24 de Febrero # 3
Union Hidalgo, Oax. Mexico 70150

This dissertation was typeset with LaTeX[†] by 'the author'.

[†]LaTeX is a document preparation system developed by Leslie Lamport as a special version of Donald Knuth's TeX Program.